

“ SPECTRAL ANALYSIS OF THE HORIZONTAL LOOP ELECTROMAGNETIC
PROFILING DATA OVER A CONDUCTIVE HALF-PLANE ”

BY

JOSEPH KIIO | NZOMO

A thesis submitted as partial fulfillment for the award of
Master of Science Degree at the University of Nairobi.

College of Biological and Physical Sciences

Faculty of Science

Department of Geology

THIS THESIS HAS BEEN ACCEPTED FOR
THE DEGREE OF *M.Sc.* 1992 *JK*
AND A COPY MAY BE PLACED IN THE
UNIVERSITY LIBRARY.

NAIROBI, 1992

University of NAIROBI Library

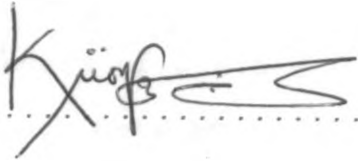


0473745 8

DECLARATION

I Joseph Kiio Nzomo, hereby declare that this is my own work and has not been presented for a Degree at any other University.

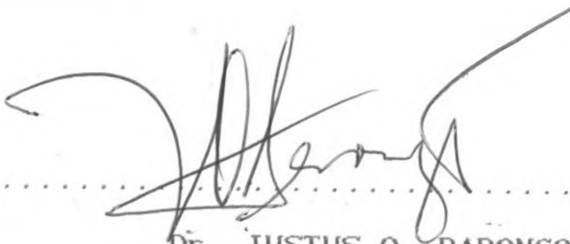
All sources of information have been specifically acknowledged by means of references.



.....

JOSEPH KIIO NZOMO

This thesis has been submitted for examination with our knowledge as University Supervisors.



.....

Dr. JUSTUS O. BARONGO



.....

Prof. J.P. PATEL

LIST OF SYMBOLS

T_x	transmitter
R_x	receiver
C_x	conductor
μ	magnetic permeability
σ	conductivity
δ	skin depth
z	depth to the top of plate
s	thickness of plate
x	distance between the reading station (midway between T_x - R_x array) and the point directly above the top of plate.
l	coil separation
E	electric field vector
H	magnetic field vector
J	current density vector
K	surface current density vector
CFT	continuous Fourier transform
DFT	discrete Fourier transform
FS	Fourier series
FT	Fourier transform

IV

ABSTRACT

Most interpretive methods in geophysical prospecting involve the analysis of a single signal which may be a spatial or time domain record of a given deterministic geophysical variable representing the anomaly of interest. In the present development, the electromagnetic (EM) response resulting from the interaction of the fields due to a thin plate-like conductor and the horizontal loop EM prospecting (HLEM) system is the pertinent geophysical variable.

The interpretation of ground EM response due to a conductive thin plate is carried out through Fourier analysis. The introductory EM response is based on the rudimentary model in which a thin conductive plate is simulated by a single current filament which lies at or near the top edge of the plate. The amplitude spectrum is derived from analytical expressions of the response of the above model through Fourier transformation. In the transform domain, highly simplified expressions result from which the depth and the quality of the conductive target may be estimated. In fact, depth can be determined directly from the slope of the amplitude spectrum which constitutes the first method of depth estimation herein described.

A second method for estimating depth using harmonic analysis is described. This method is based on the value of the wavenumber at which the real component of the Fourier transform drops off to zero. It is demonstrated that this value depends on the depth of

the wire model if the coil separation is kept constant. Spectral information on depth is available at zero or higher harmonics. This method yields two depths (making it hard to choose the correct one) and may be effectively use in areas where depth of occurrence of the orebody is roughly known. The use of the slope method to get a rough estimate of depth and the final determination thereof using the harmonic method are described.

The slope method works well for synthetic data generated from both the wire and the plate models and is moderately successful with the field data. However, the harmonic method works only for the wire model.

The estimation of conductance of the target is based on data taken at different operating frequencies of the HLEM prospecting system. Using the PLATE program, theoretical response profile data are prepared at 222, 444, 888, 1777 and 3555 hertz and then Fourier transformed. The results are used to prepare the interpretation nomograms presented in this work. This is accomplished by considering the wavenumber decay characteristics of the amplitude spectrum at low wavenumbers for a given target, where spectral noise is minimal. When field data is Fourier transformed, the nature of the spectra makes the estimation of conductance by means of the nomograms very difficulty if not impossible. In most cases, however, this parameter as well as the target dip are just as easy to evaluate directly from the observed field data using phasor diagrams and dip nomograms respectively.

VI

The overburden problem is attendant in the interpretation of data acquired from tropical terrains. Here a simple subtraction process is used to mitigate this undesirable effect. The overburden problem requires advanced analytical procedures beyond the scope of this contribution, to effectively manage it.

The spectral analysis method of EM interpretation is useful for determining depth of the target because it is unaffected by dip, size, conductance, or position of profile. A possible application of this method would be automated interpretation of large favourable data sets over many conductors.

ACKNOWLEDGEMENTS

I am deeply indebted to my supervisor Dr Justus O. Barongo. I gratefully acknowledge his guidance, support and invaluable suggestions throughout the course of this research. He was a source of constant encouragement and understanding and I benefited much from his experience in geophysical prospecting methods. Dr Barongo also introduced me to the fundamental mathematical aspects of geophysics and programming techniques using a microcomputer. I also wish to thank my second supervisor Prof. Patel for his keen interest in this research.

My entire Master of Science course was financed by the Germany Academic Exchange Service (DAAD) and I hereby gratefully acknowledge their generosity for awarding a scholarship.

I also wish to express my gratitude to the Institute of Computer Science for allowing me to use their Main Frame computer to execute some of my large programs. I wish to thank the Department of Geology for allowing me to make extensive use of their microcomputer facilities to run my smaller jobs and in word processing.

VIII

I wish to thank Mrs. Kahuthia for typing the captions in some of the diagrams and Messrs Mutonyi and Katoo for drawing the figures and diagrams in this work. I wish to thank members of my family for their continual moral support throughout the course of this research work. Lastly and not least I wish to thank Messrs. Kennedy Kibiy and Abdi Salah for their moral support and the stimulating discussions we often held as we both worked through our research projects.

TABLE OF CONTENTS

Title.....	I
Declaration.....	II
list of Symbols.....	III
Abstract.....	IV
Acknowledgements.....	VII
Table of Contents.....	IX
List of Figures.....	XII
List of Tables.....	XVIII

CHAPTER ONE

1.1 Introduction.....	1
1.1.1 Electromagnetic Methods.....	1
1.2 The Horizontal Loop System.....	3
1.3 The Search for Massive Sulphides.....	5
1.3.1 General.....	5
1.3.2 Choice of Exploration Method.....	7
1.3.3 Spectral Techniques.....	7
1.3.4 Extraneous Anomaly Sources.....	8
1.3.5 The importance of Environment.....	8
1.4 Review of Current Status of Interpretation Aids in HLEM prospecting System.....	9
1.5 Thesis Objectives and Outline.....	15

CHAPTER TWO

2.1 Basic Theory.....	19
2.1.1 Transform Analysis.....	19

2.1.2	Basic Fourier Transform Analysis.....	20
2.1.3	The Fourier Integral.....	26
2.1.4	The Inverse Fourier Transform.....	28
2.2	The Line Current Target Model.....	28
2.3	The Plate Model.....	32
2.3.1	General.....	32
2.3.2	Numerical Development of The Plate Model.....	33
2.3.3	Computational Structure.....	35
2.3.4	Limitations and Precision.....	38
2.3.5	The Half-plane Approximation.....	40
2.4	Fourier Transform of The Line Current Target Response.....	43
2.4.1	The Continuous Fourier Transform.....	44
2.4.2	The Discrete Fourier Transform.....	52
2.4.3	The Fast Fourier Transform.....	61

CHAPTER THREE

3.1	Analysis of Amplitude Spectrum.....	68
3.1.1	Estimation of Depth From The Amplitude Spectrum.....	68
3.1.2	Estimation of Depth from Harmonic Analysis of The Derived Spectrum.....	73
3.2	Fourier Analysis of Synthetic Data.....	75
3.2.1	The wire Model Data.....	77
3.2.2	The Plate Model Data.....	90
3.2.3	The effect of Dip on Amplitude Spectrum.....	96

3.3 Development of Interpretation Nomograms for
conductivity-thickness product.....101

CHAPTER FOUR

4.1 Field Studies from Western Kenya.....107
 4.1.1 Introduction.....107
 4.1.2 Outline of Geology.....107
 4.1.3 Airborne Geophysical Survey.....108
 4.1.4 Ground Geophysical Survey.....109
 4.2 Fourier Analysis of Ground HLEM data.....111
 4.2.1 Procedure Adopted in Analysing HLEM profiles.....113
 4.2.2 Analysis of Field Anomalies.....114
 4.2.3 Results of Analysis.....116

CHAPTER FIVE

5.1 Discussion of Results.....145
 5.2 Conclusions and Recommendations.....153
 References.....156
 Appendix 1 The PLATE Program.....164
 Appendix 2 Theoretical Background of The
 PLATE Program.....170

LIST OF FIGURES

PAGE

<u>Figure 2-1.</u> Flow diagram of conventional and transformational analysis (after Brigham 1974).....	21
<u>Figure 2-2.</u> Interpretation of the Fourier Transform (after Brigham 1974).....	23
<u>Figure 2-3.</u> HLEM system over a conductive half plane simulated by a line current model.....	30
<u>Figure 2-4.</u> Eigencurrents (contours of the eigenpotentials) for a 1x2 plate and 15 degrees of freedom (polynomials of order 4) (after Dyck et al., 1980).....	36-37
<u>Figure 2-5.</u> Semicomplex plane showing singularity of the integrand in equation 2.13.....	47
<u>Figure 3-1.</u> Periodic properties of the function $A_o(k_x)$	71
<u>Figure 3-2.</u> A graphical representation of the function $ A_o(K_o) $	71
<u>Figure 3-3.</u> A graphical representation of the function $\ln A_o(K_x) $	72

<u>Figure 3-4.</u> A complete graphical representation of $\ln A_o(k_x) - k_x z$	72
<u>Figure 3-5.</u> A plot of the zero harmonic wavenumber against depth.....	76
<u>Figure 3-6(a).</u> Wavenumber-domain amplitude spectrum for the wire model; coil separation (l)= 0.1 km, depth (z) = 0.01 km, slope (-z) = - 0.011.....	78
<u>Figure 3-6(b).</u> Wavenumber-domain amplitude spectrum for the wire model; coil separation (l)= 0.1 km, depth (z) = 0.02 km, slope (-z) = -0.0204.....	78
<u>Figure 3-6(c).</u> Wavenumber-domain amplitude spectrum for the wire model; coil separation (l)= 0.1 km, depth(z) = 0.04 km, slope (-z) = -0.0402.....	79
<u>Figure 3-6(d).</u> Wavenumber-domain amplitude spectrum for the wire model; coil separation (l)= 0.1 km, depth (z) = 0.06 km, slope (-z) = -0.0596.....	79
<u>Figure 3-6(e).</u> Wavenumber-domain amplitude spectrum for the wire model; coil separation (l)= 0.1 km, depth (z) = 0.1 km, slope (-z) = -0.0993.....	80

Figure 3-6(f). Wavenumber-domain amplitude spectrum for the wire model; coil separation $(l) = 0.1$ km, depth $(z) = 0.2$ km, slope $(-z) = -0.2200$80

Figure 3-7. Real component $[F_e(k_x)]$ of the Fourier transform of the wire model against wavenumber (k_x)84

Figure 3-8. Real components $[F_e(k_x)]$ of the Fourier transform of the wire model against wavenumber (k_x) ; (a) $z=0.01$ km, (b) $z=0.02$ km, (c) $z=0.04$, (d) $z=0.06$ km, (e) $z=0.1$ km, (f) $z=0.2$ km.....86-88

Figure 3-9. Wavenumber domain amplitude spectra for the plate model;(a) $z=0.01$ km, (b) $z=0.06$ km, (c) $z=0.2$ km.....93-94

Figure 3-10. Space domain profiles and their corresponding amplitude spectra for the plate model. Note anomaly response changes with dip: (a) dip= 0° (b) dip= 5° (c) dip= 10° (d) dip= 45°97-100

Figure 3-11(a). A nomogram for determination of conductivity-thickness product for ground horizontal loop EM system. Vertical scale is normalised by the amplitude of the highest

frequency and spectra are measured at 16.81 rad.....103

Figure 3-11(b). A nomogram for determination of conductivity-thickness product for ground horizontal loop EM system. Spectra are measured at 22.42rad.....106

Figure 4-1. Map to show areas flown by the Combined INPUT AEM/AEROMAGNETIC survey in Western Kenya in 1977. Data used in this study is taken from the shaded area.....110

Figure 4-2. Determination of dip of tabular conductor (after David, 1966).....115

Figure 4-3(a). (i) Horizontal loop EM profile for the anomaly A1-160 at 222 Hz. (ii) Amplitude spectrum for anomaly A1-160 line 00.....118-119

Figure 4-3(b). (i) Horizontal loop EM profile for the anomaly A1-101 at 222 Hz. (ii) Amplitude spectrum for anomaly A1-101 line 250E.....121

Figure 4-3(c). (i) Horizontal loop EM profile for the anomaly A1-148 at 222 Hz. (ii) Amplitude spectrum for anomaly A1-148 line 00.....123

Figure 4-3(d). (i) Horizontal loop EM profile for the anomaly A1-221A at 222 Hz. (ii) Amplitude spectrum for anomaly 221A line 250W.....124

Figure 4-3(e). (i) Horizontal loop EM profile for the anomaly A1-221A at 222 Hz. (ii) Amplitude spectrum for anomaly A1-221A line 500W.....126

Figure 4-3(f). (i) Horizontal loop EM profiles for the five operating frequencies for anomaly A1-161.....128-132

(ii) Amplitude spectrum for anomaly A1-161 line 00 at 222 Hz.....134

Figure 4-3(g). Amplitude spectrum for anomaly A1-161 line 125W.....135

Figure 4-3(h) Amplitude spectrum for anomaly A1-161 line 250W.....135

Figure 4-4(a). Amplitude spectrum for anomaly A1-161 line 125W at 222Hz.....136

Figure 4-4(b). Amplitude spectrum for anomaly A1-161 line 125W at 444Hz.....136

Figure 4-4(c). Amplitude spectrum for anomaly A1-161 line 125W at 888Hz.....137

	PAGE
<u>Figure 4-4(d)</u> . Amplitude spectrum for anomaly A1-161 line 125W at 1777Hz.....	137
<u>Figure 4-4(e)</u> . Amplitude spectrum for anomaly A1-161 line 125W at 3555Hz.....	138
<u>Figure 4-5(a)</u> . Amplitude spectrum for anomaly A1-161 line 250W at 222 Hz.....	139
<u>Figure 4-5(b)</u> . Amplitude spectrum for anomaly A1-161 line 250W at 444Hz.....	139
<u>Figure 4-5(c)</u> . Amplitude spectrum for anomaly A1-161 line 250W at 888Hz.....	140
<u>Figure 4-5(d)</u> . Amplitude spectrum for anomaly A1-161 line 250W at 1777Hz.....	140
<u>Figure 4-5(e)</u> . Amplitude spectrum for anomaly A1-161 line 250W at 3555Hz.....	141

LIST OF TABLES

PAGE

<u>Table 2.1.</u> Strike length of the plate model and the corresponding percentage error in depths estimated from the slope of the amplitude spectrum.....	42
<u>Table 3.1.</u> True and estimated values of depth determined from the slope of the amplitude spectrum of the wire model.....	82
<u>Table 3.2.</u> Data used to plot the real component of the Fourier transform against wavenumber, $k_x(0)$ for the wire model.....	85
<u>Table 3.3.</u> Results of using the second method (harmonic analysis) to estimate depth. The estimated values of depth are based on the zero harmonic.....	91
<u>Table 3.4.</u> Depth estimates based on data generated using the plate model.....	95
<u>Table 4.1.</u> Tabulated results of depth analysis for field anomalies.....	143

CHAPTER ONE

1.1 Introduction

1.1.1 Electromagnetic Methods

The search for fast and reliable interpretive methods in geophysical prospecting has been the prime objective of every aspiring geophysicist. The main aim of interpreting any geophysical data is to retrieve useful geologic information which can be of help to both geologists and geophysicists in an endeavour to search for minerals and oil. It is important that the raw geophysical survey data be reliable for reliable results.

With the exception of magnetic methods, the electromagnetic (EM) prospecting techniques are the most commonly used in mineral exploration. They are not suited to the search for oil because they respond best to good electrical conductors at shallow depth. As the name implies, the method involves the diffusion (Grant and West, 1965) of time varying low-frequency electromagnetic fields in and over the earth. There is a close analogy between the transmitter and the receiver and a buried conductor in the EM field situation and a trio of electrical circuits coupled by electromagnetic induction.

In a few EM systems, the source of energy may be introduced into the ground by direct contact, although generally,

inductive coupling is used, invariably the detector receives its signal by induction. Electromagnetic prospecting methods which make use of artificial primary fields generally work in the following way: An alternating magnetic field is established by passing an alternating current through a coil or along a very long wire. This field is measured with a receiver consisting of a coil connected to a sensitive electronic amplifier, meter or potentiometer bridge. The frequency of the alternating current is chosen so that an insignificant eddy current field is induced in the ground if it has an average electrical conductivity. Ordinarily this sets an upper limit on the operating frequency of about 5 KHz, although higher frequencies of upto 50 KHz may be used in certain instances. If the source and the receiver are brought near a more conductive zone, stronger eddy currents may be caused to circulate within it and an appreciable secondary magnetic field will thereby be created. Close to the conductor, this secondary or anomalous field may be comparable in strength with the primary or normal field (present in the absence of conducting zones), in which case, it can easily be detected by the receiver. Prospecting for these anomalous zones is carried out systematically by traversing the ground either with the receiver unit alone or with both the receiver and the source in combination, depending upon the system in use.

In practice, the distance between the source and the receiver is usually a few hundred and seldom a few thousand

metres. It is noteworthy that at frequencies less than 5KHz, the wavelength of the alternating source is only a small fraction of a free space wavelength, which means that, in the regions within which observations are taken, radiation and phase retardation is very slight so that effects of propagation can wholly be disregarded. Electromagnetic methods are therefore much more closely related to potential field methods, such as gravity and magnetic methods, than to seismic methods which depend upon the propagation of waves.

In the theory of electromagnetic prospecting systems, we learn that the secondary and the primary fields are not generally in phase. This phase difference is attendant in geophysical interpretation and may furnish information regarding the conductivity of the anomalous zone. In consequence, most field apparatus have been designed to determine the phase.

1.2 The Horizontal Loop EM Method

The horizontal loop EM method utilizes a phase component measuring system and is one of the oldest and perhaps one of the most universally popular of the EM methods. It uses transmitter and receiver coils which are horizontal and kept at a fixed distance apart. The receiver measures both the in-phase and the quadrature components of the secondary anomalous field, usually as a percentage of the primary

field intensity. The reference signal passes to the receiver through a cable attached to the transmitter. This cable also controls the separation between the two coils. The coils are moved along picket lines, and readings are taken at regular intervals, whereby a reading station is located at the midpoint of the transmitter-receiver array. For a fairly regular terrain, reading accuracy of about 1% can be anticipated.¹ One remarkable advantage of the HLEM system is its symmetry. Since the coils are maintained at fixed relative position, the measurements are equivalent to determining their mutual inductance. The direction of the traverse is immaterial since the rule of reciprocity ensures that measurements are not changed by swapping the transmitter and the receiver. Data acquired by means of the HLEM system are therefore relatively most easy to interpret.

The configuration of the HLEM system adopted in this study is the in-line, moving source (Figure 2-3). It is also known as Slingram and Ronka EM. Like many other systems, it was developed in Sweden and has been popular in North America since about 1958 (Telford et al., 1990).

In contrast to airborne time domain systems, the ground HLEM has low penetration power. The high penetration capability of the airborne systems is owed to their large geometry and high dipolar moment (10^5 a/m^2), (Keating, 1987). A rule used for HLEM method is that the maximum

¹ requires coil separation control of 0.333% (1m in 300)

detectable depth is one half of the coil separation. From the analytical point of view, even for a very good conductor, the maximum response is not much above background for depths greater than half the coils' separation. Moreover, the small power available for the portable transmitter is also a practical limitation of the extent of penetration (Telford et al., 1990)

1.3 The search For Massive Sulphides

1.3.1 General

An introduction to a discussion on a geophysical technique employed in the search for massive sulphide ores requires a definition of the term massive sulphide. In Lindgren (1933) classification, such a body would be an emanation from an igneous intrusive and would so be a contact metamorphic deposit or an allied vein and hence epigenetic in the truest sense. In the recent past however, field evidence has suggested metamorphism of syngenetic deposits as the origin of some massive sulphide ores (Stanton, 1960; Keating, 1960).

To a geophysicist, the mode of origin of massive sulphides would be less material, more important would be any simple physical attributes that can serve as indicators of their existence. The organisers of the Symposium on Massive Sulphides in Canada published in the Canadian Mining and Metallurgical Bulletin, February and March, 1960 defines a

massive sulphide as a body that consists of one single mass of an extent of at least 1000 square feet and made up of at least 80 percent or more sulphides (Gilbert, 1960). Many of the contributors found it necessary to reduce the ore content to 50 percent in order to include all the bodies that they considered to be massive sulphides. With this lower limit, the minimum density would be about 3800 kg/m^3 as one recognised physical attributes of a massive sulphide ore body. The iron oxides are frequent associates of some of the sulphides and vice versa. From the physical attributes of the individual minerals, one can predict fairly moderate conductivities² for mineral assemblages that include sphalerite and haematite and high magnetic susceptibility for those assemblages that include pyrrhotite and / or magnetite.

The geophysicist would then define a massive sulphide as a very dense, typically very conductive and frequently magnetic occurrence (McKay and Patterson, 1960; Ward, 1958). The Encyclopaedic Dictionary of Exploration Geophysics prepared by the Society of Exploration Geophysicists defines massive sulphide as rocks that are more than 20 percent sulphides by volume (as opposed to disseminated sulphides), which involve electrical phenomena that behave like massive electrical substances.

² For the purpose of describing massive sulphides sphalerite is considered to be poorly conductive.

1.3.2 Choice of Exploration Method

The search for massive sulphides is either done in limited or regional scale. The former is concerned with ground geophysical methods while the latter is solely concerned with airborne methods. Regardless of scale, the prime objective of choosing a method is to secure maximum information at minimum cost and to provide service which is but part of an overall exploration sequence (Ward, 1958; Riley, 1959). As well, the choice of the method will depend on expected depth of occurrence, the geometry of typical occurrences in any given district, etc. Generally certain undeniable patterns which seem to offer the most advantages must be developed. It has generally been established that the high electrical conductivity of massive sulphides is the most readily exploited of the physical properties and so an electrical or an electromagnetic method would be most appropriate (Ward, 1958; McKay and Patterson, 1960). Airborne electromagnetic methods used in conjunction with magnetic methods serve to ascertain the occurrence of massive sulphides which is easily apparent from the coincidence of both anomalies.

1.3.3 Spectral Techniques

Many recent publications (Odegard and Berg, 1965; Rao and Avasthi, 1973; Sharma and Geldard, 1968; Barongo, 1977; Bartel and Becker, 1988, 1990; Murthy and Mishra, 1980; Bhimasankaran et al.,

1977) reveal the growing interest of geophysicists in adopting the technique of frequency transformation as an elegant method of interpretation. The ease with which complicated potential field data can be analysed in the frequency domain makes the approach very useful. In the present development, an interpretive method for the horizontal loop electromagnetic profiling data through Fourier transformation is formulated. In the transform domain, the interpretation of such data is considerably simplified vis a vis conventional techniques.

1.3.4 Extraneous Anomaly Sources

In regional search for massive sulphide ores, many extraneous anomaly sources arise, as exemplified by graphitic zones. These are a source of difficulty in interpretation and should be eliminated cheaply and preferably without drilling. This calls for auxiliary methods such as magnetics which act as secondary tools. Thus, it would be inadequate in most cases to rely on only one method of exploration.

1.3.5 The Importance of Environment

Because of the noted characteristics of massive sulphide deposits, the geophysicist expects to employ various prospecting methods, singly or in sequence, in order to detect and delineate these deposits. The presence of ore

is not guaranteed on the basis of definition only, so it is imperative to study the environment and evaluate case histories. The environmental considerations include, the nature of host rock, especially the composition and fluid permeability, main alteration minerals, structural controls of the deposits and proximity to a related parent rock.

1.4 Review of Current Status of Interpretation Aids In HLEM Prospecting System

The interpretation of electromagnetic anomalies using conventional techniques is basically an exercise of model fitting. The procedure adopted is often to compare observed anomalies with calculated or measured responses of the apparatus and conductivities (Grant and West , 1965). If the anomaly pattern can be satisfactorily matched with one of these theoretical responses , we can then conclude that the appropriate model resembles the geological body in its more important particulars. Discrepancies are bound to occur and their nature gives indication of where these differences lie. A collection of theoretical curves called type curves is used in the direct approach to quantitative interpretation by comparison of one or two specially selected anomaly profiles.

The horizontal loop electromagnetic (HLEM) prospecting system is widely used in prospecting for massive sulphide deposits. It is a horizontal coplanar system with

vertically disposed magnetic dipoles. The interaction of the primary dipole field with a buried conductor generates a secondary magnetic field which consists of an inphase and an out-of-phase (or quadrature) component with respect to the primary field. These two components are measured by the receiver coil as percentages of the primary dipole field. Interpretation of the data obtained therefrom is rather difficult (David, 1966).

The derivation of the theoretical solution of the response of a dipping tabular conductor is rather involving. Wait (1951,1954,1955,1956), Slitcher and Knopoff (1959) gave theoretical solutions for the case of an infinite half-plane of infinite conductance in free space, but later West (1960) showed the inadequacy of this solution in many circumstances. Approximate solutions for a half-plane model of infinite conductance are also known (Wesley, 1958b; Wait, 1959). A numerical solution involving the use of eigenpotentials for a finite, thin plate of finite conductance in free space has been obtained by Annan (1974). Quite recently, Weidelt (1983), obtained an exact solution for an infinite half-plane of finite conductance in free space.

Owing to complexity inherent in deriving theoretical solutions for typical field conditions, scale models have gained popularity. These allow a wide range of conditions to be studied simply, but the reliability of the results is

limited by non-simulation of field conditions. The inphase-quadrature relationship is also important as an interpretative procedure and is harnessed in multifrequency prospecting systems; HLEM inclusive (West, 1960; Dolan, 1960). In case of thin sheet, West(1960) has shown that the most useful response parameter, α , is given by the product, $\sigma\mu\omega t$, where σ is the conductivity in Siemens per metre, μ is the magnetic permeability in Henrys per metre, t is the conductor thickness in metres and ω is the coil separation in metres. A wide range of conditions is achieved in the laboratory modelling by varying frequency and consequently the response parameter for the same body and coil configuration. One disadvantage with laboratory scale modelling is that, inhomogeneities naturally occurring in sulphide deposits cannot be duplicated in the model. However, values of the response parameter that cover the useful prospecting range of naturally occurring massive sulphide deposits are used to mitigate this problem.

In the conventional interpretation of HLEM data over a conductive half-plane target, model curves are constructed at various dip values. The shape of the HLEM anomaly curve depends on the dip of the conductive sheet. Based on the areas under the two shoulders of the curve, it is possible to derive the value of dip. Using a technique developed by Parasnis and Hedstrom (1958), the secondary field is plotted as a complex variable while keeping the ratio of transmitter-receiver separation to depth to the top of the

conductor and the response parameter constant for a given half-plane. A series of parametric curves is obtained for various dips by plotting the maximum anomalies in both the inphase and the quadrature components. Curves are then drawn through these points joining those with the same depth in units of coil separation and equal response parameter. These are known as phasor diagrams. In carrying out interpretation dip is first estimated and the most appropriate curve is referred in order to determine the depth to the top and the response parameter of the conductor.

The use of phasor diagrams and modelled horizontal loop profiles in the interpretation of HLEM data has shown remarkable success as is exemplified by several case histories (Corbet, 1961; Rattew, 1961; Fleming and Brooks, 1960). However, some difficulties and drawbacks are attendant in the use of these methods. Notably, when the response parameter is equal to 100, the quadrature component is only a few percent of the primary field and as such, no useful interpretation of quality can be made. The frequency and coil separation are selected on the basis of the expected depth-to-top. Moreover the preparation of phasor diagrams is slow and tedious. The standard interpretation nomograms for HLEM data are frequently calculated for certain target size and orientation and significant interpretation errors may occur if the parameters of the anomalous target do not match those of the chosen nomograms. This is a very significant

drawback in the space domain interpretation and as indicated by Ferneyhough (1985), the strike and dip of the conductor have a large effect on the correct depth interpretation. To overcome this problem, researchers have resorted to the use of spectral analysis techniques (e.g., Barongo, 1977; Murthy and Mishra, 1980; Barongo, 1985; Bartel and Becker, 1988). Analysis of geophysical field data in the frequency domain is not a new concept in exploration geophysics. Its simplicity has enabled geophysicists to perform useful operations such as vertical derivatives, upward and downward continuation and residuals of potential field data. The method has been used in the interpretation of gravity anomalies (e.g., Odegard and Berg, 1965) and magnetic anomalies (e.g., Murthy and Mishra, 1980) to yield parameters of simple shapes. Its recent extension to EM data interpretation has been due to its simplicity and straightfowardness vis a vis the analysis of numerical model results and phasor diagrams using conventional techniques described heretofore. Virtually all industrial practice relies on nomograms constructed from laboratory scale-model data except one moderately successful attempt to use inversion theory (Keating, 1987).

In the spectral method, profiles obtained in the space domain are converted into the wavenumber domain by means of a Fourier transform (FT) algorithm. The data are now a function of wavenumber with units of inverse distance.

Spectral analysis allows for a direct and an independent interpretation of depth and quality of the anomalous conductor. It is important to realise that here, all the available data along the profile are analysed, unlike most other methods where data from characteristic points only are used. This makes the Fourier transform approach very useful.

The simplest way to approximate the response of a thin, dipping tabular conductor is to simulate it by a line current source at or near the top edge of the conductor. In the horizontal loop prospecting system, both transmitter and receiver coils move in tandem and at right angles across the simulated wire source. Spectral analysis is first applied to the line current response and later extended to numerically generated half-plane model data. Depth and quality of the conductor can reliably be estimated from spectral characteristics of the computed amplitude spectrum. Data taken at different operating frequencies can be used to estimate the conductance of the half-plane. This appears as conductivity-thickness product which is a very useful parameter in characterizing massive sulphides. One important thing to note in this work is that it involves solving of the 'forward problem'. In general the 'forward theory' in contrast to the 'inverse theory' is defined as the process of predicting the results of measurements (predicting data) data on the basis of some general principle or model and a set of specific conditions relevant to the problems at hand

whereas the inverse theory roughly speaking addresses the inverse problem: starting with the data and a general principle or model and then determining the estimates of the model parameters (Williams, 1984). This concept may be summarised as follows:

forward problem:

model parameters \longrightarrow model \longrightarrow prediction of data,

inverse problem:

data \longrightarrow model \longrightarrow estimates of model parameters.

Note that the inverse theory does not provide the model but provides information about the unknown numerical model parameters that go into the model. The forward problem is generally easier to solve than the inverse problem, though, the latter can provide means of assessing the correctness of a given model or discriminating between several possible models.

1.5 Thesis Objectives and Outline

The basic objective of this thesis is to demonstrate the applicability of using Fourier transformation on horizontal loop electromagnetic profiling data over a conducting, dipping half-plane to interpret for depth and quality of the conductor. The study is aimed at searching for massive sulphide deposit whose common natural geometry

of occurrence is a thin tabular conductor with both large strike and depth extents or simply a half-plane. In carrying out Fourier transformation, data from the whole anomaly profile are considered and in the transform domain interpretation is quite simplified in which case the data are now a function of wavenumber.

First, a wire model is chosen to represent the current pattern in the tabular conductor (which is justifiable from electromagnetic point of view) for analytical purposes. Basic analytical expressions are thus derived. In the final analysis data derived from a thin dipping tabular conductor are used. The conductor is presumed to be embedded in non-conducting medium which brings the necessity of addressing the overburden problem common in tropical geological environments.

The thesis hence is aimed at achieving the following:

(a) development of a procedure for interpreting the depth to the top of a thin, dipping, tabular conductor through Fourier transformation.

(b) construction of interpretation nomograms based on amplitude spectrum derived from the Fourier transformation. These can be used to interpret for conductivity thickness-product of the target.

(c) adaptation of the plate program to a microcomputer for thin plate modelling

The thesis is divided into five chapters. The present chapter has introduced the goal of the thesis. It also reviews the current status of interpretation methods and places the thesis in the context of current geophysical technology. Chapter two discusses the entire theoretical background of the research and mainly dwells on Fourier transforms. The plate model is also herein discussed with special regard to its geological justification as representative of massive sulphide orebodies, and its EM response to an oscillating dipole magnetic field. The selection of plate size that approximates a half-plane is also touched.

Chapter three examines the analytic expressions of the derived spectrum and a comprehensive account is given on how useful parameters of the target conductor may be derived from such expressions. The method developed is then tested on synthetic data generated from both the wire and the plate model. A method for constructing interpretation nomograms for conductivity-thickness product is also explained.

Chapter four dwells on the application of the spectral analysis method on field data obtained from the Greenstone Belt western Kenya. Results of analysis and conclusions

that can be drawn from the present study and recommendations are given in chapter five.

Finally a list of relevant references and appendices covering the PLATE program and its theoretical background are given.

CHAPTER TWO

2.1 Basic Theory

2.1.1 Transform Analysis

The present study is based on transform analysis which is related to the Fourier transform. Fourier transforms are examined with respect to the basic properties of transform analysis.

Transform analysis techniques find everyday use from one problem to another, notwithstanding that the term is not a familiar analysis description. For example, the logarithm is infact a transform which we have all used and can be used to demonstrate and solidify the meaning of transform analysis. We can solve a simple problem such as determining the quotient, $Y = X/Z$, by conventional and transform analysis procedures. Conventional analysis implies that we must determine Y , by long hand division which represents a time consuming and complex process. However, there is a simpler and less tedious alternative none other than transform analysis procedure. The first step is to convert or transform the problem statement. For the example problem, we choose the logarithm to transform division to subtraction operation. Owing to this simplification, transform analysis then requires a table look up of $\log(X)$ and $\log(Z)$, and a subtraction

operation to determine $\log(Y)$. We next find the inverse transform (anti-logarithm) of $\log(Y)$ by table look-up and complete the problem solution. We note that, by using transform analysis techniques, we have reduced the problem complexity of this example we have considered. Figure 2-1 illustrates this basic operation.

In general, transform analysis often results in simplified problem solving analysis. One such transform analysis technique is the Fourier transform. This transform has been found to be especially useful for problem simplification in many fields of scientific endeavours (Brigham, 1974).

2.1.2 Basic Fourier Transform Analysis

The logarithm transform considered previously is easily understood because of its single dimensionality; that is the logarithm function transforms a single value X into a single value $\log(X)$. The Fourier transform is not as easily interpreted because we must now consider functions defined from $-\infty$ to $+\infty$. Hence contrasted to logarithm, we must now transform a function of another variable, also defined from $-\infty$ to $+\infty$.

A straight forward interpretation of the Fourier transform is illustrated in Figure 2-2. As shown the

CONVENTIONAL ANALYSIS

TRANSFORM ANALYSIS

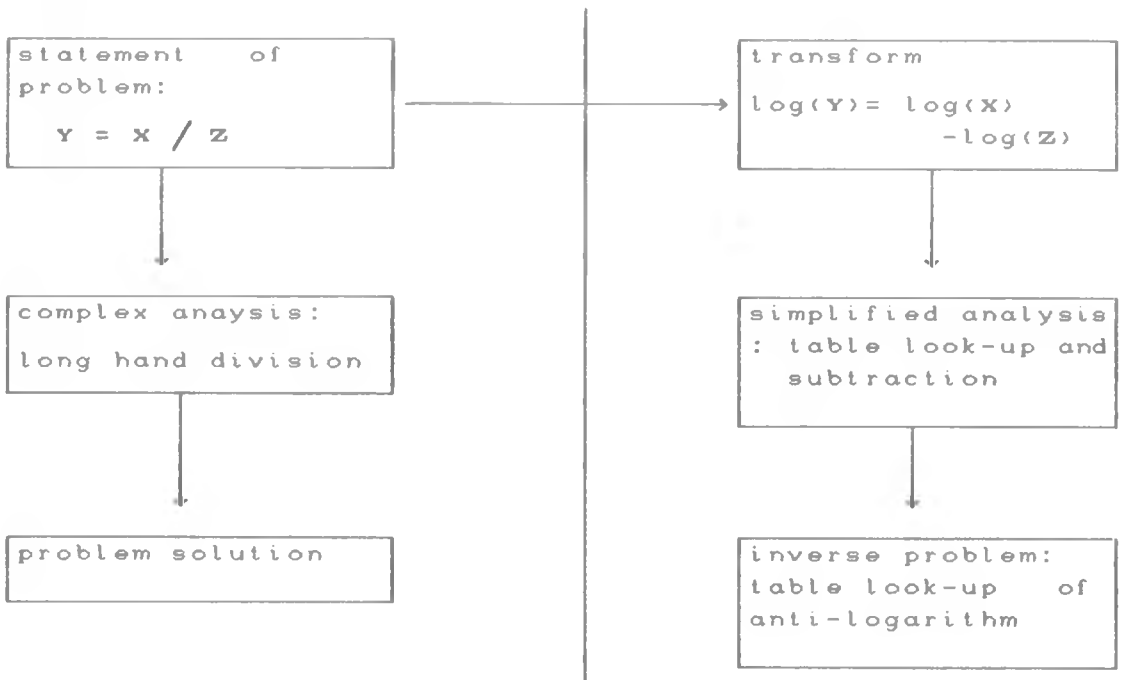


Figure 2-1. Flow diagram of conventional and transform analysis (after Brigham, 1974).

essence of the Fourier transform of a waveform is to decompose or separate the waveform into a sum of sinusoids of different frequencies. If these sinusoids sum to the original waveform, then we have determined the Fourier transform of the waveform. The pictorial representation of the Fourier transform is a diagram which displays the amplitude and frequency of each determined sinusoid (Figure 2-2).

The quantitative and qualitative investigation of a single signal is called single variant analysis. If the study relates time domain and frequency domain behaviour together, the study is called single variant spectral analysis (Taylor et al., 1976). Here, the time and frequency properties of a signal are interrelated mathematically. Through Fourier transformation, information about the periodic and the aperiodic character of the signal can be obtained. Fourier transforms can be used to investigate the frequency domain properties of a time domain signal. Inverse Fourier transform generates a time domain image of a signal characterized in the frequency domain. The signal mentioned above can be some geophysical variable whose behaviour is deterministic (or can be predicted).

The decomposition of an arbitrary function waveform into sinusoidal components has been known and used by the technical community for over a century. Using transform methods, tremendous breakthroughs have been

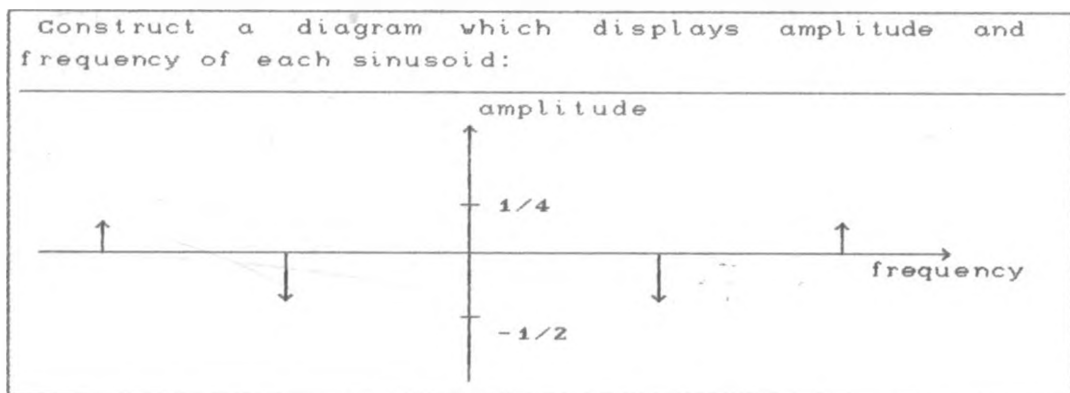
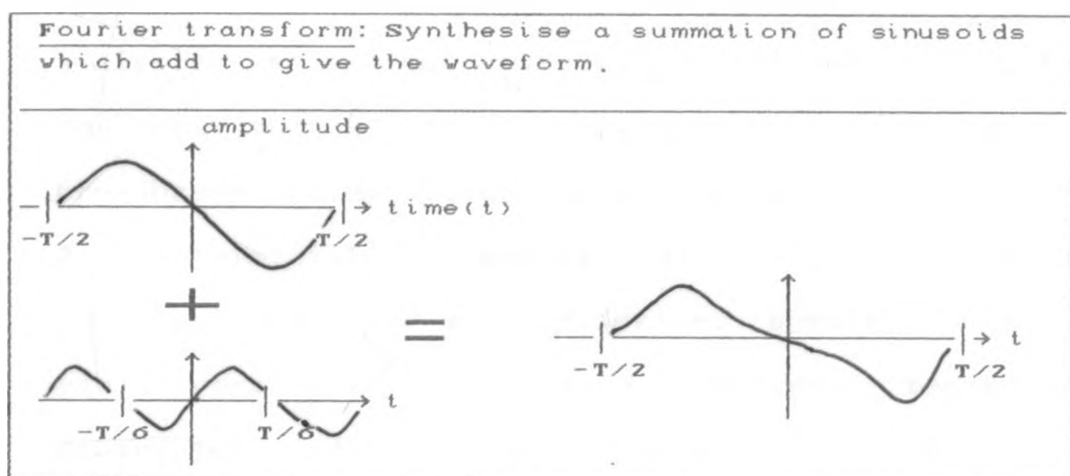
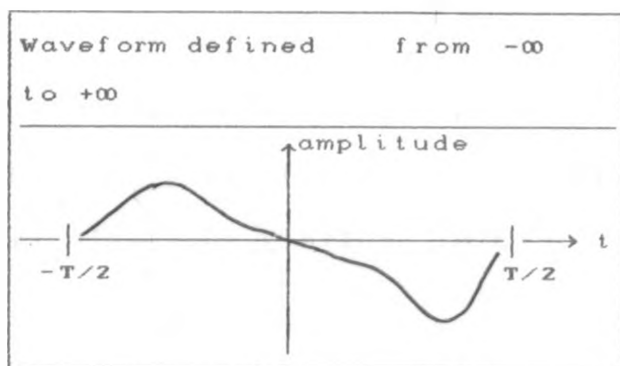


Fig. 2-2 Interpretation of the Fourier Transform
(after Brigham, 1974).

made in the study of linear systems and random processes among others. The advent of computers and the development of efficient standard algorithms have considerably increased the speed of performing numerical Fourier transforms for instance, the Cooley-Tukey FFT algorithm (Taylor, 1976).

Even though a time series signal record may not contain truly periodic components, the methods of spectral analysis can provide extremely valuable insights into the behaviour of the causal process of the signal. This broadbased concept forms the mainstay of this research. A deterministic geophysical variable will be Fourier-transformed and the derived spectrum analysed to yield parameters of prime interest regarding the geophysical body on which the derivation of the variable is based. (In the present analysis, the signal employed is recorded in spatial domain, hence in the frequency domain, frequency will be referred to as cycles per unit distance and the period in distance units. Infact, it makes it easy to visualise the analysis without loss of generality)

The data representing most geophysical phenomena can be regarded as deterministic in that they can be represented by an explicit mathematical relationship (Bendat et al., 1971). Deterministic data can be subdivided into periodic and complex periodic data. Most geophysical data fall in the latter category which can be defined by a

waveform repetitive at regular intervals so that :

$$f(t) = f(t + nT_p) \quad (2.1)$$

$$n = 1, 2, 3, \dots$$

We define a fundamental period T_p or the basic interval required for one full oscillation and consequently a fundamental frequency f_1 , in cycles per unit time. With few exceptions in practice, complex periodic data are capable of expansion into Fourier series according to the following formulae :

$$f(x) = a_0/2 + \sum_{n=1}^{\infty} a_n \cos(n\omega) + b_n \sin(n\omega) \quad (2.2)$$

$$\text{where: } \omega = 2\pi f_1$$

$$a_n = 1/T \int_0^T f(t) \cos(n\omega) dt$$

$$b_n = 1/T \int_0^T f(t) \sin(n\omega) dt$$

$$n = 0, 1, 2, 3, \dots$$

An alternative way to express the Fourier series for complex periodic data is as follows:

$$f(t) = X_0 + \sum_{n=1}^{\infty} X_n \cos(2\pi f_1 t - \theta_n) , \quad (2.3)$$

where:

$$X_0 = a_0 / 2 ,$$

$$X_n = \sqrt{a_n^2 + b_n^2} ,$$

$$\theta_n = \tan^{-1}(b_n / a_n) ,$$

$$n=1,2,3,\dots$$

The above equation (2.3) simply means that, complex periodic data consist of a static component X_0 and an infinite number of sinusoidal components called harmonics of amplitudes X_n and phases θ_n . The frequencies of the harmonic components are all integral multiples of the fundamental frequency f_1 . The above expression (equation 2.3) can be characterised by a discrete spectrum which is an expression of the variation of the amplitude with frequency.

2.1.3 The Fourier Integral

The Fourier integral is defined by the expression :

$$H(f) = \int_{-\infty}^{\infty} h(t) \exp(-i2\pi ft) dt \quad (2.4)$$

If the integral exists for every value of the parameter, f , then equation (2.4) defines $H(f)$, the Fourier transform of $h(t)$. Typically, $h(t)$ is termed a function of the variable time and $H(f)$ is termed a function of the variable frequency. The general Fourier transform is a complex quantity such that:

$$H(f) = R(f) + iI(f) = |H(f)| \exp(j\theta f), \quad (2.5)$$

where:

$R(f)$ is the real part of the Fourier transform,

$I(f)$ is the imaginary part of the Fourier transform,

$|H(f)|$ is the amplitude or the Fourier spectrum of $h(t)$ and is given by $[R^2(f) + I^2(f)]^{1/2}$

$\theta(f)$ is the phase angle of the Fourier transform and is given by $\tan^{-1}[I(f)/R(f)]$.

2.1.4 The Inverse Fourier Transform

The inverse Fourier transform is defined as:

$$h(t) = \int_{-\infty}^{\infty} H(f)\exp(i2\pi ft)df \quad (2.6)$$

Inverse transformation allows the determination of a function of time from its Fourier transform. If the function $h(t)$ and $H(f)$ are related by equations (2.4) and (2.6), the two functions are termed as a Fourier transform pair.

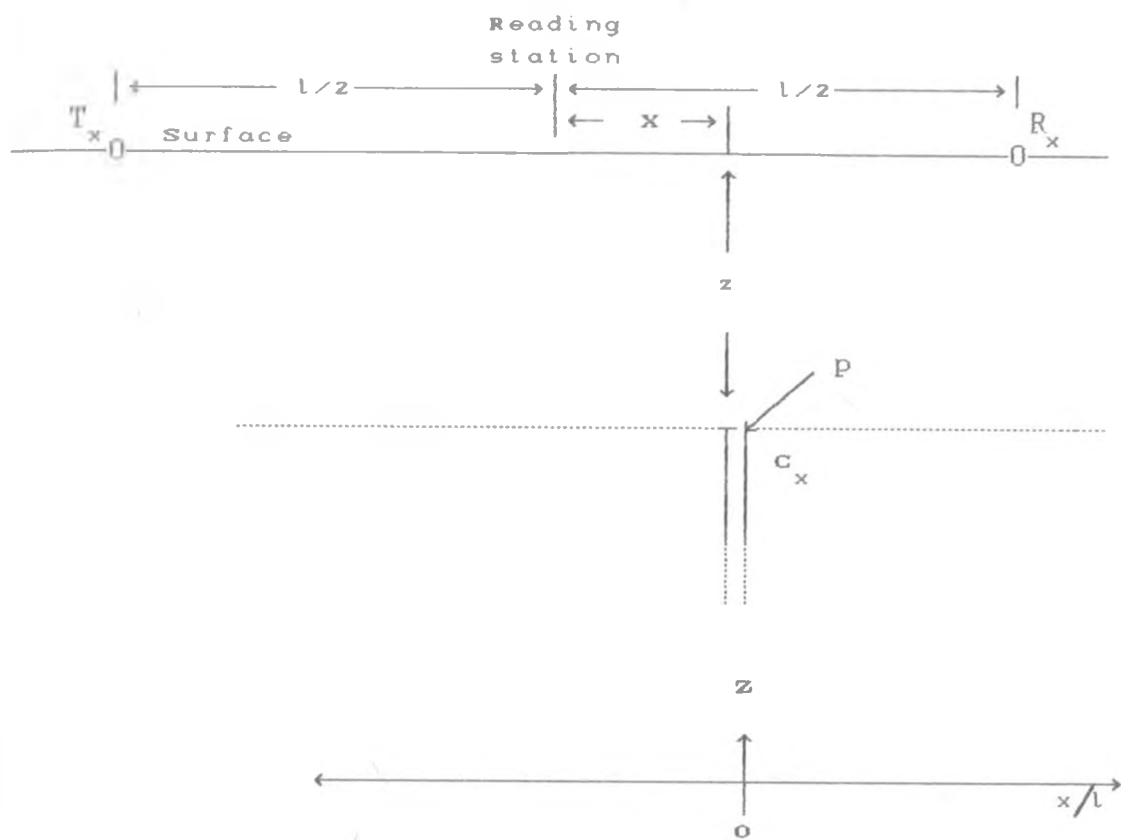
2.2 The line Current Target

A very simple and common configuration for conductive massive sulphide ore zones is a thin sheet, long in one horizontal dimension and extending to a great depth (Telford et. al., 1990). As suggested by Keller and Frischknecht (1966), the simplest approximation to the eddy current distribution in a tabular conductor is a long filament of current of given strength that coincides with the upper edge of the thin plate conductor in the vicinity of a dipole field. The HLEM prospecting system utilises the principle of induction and in the present research, it is used as a two loop profiling system of which there are various configurations. In induction methods, a small current loop is used as a source and a

similar receiver loop is employed. If the separation between the source and the receiver loop is more than five times the diameter of either loop, both loops may mathematically be treated as dipoles (Wait, 1954). The concept of mutual coupling is used when dealing with two loop systems (Keller and Frischknecht, 1966). Of the various two loop configurations used in geophysical prospecting, the mathematical development is essentially the same. In the HLEM prospecting system, we deal with the vertical magnetic moments of the transmitted and the measured dipole fields. The circuit analogy for the equivalent current axis in this system is easily worked out using the geometry shown in Figure 2-3. The above geometry accounts for mutual inductance between the current axis and a small current loop given by (Telford et. al. 1990):

$$M = \frac{0.02a^2(l/2 + x)}{(z^2 + (l/2+x)^2)} \quad (2.7)$$

and the vertical component of the secondary magnetic field at the receiver becomes:



Explanation of symbols:

T_x : Transmitter coil.

C_x : Half-plane conductor.

R_x : Receiver coil.

z : Depth to the top of conductor.

l : Coil separation.

x : distance between the midpoint of coils and the point directly above the conductor on the surface.

P : Position of current filament (marked by an arrow)

Figure 2-3. HLEM system over a conductive half-plane simulated by a line current model

$$H_z^S = \frac{-0.01a^2 ip(l^2/4-x^2)}{\beta L(z^2+(l/2-x)^2)(z^2+(l/2+x)^2)} \quad (2.8)$$

while the directly coupled component becomes:

$$H_z^P = \frac{-i_p a^2}{4l^3} \quad (2.9)$$

In this system we measure the ratio H_z^S / H_z^P . Putting $\alpha = x/l$ and simplifying the expression we get:

$$\frac{H_z^S}{H_z^P} = \frac{(4\alpha^2 - 1)}{6.25\beta L/l \{4z^2/l^2 + (1+2\alpha^2)\} \{4z^2/l^2 + (1-2\alpha^2)\}}, \quad (2.10)$$

where:

$$\beta = (1+1/Q^2)^{1/2}$$

$$Q = R/\omega L$$

ω = operating frequency in radians per second

R = resistance of the simulated current axis

L = self inductance of the simulated current axis

This final expression represents the HLEM response

over a conducting half plane that is simulated by a current axis which forms the fundamental model in this study.

2.3 The Plate Model

2.3.1 General

The program PLATE (Dyck et al., 1980) which is based on a development by Annan (1974) is a powerful algorithm that is highly versatile and is capable of simulating most commercial EM systems. The current work is solely concerned with solving the forward problem and makes extensive use of the plate model.

A very common and simple configuration of naturally occurring massive sulphides is a thin vertical/dipping sheet. This makes the PLATE program ideal as a modelling tool in the search for massive sulphides. The common natural geometry of occurrence of massive sulphides has been geologically justified by a study carried out by Avarantchev (1980) on a list of deposits of north-western Quebec. This study covers the Quebec part of the Abitibi greenstone belt. Out of a total of 2000 deposits, 307 had an unknown shape, and 92% of the rest had a shape that can be modelled approximately by a plate or half-plane. This justification from geological and geophysical points of view forms a firm basis for analysis aimed at searching for massive sulphides using

the plate model. It will be noticed that a line current target is first used to approximate the behaviour of a thin plate conductor and forms the working basis of this study. This is only for analytical purposes, in as much as, the PLATE program is used to generate the response of the more realistic dipping plate model in the final analysis.

2.3.2 Numerical Development of the Plate Model

The inductive response of a rectangular thin plate in free space was solved by Lamontagne and West (1971). They solved Maxwell's equations by using the finite-difference method. Annan (1974), though with a substantially different approach, devised a numerical procedure for determining the EM response of a dipping rectangular thin plate conductor for any of the various types of EM sources though the basic idea remained the same notwithstanding. The inductive response of a thin rectangular plate conductor is done numerically since, an analytical solution is difficult to implement. Wesley (1958) derived the response of a vertical infinitely conducting half-plane and lately Weidelt (1983) has published a solution for the EM response of a dipping half-plane with finite conductance. It hence logically follows that the response calculated using the PLATE program should approximate this latter model.

In Annan's method, the secondary field of a thin plate excited by an EM primary source is considered as being

generated by a set of equivalent sources distributed on the surface of the plate. Annan (1974) has applied this concept to a number of problems.

The application of the equivalent source method reduces the problem of an inductively thin plate to a surface integral equation in terms of unknown surface currents and a known source field. The solution is obtained by a standard finite element technique: the Galerkin method. This results in a set of linear equations that are solved in terms of a weighted eigenvalue problem. The solution is a set of eigenpotentials which are equivalent to a set of non-interacting current loops the sum of which represents the induced current system on the plate. Finding the set of eigencurrents is complicated, but need be done only once for a plate of given aspect ratio (width to strike length ratio), on which the eigenpotentials solely depend. After this, only 10-20 coefficients in the eigencurrent summation are required for description of most induced current systems on the thin plate model. Thus, for a wide range of likely practical cases the eigenpotentials are generated, stored and conveniently used during modelling. Notably, this makes it easy to adapt the PLATE program to a microcomputer by ignoring the intermediate subroutines that evaluate the eigenpotentials thereby consuming considerable amounts of RAM memory. Instead, eigenpotential files are referenced thus eliminating large sections of the program. Also the eigenpotentials and other

parameters can be calculated separately by means of modular programming on a microcomputer. This mode of programming has been implemented in the present study where modules capable of running on an IBM PS/2, Model 30 with a DOS limited RAM of 640 K, have been developed to compute all the parameters of the plate model before the final response is synthesised. This is discussed in the documentation of the programs used in this work (not included in this thesis).

Another convenience of Annan's method is that, each eigencurrent has exactly a frequency response like a simple loop circuit, hence it is quite easy to calculate responses for a broad spectrum of frequencies or time domain EM systems. Figure 2-4 shows a map of a set of eigencurrents for a plate of aspect ratio of 1x2 (Dyck et al., 1980).

2.3.3 Computational Structure

There are four main steps in Annan's procedure (Annan, 1974), viz:

1. The eigencurrents are first prepared. This requires only the aspect ratio of the plate.
2. The coupling between the EM source and the plate must then be calculated. This is done by finding the normal component of the transmitter's magnetic field on a grid

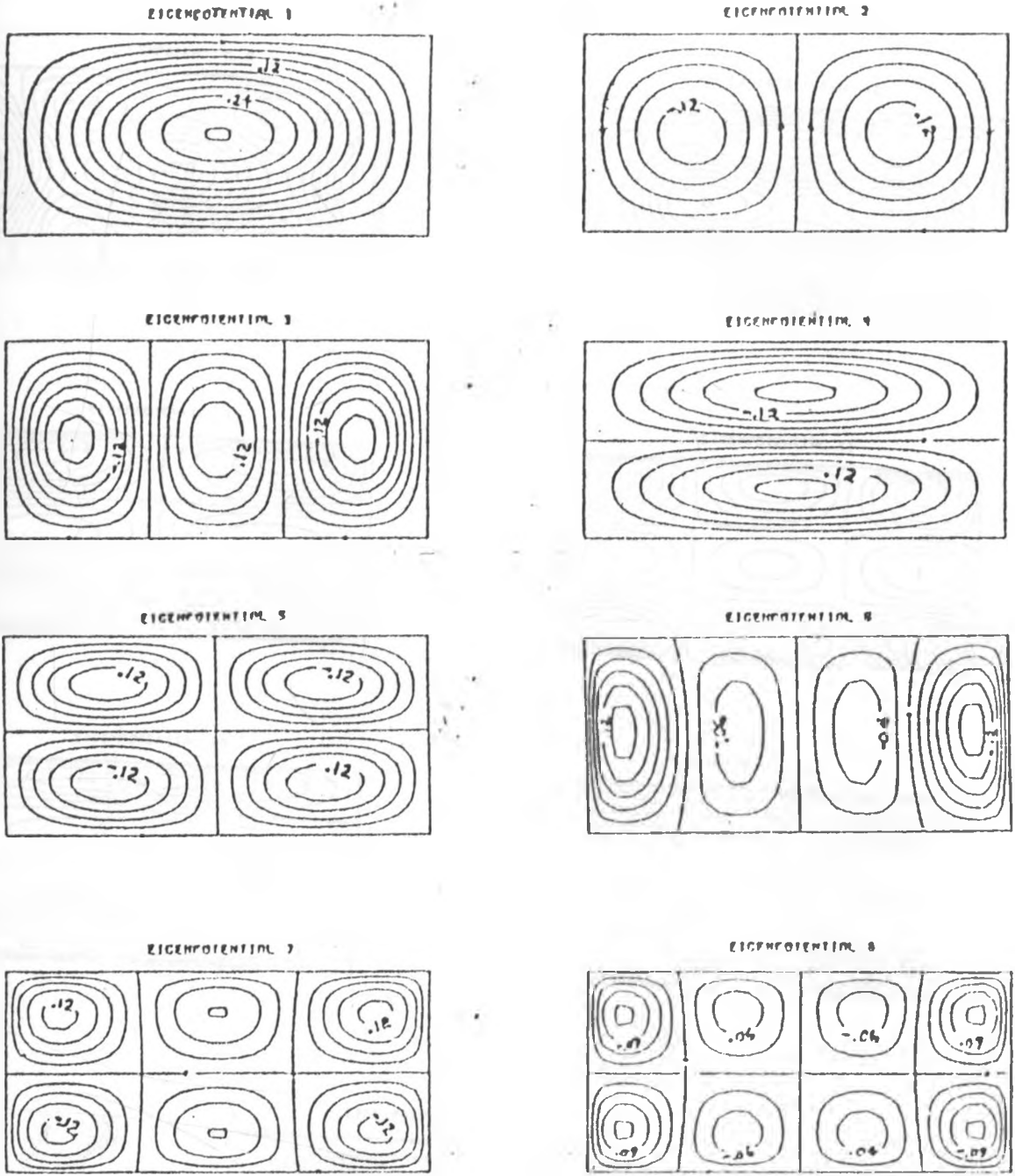
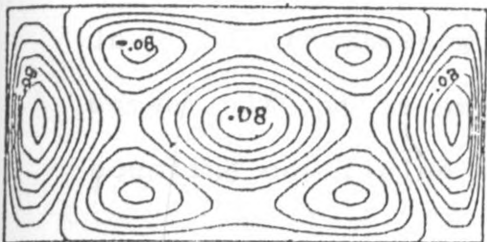
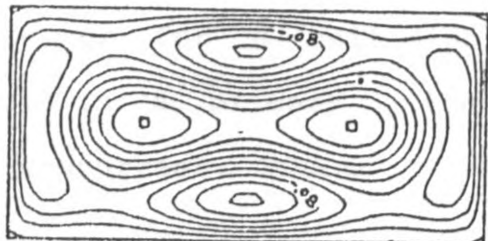


Fig 2-4 Eigencurrents (contours of eigenpotentials) for a 1x2 plate and 15 degrees of freedom (polynomials of order 4) (After Dyck, 1980)

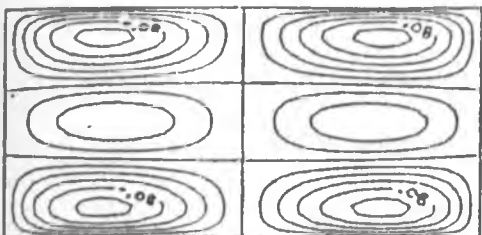
EIGENPOTENTIAL 9



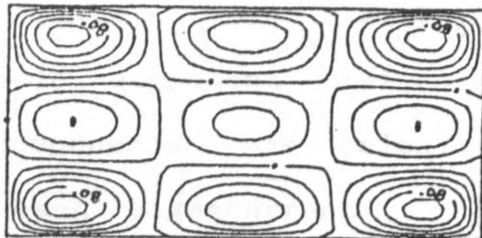
EIGENPOTENTIAL 10



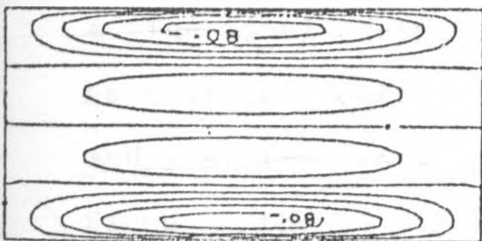
EIGENPOTENTIAL 11



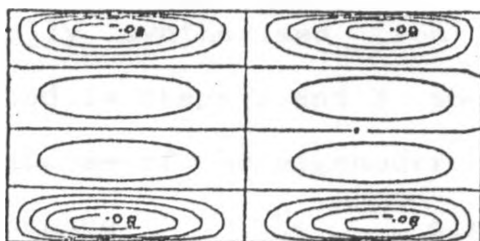
EIGENPOTENTIAL 12



EIGENPOTENTIAL 13



EIGENPOTENTIAL 14



EIGENPOTENTIAL 15

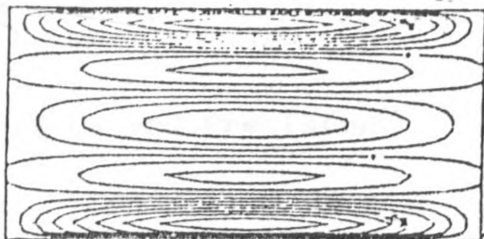


Fig 2-4 cont'd

of points on the plate, and then performing numerical integrations of the field and the eigenfunctions. The field is calculated for a unit current in the transmitter loop if the transmitter is large, or for a unit dipole moment if it is small. The result is a primary field coupling coefficients for each eigencurrent.

3. The coupling between the EM receiver and the plate is computed. This is done by subdividing each eigencurrent into current elements each with a corresponding magnetic field component at the receiver. The magnetic field components are calculated and summed up (integrated) for each eigencurrent, thus giving a set of secondary field coefficients.

4. The final response is finally synthesised from the geometrical coefficients generated in steps 2 and 3 above, and the frequency or time response of the eigencurrents. Since the eigencurrents behave like simple non-interacting loop circuits, this calculation is easily redone for different plate conductances and frequencies.

2.3.4 Limitations and Precision

In reasonably favourable situations, Annan's method is capable of computing responses to about the same accuracy as physical scale model measurements. Errors may arise in two ways: 1) through having insufficient number of

eigencurrents to represent the actual induced current system in the plate, and 2) in numerical integrations that compute the coupling between the receiver, the transmitter and the various eigencurrents. In fact, the present version of the plate program does not allow the user any control over the integration parameters, for instance, a finer subdivision of the integration interval to increase the accuracy of the results.

For tightly coupled circuits or, in other words, if the plate is very large and the EM system is very close to a part of it so that appreciable induction occurs only in a very small part of the conductor, then very high order eigencurrents would be required to describe the induction properly. The program is limited to only 15 eigencurrents, which is the chief limitation of this system. As was noted in this study, the program PLATE breaks down when responses for shallow depths of about 10 metres and a plate length of 1200 metres were attempted at moderately high conductivities(about 50 S). As a rough guide the program fails when: $W.S/[x_1 . x_2] > 100$ where; W is plate width, S is strike length of the plate, x_1 is distance of the receiver to the closest part of the plate, x_2 is distance of the transmitter to the closest part of the plate.

In the present study the half plane is simulated by line current axis located at or near the top edge and the edge effects of the current flow cannot be ignored.

Moreover, we do not expect all the currents to be absolutely confined to the top edge. The sum total of these effects is to displace the position of the current axis towards the centre of a given plate size. This introduces a systematic error whose management is beyond the scope of the present work.

2.3.5 The Half-plane approximation

The choice of a plate model that effectively approximates a half-plane is based on important conclusions arrived at by Keating (1987). A criterion used to determine the plate size that can be considered infinite is that the maximum amplitude of the response stabilises with increasing plate size (Palacky, 1975). The choice of the size made a function of expected conductance of a particular target. It need only be about 600 metres when the conductance is 20 or 50 S, which is a commonly used length to model a half-plane. If low conductance is expected, a larger strike length of the order 900m should be used. As noted earlier in the preceding section, the plate size can influence the minimum detectable depth. This is more so for ground EM systems whose geometries are smaller compared to airborne systems. In this study a strike length of 900m is used to generate interpretation nomograms for conductance. This plate size

allows the response of depths as low as 30m to be determined. The preference of this plate size (though too big for correct determination of depth from slope of the amplitude spectrum for reasons to be discussed later) is ideal for conductance interpretation nomograms. However, for purposes of demonstrating the effectiveness of determining the estimate of depth from the slope of the amplitude spectrum, a plate strike length of 600m was used. The selection of this plate size (300x600) was based on a study carried out in which the conductivity-thickness product*, depth, and frequency were kept constant while the strike length was varied between 300 and 900 metres. Both the EM response and the corresponding spectrum were computed for each plate size using a frequency of 888Hz, a conductivity-thickness product of 50S and a depth of 20 metres throughout. Depth was henceforth estimated from the slope of the amplitude spectrum. The percentage error was also recorded. Table 2.1 shows the results of this test from which it can be noted that the estimated depths are always in excess of the correct depths. The percentage error minimises at a strike length of 600 metres. This strike length was hence used to show the validity of estimating depth from the slope of the amplitude spectra.

*conductivity-thickness product or conductance is given here since conductivity alone cannot be determined for the plate model.

Table 2.1 Strike length of the plate model and the corresponding percentage error in the depths estimated from the slope of the amplitude spectrum.

Strike length (m)	%error
300	26.20
400	23.41
500	23.28
600	21.39
700	23.53
800	23.12
900	24.90

2.4 Fourier Transform of The Line Current Target Response

The usefulness of spectral analysis for HLEM data interpretation can be seen by first considering the Fourier transform of the elementary analytical expression which represents the approximate behaviour of a more realistic model which will later be examined numerically. The conventional definition of the Fourier transform is given by (Bartel and Becker 1990):

$$F(k_x) = \int_{-\infty}^{\infty} f(x) \exp(ik_x x) dx \quad (2.11)$$

Using a right handed cartesian system of co-ordinates in two dimensions, the x-coordinate is taken along the traverse path, assumed to be perpendicular to the strike of the target and lying directly above the centre.

The secondary magnetic field as a function of x is thus transformed into a function of the angular wavenumber k_x ($= [2\pi n / 2L]$, $n = 0, 1, 2, \dots$) which has units of radians per kilometre. L is the half-range of the anomaly profile. In deriving the Fourier transforms, we have two cases to consider, viz; the continuous Fourier transform (CFT) and the discrete Fourier transform (DFT). Although they are conceptually similar, their derivation are different and they hence will be considered

separately. Infact, the DFT arises from the CFT by a suitable limiting process.

2.4.1 The Continuous Fourier Transform

As derived earlier, the expression for the ratio of the primary to the secondary magnetic fields after interaction with a subsurficial conductor is given by equation (2.10) (see also Telford et al.,1990).

The quantity Q is the response parameter. To simplify the analysis, we define a quantity C ($= 1/6.25\beta L$) so that after eliminating α , equation (2.5) becomes:

$$H_z^S / H_z^P = C f(x) , \quad (2.12)$$

where:

$$f(x) = \frac{l^2(4x^2 - l^2)}{\{4z^2 + (1-2x)^2\}\{4z^2 + (1+2x)^2\}}$$

The CFT of equation (2.12) is given by:

$$F(k_x) = C \int_{-\infty}^{\infty} f(x) \exp(-ik_x x) dx, \quad (2.13)$$

Here, $F(k_x)$ is the description of $f(x)$ in the frequency domain or wavenumber domain. To obtain a complex transform we employ the residue theorem of complex variable analysis. The integrand of equation (2.13) can be written as:

$$f(x) \exp(-ik_x x) = pq \quad (2.14)$$

where:

$$p = \frac{2x + 1}{4z^2 - (1-2x)^2}$$

$$q = \frac{(2x - 1)l^2 \exp(-ik_x x)}{4z^2 - (1+2x)^2}$$

The above equation (2.14) satisfies Dirichlet conditions except at the simple poles $x = iz + 1/2, -iz + 1/2$

and $x = iz - l/2, -iz - l/2$, where $i = (-1)^{1/2}$. The HLEM configuration allows us to make reference to the lower half of the complex plane (Figure 2-5) where the relevant poles in solving equation (2.13) are shown. We notice that these are simple poles and consequently the evaluation of the residues is of particular simplicity since in general:

$$\text{Res}\{f(z), a\} = \lim_{z \rightarrow a} f(z)(z-a) = a_{-1} \quad (2.15)$$

where the residue a_{-1} is evaluated at the pole $z = a$. The residue at $x = -iz + l/2$ hence becomes:

$$\text{Res}\{f(x), -iz + l/2\} = \frac{l(l-iz)\exp(ik_x l/2) \exp(-k_x z)}{8(l - 2iz)} \quad (2.16)$$

and similarly the residue at $x = -iz - l/2$ is given by:

$$\text{Res}\{f(x), -iz - l/2\} = \frac{-l(l-iz)\exp(ik_x l/2)\exp(-k_x z)}{8(l + 2iz)} \quad (2.17)$$

The reference plane consists of a closed contour; a semicircle C' and a radius R (where $R > 0$).

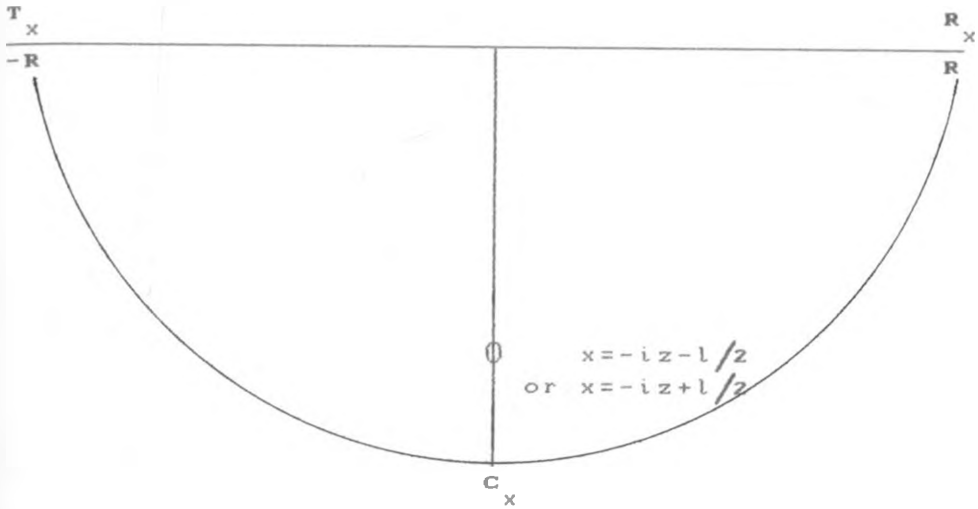


Fig. 2-5 Semicomplex plane showing the singularity of the integrand in equation 2.13

Integrating counterclockwise around the contour $R_x T_x C_x R_x$ and using the residue theorem we obtain:

$$\int_{C'} f(x) dx - \int_{-R}^R f(x) dx = 2\pi i \{\text{sum of residues}\}$$

hence:

$$C \left\{ \int_{C'} f(x) \exp(-ik_x x) dx - \int_{-R}^R f(x) \exp(-ik_x x) dx \right\} = 2\pi i \{\text{sum of residues}\}$$

In the limit as $R \rightarrow \infty$, the first integral vanishes so that we have:

$$F(k_x) = C \int_{-\infty}^{\infty} f(x) \exp(-ik_x x) dx$$

$$= -2\pi i (A e^{-ik_x l/2} + B e^{ik_x l/2}) e^{-k_x z} \quad (2.18)$$

where:

$$A = \frac{1(1-iz)}{8(1-2iz)},$$

$$B = \frac{-1(1-iz)}{8(1-2iz)}$$

In order to obtain a complete expression for the spectrum , it is necessary to separate the function $F(k_x)$ into its real and imaginary parts. Complex numbers A and B can easily be reduced by rationalisation so that:

$$A = a + ib, \tag{2.19}$$

where:

$$a = \frac{1(1^2+2z^2)}{8(1^2+4z^2)}$$

and:

$$b = \frac{zl^2}{8(1^2+4z^2)}$$

Similarly:

$$B = c + id, \tag{2.20}$$

where:

$$c = \frac{-l(l^2 + 2z^2)}{8(l^2 - 4z^2)}$$

and:

$$d = \frac{zl^2}{8l(l^2 + 4z^2)}$$

From Euler's identities, one derives the expressions:

$$\left. \begin{aligned} \exp(ik_x l/2) &= \cos(k_x l/2) + i \sin(k_x l/2) \\ \exp(-ik_x l/2) &= \cos(k_x l/2) - i \sin(k_x l/2) \end{aligned} \right\} \quad (2.21)$$

Substituting equations (2.19) and (2.20) and equations(2.21) into equation (2.18) and using the fact that $i^2 = -1$, then simplifying, we obtain:

$$F(k_x) = 2\pi C (e + if) \exp(-k_x z) \quad , \quad (2.22)$$

where:

$$e = \operatorname{Re}\{F(k_x)\} = b \cos(k_x l/2) + c \sin(k_x l/2) + d \cos(k_x l/2) - a \sin(k_x l/2)$$

and:

$$f = \operatorname{Im}\{F(k_x)\} = d \sin(k_x l/2) - a \cos(k_x l/2) - b \sin(k_x l/2) - c \cos(k_x l/2) .$$

Here "Re" and "Im" mean real part and imaginary part of, respectively. Substituting the values of a, b, c and d into equation(2.22) the real part becomes:

$$\operatorname{Re}\{F(k_x)\} = \frac{z l^2 \cos(k_x l/2) - (l^2 + 2z^2 l) \sin(k_x l/2)}{4l^2 + 16z^2} \quad (2.23)$$

Similarly:

$$\operatorname{Im}\{F(k_x)\} = \frac{\left[(l^3 + 2z^2 l) \cos(k_x l/2) - z l^2 \sin(k_x l/2) - (l^3 + 2z^2 l) \cos(k_x l/2) + z l^2 \sin(k_x l/2) \right]}{4l^2 + 16z^2}$$

or:

$$\operatorname{Im}\{F(k_x)\} = 0 . \quad (2.24)$$

Thus, the spectrum of f(x) becomes highly simplified to the real part only. The final expression for the spectrum can now be written:

$$F(k_x) = 2\pi C A_0(k_x) \exp(-k_x z) , \quad (2.25)$$

where:

$$A_o(k_x) = \frac{zl^2 \cos(k_x l/2) - (l^3 + 2z^2 l) \sin(k_x l/2)}{4(l^2 + 4z^2)}$$

which is the continuous Fourier transform (CFT) of the line current response function $f(x)$.

2.4.2 The Discrete Fourier Transform

The continuous Fourier transform (CFT) of the preceding section converts a class of spatial domain signals into the frequency domain. The spectrum of $f(x)$ or simply $F(k_x)$ is the description of $f(x)$ in the frequency domain. $F(k_x)$ is characterised by a complex number representing phase and magnitude. A special case of the Fourier transform is the Fourier series (FS). If $f(x)$ is periodic over some interval, say $(-L,+L)$, it is possible to express the frequency domain behaviour of $f(x)$ as a discrete rather than a continuous series. When the response function of an equivalent current axis model is resolved into its real and imaginary components, the discrete cosine transform of the even component gives the real component of the Fourier transform of $f(x)$, while the discrete sine transform of the odd component gives the imaginary component of the Fourier transform of $f(x)$. The resolution of the function $f(x)$ makes use of the following formulae:

$$\begin{aligned} f_e(x) &= 1/2[f(x)+f(-x)] \\ f_o(x) &= 1/2[f(x)-f(-x)] \end{aligned} \tag{2.26}$$

where:

$f_e(x)$ = the even component of $f(x)$
 $f_o(x)$ = the odd component of $f(x)$

We can also determine if a function is odd or even. Thus, a function is even if $f(x) = f(-x)$ and odd if $f(x) = -f(-x)$. If neither of the above conditions holds, then the formulae in equations(2.26) should be used to calculate both the components.

Assuming that $f(x)$ is periodic with period $2L$ and satisfies Dirichlet conditions, that is, the function is piece-wise continuous and integrable over any interval, then its real Fourier series is given by:

$$f(x) = a_0 / 2 + \sum_{n=1}^{\infty} \left[a_n \cos(k_x x) + b_n \sin(k_x x) \right], \tag{2.27}$$

where:

$$k_x = \pi n/L ,$$

$$a_0/2 = 1/2L \int_0^L f(x)dx \quad \text{or} \quad a_0 = 1/L \int_0^L f(x)dx ,$$

$$a_n = 1/L \int_0^L f(x)\cos(k_x x)dx ,$$

$$b_n = 1/L \int_0^L f(x)\sin(k_x x)dx .$$

We can easily arrive at the complex Fourier series by using the Euler identities (see equation(2.21)). From such, one derives the relations :

$$\cos(x) = 1/2 [\exp(ix)+\exp(-ix)] ,$$

$$\sin(x) = 1/2 [\exp(ix)-\exp(-ix)] .$$

Substituting these in equation(2.27), we arrive at the complex Fourier series:

$$f(x) = a_0/2 + \sum_{n=1}^{\infty} \left[\frac{1}{2} (a_n - ib_n)\exp(ik_x x) + \frac{1}{2} (a_n + ib_n)\exp(-ik_x x) \right] . \quad (2.28)$$

If we define c_n as:

$$c_n = (a_n - ib_n)/2 = 1/2L \int_{-L}^L f(x) \{ \cos(k_x x) - i \sin(k_x x) \} dx$$

$$= 1/2L \int_{-L}^L f(x) \exp(-ik_x x) dx \quad (2.29)$$

and c_{-n} as:

$$c_{-n} = (a_n + ib_n)/2 = \int_{-L}^L f(x) \{ \cos(k_x x) + i \sin(k_x x) \} dx$$

$$= 1/2L \int_{-L}^L f(x) \exp(ik_x x) dx, \quad (2.30)$$

the complex Fourier series then becomes:

$$f(x) = a_0/2 + 1/2 \sum_{n=1}^{\infty} \left[c_n \exp(ik_x x) + c_{-n} \exp(-ik_x x) \right]. \quad (2.31)$$

We note that $a_n + ib_n$ is a complex conjugate of c_n and it can easily be shown that $c_n^* = c_{-n}$ (where c_n^* is a complex conjugate of c_n). The integral in equation (2.29) gives $1/2a_0$ when $n = 0$; when $n > 0$ the integral equals $1/2(a_n - ib_n)$ and when $n < 0$, it equals $1/2(a_{-n} + ib_{-n})$. Thus the complex Fourier series in equation(2.28) can be written in a concise statement :

$$f(x) = \sum_{n=-\infty}^{\infty} c_n \exp(-ik_x x),$$

where:

$$c_n = 1/2L \int_{-L}^L f(x) \exp(-ik_x x) dx \quad (2.32)$$

This is true whenever the series converges to $f(x)$.

The set of coefficients c_n is the Fourier spectrum or simply the spectrum of $f(x)$. If the finite sub-interval $2L$ is large enough, we have:

$$\begin{aligned} c_n &= 1/2L \int_{-\infty}^{\infty} f(x) \exp(-ik_x x) dx \\ &= 1/2L F(k_x), \end{aligned} \quad (2.33)$$

where $F(k_x)$ is the Fourier transform of $f(x)$. From equation (2.29) and (2.30):

$$\left. \begin{aligned} a_n &= c_n + c_{-n} = 2\text{Re}\{c_n\} \\ b_n &= c_n - c_{-n} = -2\text{Im}\{c_n\} \end{aligned} \right\}, \quad (2.34)$$

hence it follows that:

$$a_n = 1/L \operatorname{Re} \left[F(k_x) \right],$$

$$b_n = 1/L \operatorname{Im} \left[F(k_x) \right]. \quad (2.35)$$

Since:

$$\begin{aligned} F(k_x) &= \int_{-L}^L f(x) \exp(-ik_x x) dx \\ &= \int_{-L}^L f(x) \cos(k_x x) dx - i \int_{-L}^L f(x) \sin(k_x x) dx, \quad (2.36) \end{aligned}$$

then:

$$a_{-n} = 1/L \int_{-L}^L f(x) \cos(k_x x) dx \quad (2.37)$$

so that:

$$\operatorname{Re} \left[F(k_x) \right] = \int_{-L}^L f(x) \cos(k_x x) dx. \quad (2.38)$$

Similarly:

$$b_n = 1/L \int_{-L}^L f(x) \sin(k_x x) dx, \quad (2.39)$$

so that:

$$\operatorname{Im} \left[F(k_x) \right] = - \int_{-L}^L f(x) \sin(k_x x) dx. \quad (2.40)$$

where Re and Im refer to 'real part of' and 'imaginary part of' respectively (Geldart and Sharma, 1968). If we now replace $f(x)$ in equation (2.38) with an even function term $f_e(x)$ and in equation (2.40) with an odd function term $f_o(x)$, we obtain:

$$\begin{aligned} F_e(k_x) &= \int_{-L}^L f_o(x) \cos(k_x x) dx \\ &= 2 \int_0^L f_o(x) \cos(k_x x) dx \end{aligned} \quad (2.41)$$

and:

$$\begin{aligned} F_o(k_x) &= - \int_{-L}^L f_o(x) \sin(k_x x) dx \\ &= -2 \int_0^L f_o(x) \sin(k_x x) dx \end{aligned} \quad (2.42)$$

where:

$$F_e(k_x) = \operatorname{Re} \left[F_o(k_x) \right] = \text{cosine transform of } f_o(x),$$

and:

$$F_o(k_x) = \operatorname{Im} \left[F_o(k_x) \right] = \text{sine transform of } f_o(x). \quad (2.43)$$

The discrete cosine transform of the even component is

hence given by:

$$\begin{aligned}
 F_o(k_x) &= 2\Delta x \sum_{m=0}^{N-1} f_e(x) \cos(k_x m \Delta x) \\
 &= 2\Delta x \sum_{m=0}^{N-1} f_e(m \cdot \Delta x) \cos \left[\frac{\pi}{L} n \cdot m \cdot \Delta x \right],
 \end{aligned}$$

$$n = 0, 1, 2, \dots, N-1, \tag{2.44}$$

where N is the number of observation points on one side of the profile only and Δx is the interval of observation or the sampling interval. Taking the fundamental frequency to be $2\pi/2L (= \pi / \Delta x N)$, equation (2.44) reduces to:

$$F_e(k_x) = 2\Delta x \sum_{m=0}^{N-1} f_e(m \Delta x) \cos \left(\frac{\pi}{N} \cdot m \cdot n \right),$$

$$n = 0, 1, 2, \dots, N-1. \tag{2.45}$$

Likewise, the imaginary part which is the sine transform of the odd component is given by:

$$F_0(k_x) = -2\Delta x \sum_{m=0}^{N-1} f_0(m \cdot \Delta x) \sin(\pi / N \cdot m \cdot n), \quad (2.46)$$

$$n = 0, 1, 2, \dots, N-1$$

Thus equations (2.45) and (2.46) conclude the derivation of the discrete Fourier transform of a general function $f(x)$, subject to Dirichlet conditions. The amplitude and phase of the derived spectrum can be obtained by applying the usual operations with complex numbers.

2.4.3 The Fast Fourier Transform (FFT)

The Cooley-Tukey FFT or the fast Fourier transform is an algorithm that can compute the discrete Fourier transform (DFT) much more rapidly than other available algorithms. The FFT is hence a more efficient method of producing discrete transforms. Due to the algorithmic nature of the FFT, it can be better understood by addressing only its computational aspect (Brigham, 1974). Briefly the development of the FFT proceeds as follows (Taylor, 1976): Let a time series input be given and denoted by: $x(k)$, $k=0,1,..N-1$. Let the series be further decomposed into two disjointed sequences say $y(k)$ and $z(k)$, where:

$$\left. \begin{aligned} y(k) &= x(2k) \\ z(k) &= x(2k+1) \end{aligned} \right\} k=0,1,2,\dots,N-1. \quad (2.47)$$

Thus, the sample values of $x(k)$ are loaded alternately into the array y and z . Let the DFT representation of the time series $y(k)$ and $z(k)$ be taken and denoted by $Y(i)$ and $Z(i)$, respectively. In particular, $Y(i)$ and $Z(i)$ would satisfy:

$$\left. \begin{aligned} Y(i) &= \sum_{k=0}^{N/2-1} y(k) W_N^{2ik} \\ Z(i) &= \sum_{k=0}^{N/2-1} z(k) W_N^{2ik} \end{aligned} \right\} k=0,1,\dots,N-1, \quad (2.48)$$

noting that:

$$\begin{aligned} W^i z(i) &= W^i \sum_{k=0}^{N/2-1} x(2k+1) W_N^{2ik} \\ &= \sum_{k=0}^{N/2-1} x(2k+1) W_N^{i(2k+1)} \end{aligned} \quad (2.49)$$

The Fourier representation of $X(k)$ can be synthesised from the disjoint transforms $Y(i)$ and $Z(i)$ as follows:

$$X(i) = \sum_{k=0}^{N/2-1} \left[x(2k)W_N^{2ik} + x(2k+1)W_N^{i(2k+1)} \right],$$

or in terms of equation(2.48):

$$X(i) = Y(i) + W^i Z(i). \tag{2.51}$$

Utilising symmetry properties of DFT in which spectral components of $x(t)$, existing from $N/2$ to $N-1$, can be interpreted as negative frequency locations, the periodic behaviour of $X(f)$ gives rise to the relation:

$$x(-k) = x(N-k). \tag{2.52}$$

Then it follows that $x(k)$ and $x(-k)$ form a conjugate pair, that is :

$$x(k) = x(-k)^* \tag{2.53}$$

where the asterik denotes complex conjugation. Using equation(2.52), a further simplification may be effected by extending $X(i)$ thus:

$$\left. \begin{aligned} X(i) &= Y(i) + W^i Z(i) \\ X(i+N/2) &= Y(i) - W^i Z(i) \end{aligned} \right\} i=0,1,\dots,N/2-1. \quad (2.54)$$

Using the results of equation(2.53), one may represent the negative frequency components as follows:

$$X(-i) = X^*(i) = Y^*(i) - W^i Z^*(i) = Y(-i) - W^{-i} Z(-i), \quad (2.55)$$

where the asterik denotes complex conjugation. If, for instance $N=8$, the DFT for $x(k)$ requires $N^2 = 64$ operations, whereas the FFT approach requires only $2(N/2)^2 = 32$ operations to produce the same spectrum. Thus, partitioning the data into two subseries reaps significant computational savings. Further decomposition of the data results into additional savings which satisfies the the following relationship:

$$N = \prod_{i=1}^m n_i = n_1 \times n_2 \times \dots \times n_m, \quad (2.56)$$

where n_i is a prime number. If all n_i 's have a value of two (e.g. $8 = 2 \times 2 \times 2 = 2^3$), the algorithm is said to be of radix(2), that is the total number of data points is expressible in powers of two. The FFT adopted in this work

is radix(2) notwithstanding that it is desirable to use a mixed radix algorithm which would for instance interpret $N=12$ as $2^2 3^1$, that is, $n_1 = n_2$ and $n_3 = 3$. It is very important to note that in order to adjust a sample space into radix(2) format, the data is padded with zeroes bearing in mind that the more data points one has the more realistic is the computed spectrum. In other words spectral resolution is increased by having more data points which is synonymous with increasing the basic interval or range. In this work, a sample space of 1024 data points is used. Although the utility of the FFT analysis is great, there are latent error sources imbedded in this method, which the user ought to be attendant to. These fall into three categories: aliasing, leakage and picket-fence effect. Each of the above error-sources is discussed below.

1. Aliasing effect.

As the name implies, one signal may be impersonated by another (an alias). Here the sampling rate is too slow to completely characterise the input signal. Consequently, a low frequency bogus signal impersonates the higher frequency input signal. The aliasing problem is easily removed by sampling at least twice the rate of the highest frequency residing in the signal, a sampling or Nyquist condition.

2. Leakage.

This is an undesirable harmonic distortion whose understanding may be exemplified by considering a signal $x(t)$ given by:

$$x(t) = \sin(2\pi f_0 t) \quad (2.57)$$

with a fundamental period T_0 where,

$$T_0 = 1/f_0.$$

If $x(t)$ is now sampled above Nyquist frequency rate for T seconds and suppose further that $T = T_0$, then the resulting Fourier representation of $x(t)$ would have a non-trivial component at f_0 Herz only. However, suppose that the same sample rate is used, but the sampling continued for more than T_0 , i.e. $T = \alpha T_0$. Suppose further that α is non-integer, then the resulting Fourier transform of the new time series would have more than one non-trivial frequency components because the new time series is not periodic in the sampling interval. The harmonic distortion introduced by leakage problem can be minimised by using a sampling interval comparable with the fundamental period of the signal to be analysed.

3. Picket fence effect.

The DFT can be envisaged as a set of narrow band pass filters whose centre frequencies are located at k/T Hz, where $k=0,1,\dots,N-1$. Thus, the FFT filter response curve resembles a picket fence. The frequency components of an input signal $x(t)$ that reside at $k/T = kf_0$ will be transformed without distortion, however, frequency components of $x(t)$ that reside in non-integer multiples of f_0 are transformed with distortion. This distortion constitutes the error introduced by the picket fence effect which can be minimised by ensemble averaging techniques and interpolation methods.

CHAPTER THREE

3.1 Analysis of Amplitude Spectra

The frequency functions derived in preceding sections can be used to make useful interpretations for the thin conductive plate model. The transformed expression clearly demonstrates that its decay is primarily controlled by the depth to the top of the model. This affords a direct derivation of the depth from the computed spectrum of the measured anomaly (equation 2.25). Depth can also be estimated from harmonic analysis of the same equation. Each of the above two methods will be elaborated separately in the following sections.

3.1.1 Estimation of Depth from Amplitude Spectra

A logarithmic transformation of equation (2.25) yields the expression:

$$\ln F(k_x) = -k_x z + \ln 2\pi C A_o(k_x) \quad (3.1)$$

where the symbols have the meaning defined earlier. Loosely, equation (3.1) can be regarded as of general linear form:

$$y = mx + c,$$

where:

$$m = -z$$

and:

$$c = \ln 2\pi C A_o(k_x). \tag{3.1}$$

The factor C is not generally a constant and its behaviour can be clarified by examining the function $A_o(k_x)$ which can be transformed into a sine or cosine function in order to determine its periodic properties. It can be written in the form:

$$A_o(k_o) = P_o \sin(k_x l/2 - \Phi), \tag{3.3}$$

where:

$$P_o = \frac{l(a^2 + b^2)^{1/2}}{4(l^2 + 4z^2)}, \quad \Phi = \cos^{-1} \left\{ a / (a^2 + b^2)^{1/2} \right\}$$

and:

$$a = l^2 + 2z^2,$$

$$b = zl.$$

From equation (3.3) we see that $A_o(k_x)$ is a periodic function of amplitude P_o and phase Φ which are all directly proportional to transmitter-receiver separation (l) and depth (z). For a given value of l the period of the

function is constant and is given by:

$$T = 4\pi / v, \quad (3.4)$$

hence the function $A_o(k_x)$ takes the graphical shape depicted in Figure 3-1.

In the evaluation of the spectrum of $F(k_x)$, we have to evaluate $\ln A_o(k_x)$. We note that the absolute value of $A_o(k_x)$ takes the shape depicted in Figure 3-2. At the points marked d' the amplitude falls to zero hence $\ln A_o(k_x)$ is infinite and these are the points of discontinuity of the function $\ln A_o(k_x)$. This is shown in Figure 3-3. We can hence define a maximum value of $\ln A_o(k_x)$ which is finite and constant for all k_x . The interpretation for depth is based on the upper limit of the logarithmic function for as much as the lower limit is infinite in the negative sense. This upper limit or envelop is shown by the dotted line in Figure 3-3. If the term $-k_x z$ is superimposed on $\ln A_o(k_x)$ by addition (see equation (3.1)) a complete graphical representation of the continuous spectrum of $f(x)$ is obtained as shown in Figure 3-4. The slope of the dotted line which delimits the upper bound of the exponentially decaying envelop gives the depth estimate to the top of the thin conductive plate. The same concept can be extended to the discrete case whose DFT has similar form.

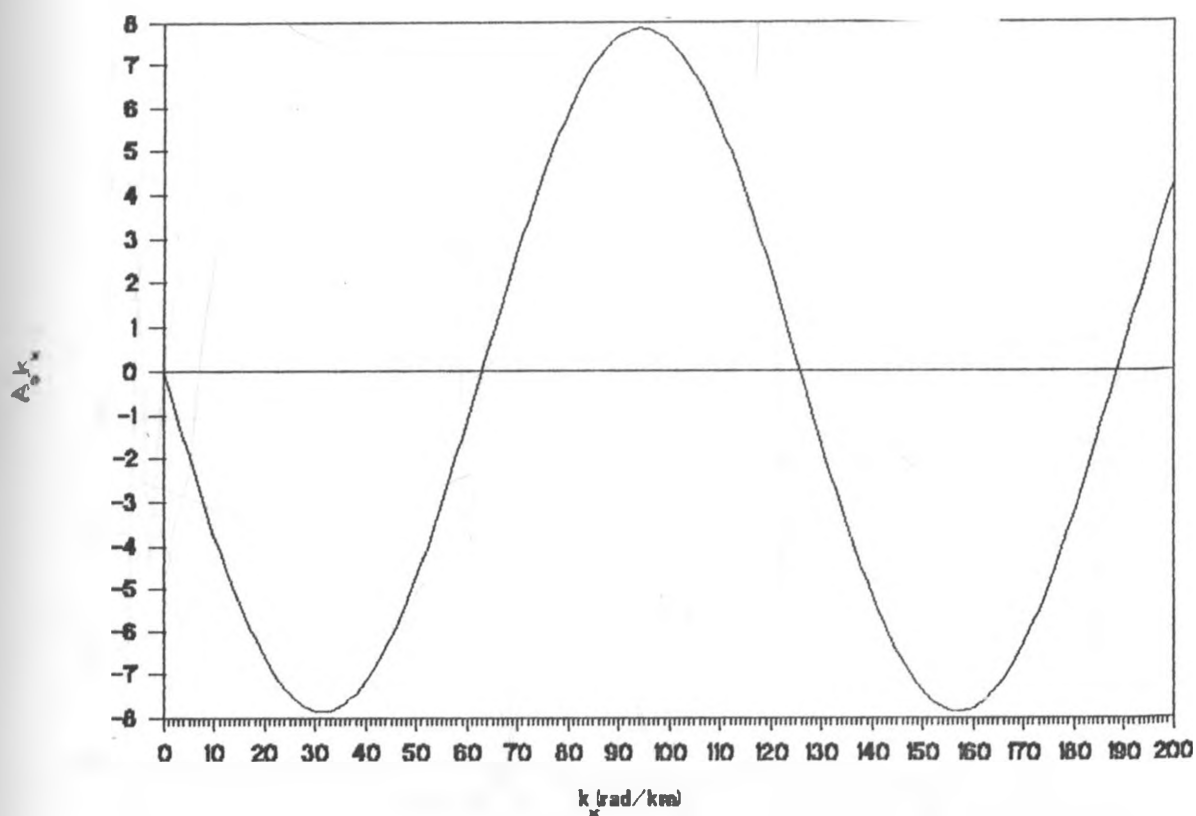


Fig. 3-1 Periodic properties of the function $A_0(k_x)$

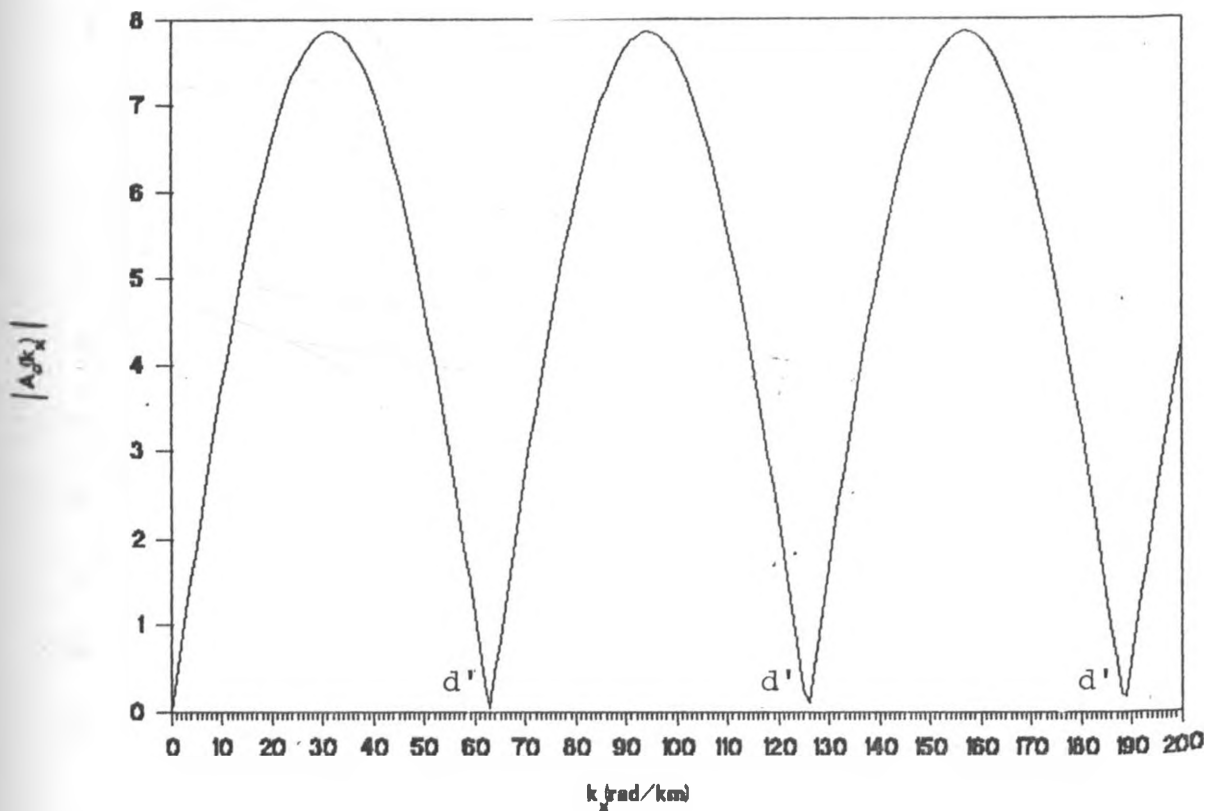


Fig. 3-2 Graphical representation of the function $|A_0(k_x)|$

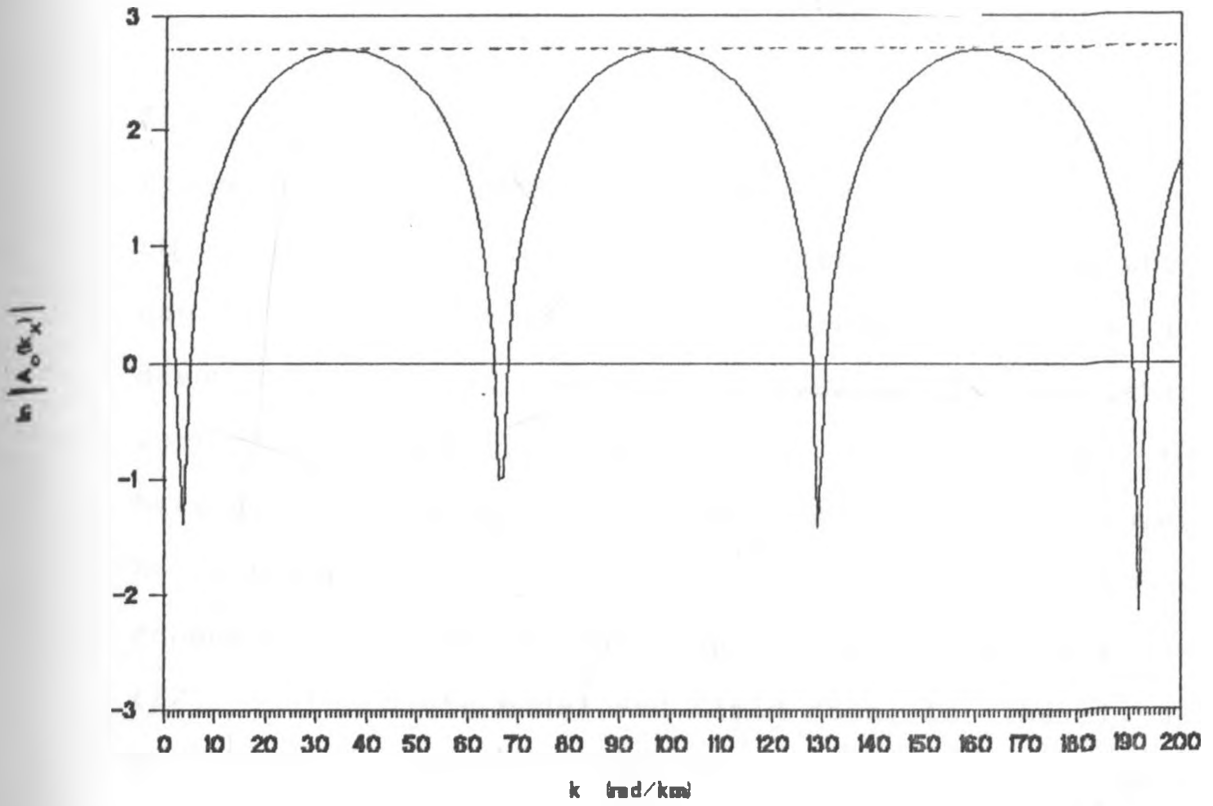


Fig. 3-3 Graphical representation of the function $\ln |A_0(k_x)|$

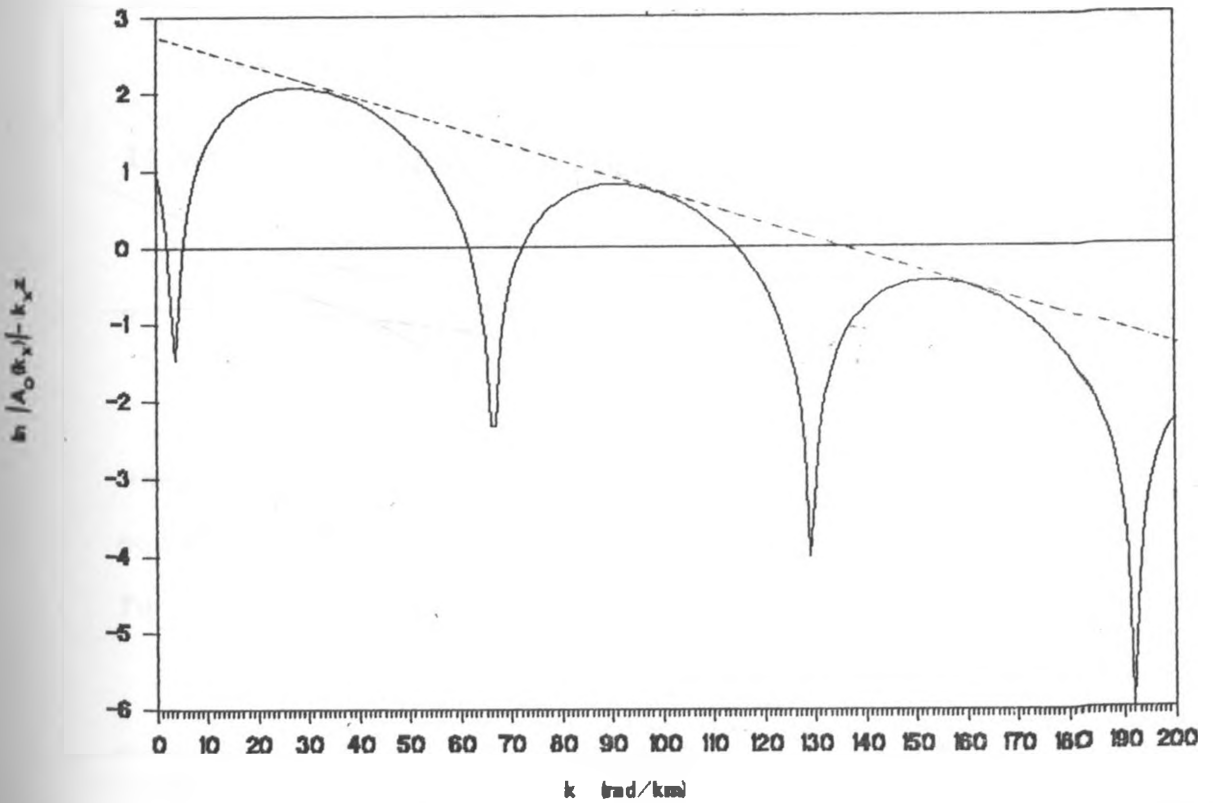


Fig. 3-4 Complete Graphical representation of the function $\ln |A_0(k_x)| - k_x z$

3.1.2 Estimation of Depth from Harmonic Analysis of The Derived spectrum

The depth to the top of the conductive target can also be estimated from equation(2.25). We make use of the fact that the spectrum falls to zero at definite points from which we can derive quantitative information regarding depth. It is demonstrated that , spectral information is available at zero harmonic making it unnecessary to consider higher harmonics for interpretation. Moreover, it may sometimes be inevitable to consider the second or higher harmonics depending upon the resolution of the fast Fourier transform (FFT) on the plate model and field data. In the transform domain $F(k_x)$, drops to zero when :

$$2l \cos(k_x l/z) - (l^2 + 2z^2) \sin(k_x l/z) = 0. \tag{3.5}$$

If we define a phase angle γ such that:

$$\gamma = \cos^{-1} \left\{ a / (a^2 + b^2)^{1/2} \right\}, \tag{3.6}$$

where a and b are as defined in the preceding section, equation (3.5) can be transformed into a sine (or cosine) function:

$$\frac{a}{(a^2 + b^2)^{1/2}} \sin(k_x l/z) - \frac{b}{(a^2 + b^2)^{1/2}} \cos(k_x l/z) = 0$$

or:

$$\cos(\gamma)\sin(k_x l/2) - \sin(\gamma)\cos(k_x l/2) = 0,$$

hence:

$$\sin(k_x \frac{l}{2} - \gamma) = 0. \tag{3.7}$$

The relationship expressed in equation (3.7) is true if:

$$k_x \frac{l}{2} - \gamma = n\pi, \quad n=0,1,2,\dots \tag{3.8}$$

The value of n defines the harmonics. If we write the n^{th} harmonic as $k_x(n)$, then equation (3.8) becomes:

$$\frac{k_x(n) l}{2} - \gamma = n\pi, \quad n=0,1,2,\dots \tag{3.9}$$

We see, from equation (3.9), that the phase angle γ is a function of depth (z) and is the first value of k_x for which $F(k_x)$ falls to zero, thus making it the only significant term in estimating depth. It follows that the zero harmonic can be chosen to estimate depth since the

term $n\pi$ is not a function of depth but merely adds a constant value to the phase angle. We can hence write:

$$k_x(0) l/2 = \gamma$$

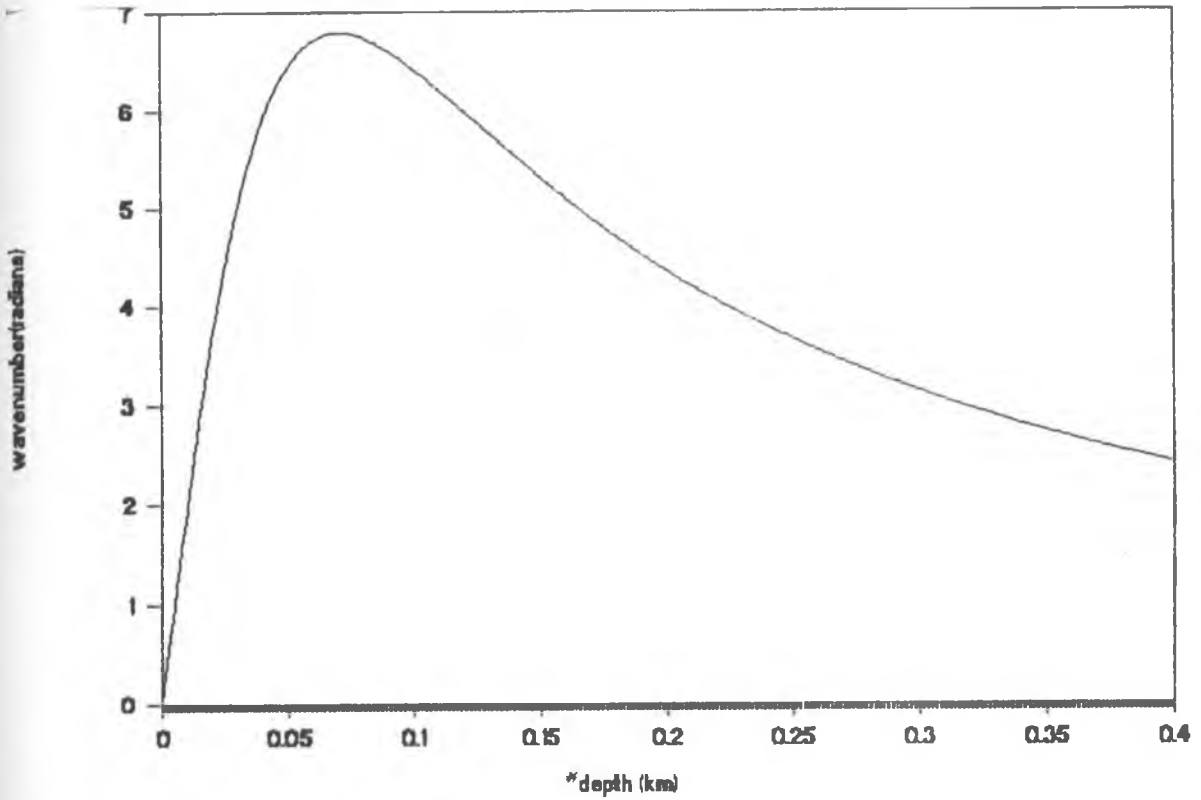
or:

$$k_x(0) = 2\gamma / l . \tag{3.10}$$

The transmitter-receiver separation l remains constant, hence we can vary depth, calculate the value of γ and consequently calculate the corresponding values of the harmonic. An important fact here is that , the depth estimation is independent of constant C (compare equations(3.5) and (2.22)) and the dip of the thin plate model. Figure 3-5 shows the plot of the zero harmonic against depth, which may be used to estimate depth immediately the value of the zero harmonic is known.

3.2 Fourier Analysis of Synthetic Data

Synthetic data that are analysed in this work are based on the response of an equivalent current axis model that simulates a finite thin conductive plate, and the response of the plate model calculated using the PLATE program (Dyck et al., 1980). The profile length is chosen so as to ensure good resolution of the Fourier transform. To the same effect, the sampling interval is made small enough. In this



*The ambiguity of this plot in finding the depth is well exemplified. Moving horizontally, the graph is encountered twice for all values of wavenumber less than about 6.8 radians.

Fig. 3-5 A plot of the zero harmonic wavenumber against depth.

analysis the target parameter of interest is depth. Here it is desired to show how one can estimate the depth to the top of the target from anomaly profiles alone. First the profiles are prepared using known depths and then the depth is recovered from the anomaly profiles by means of spectral analysis. If this method is demonstrated to work, then it would mean that anomaly profiles from the field can be directly subjected to the same procedure to recover depth.

3.2.1 The wire Model data

The analytical expression for the response of the wire model was programmed using a simple FORTRAN 77 program. The full range profile used was 30 km and a coil separation of 100 m. Depth was varied between 0.01 to 0.2 km thus obtaining a set of profiles for analysis. A 1024-point complex FFT was executed on an IBM PS/2 computer to obtain the profiles in the wave-number domain. A sampling interval of 0.01 km (10m) was used. The estimation of depth was carried out using the two methods described in chapter 2.

In the first method, the amplitude spectra are plotted and as described previously it is expected to take the shape of series of peaks whose crests lie along a straight line. The slope of this line can be determined and represents the depth to the top of the wire model. The amplitude spectra for the responses using depths stated above were plotted and are shown in Figures 3-6(a) to (f).

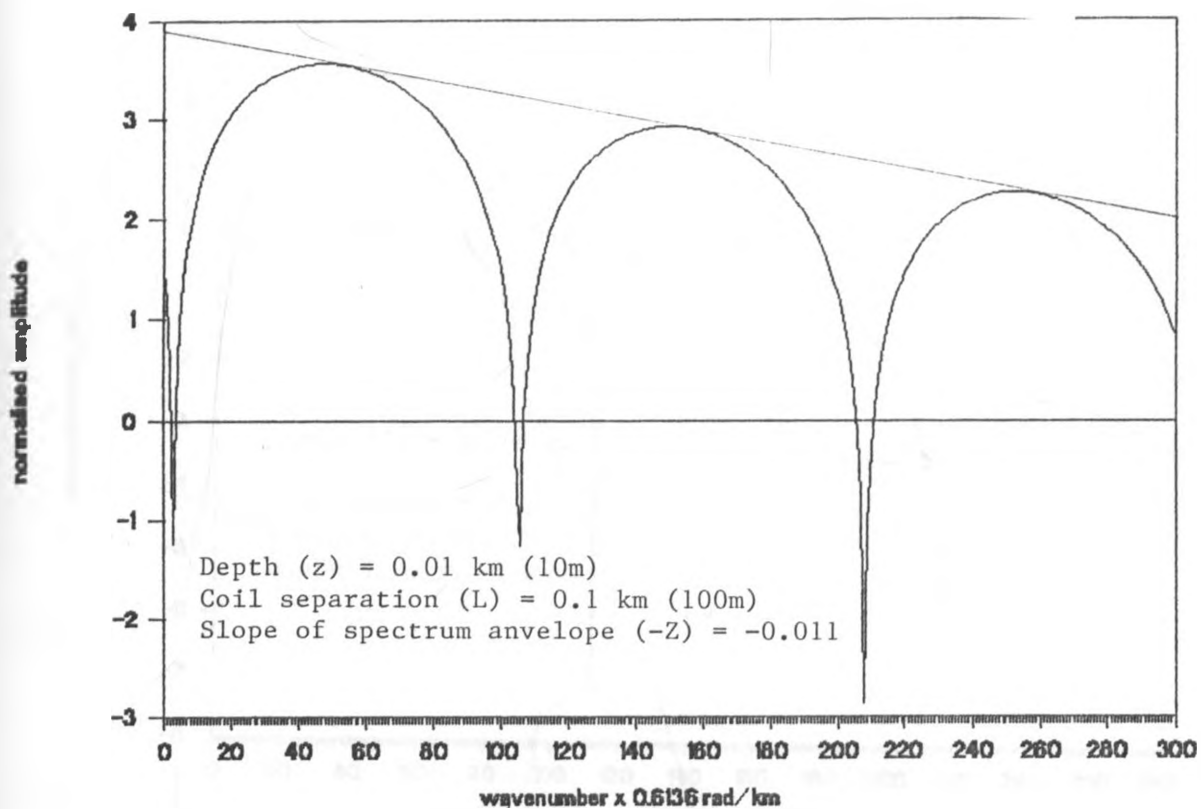


Fig. 3-6(a) Wavenumber-domain amplitude spectrum for the wire model

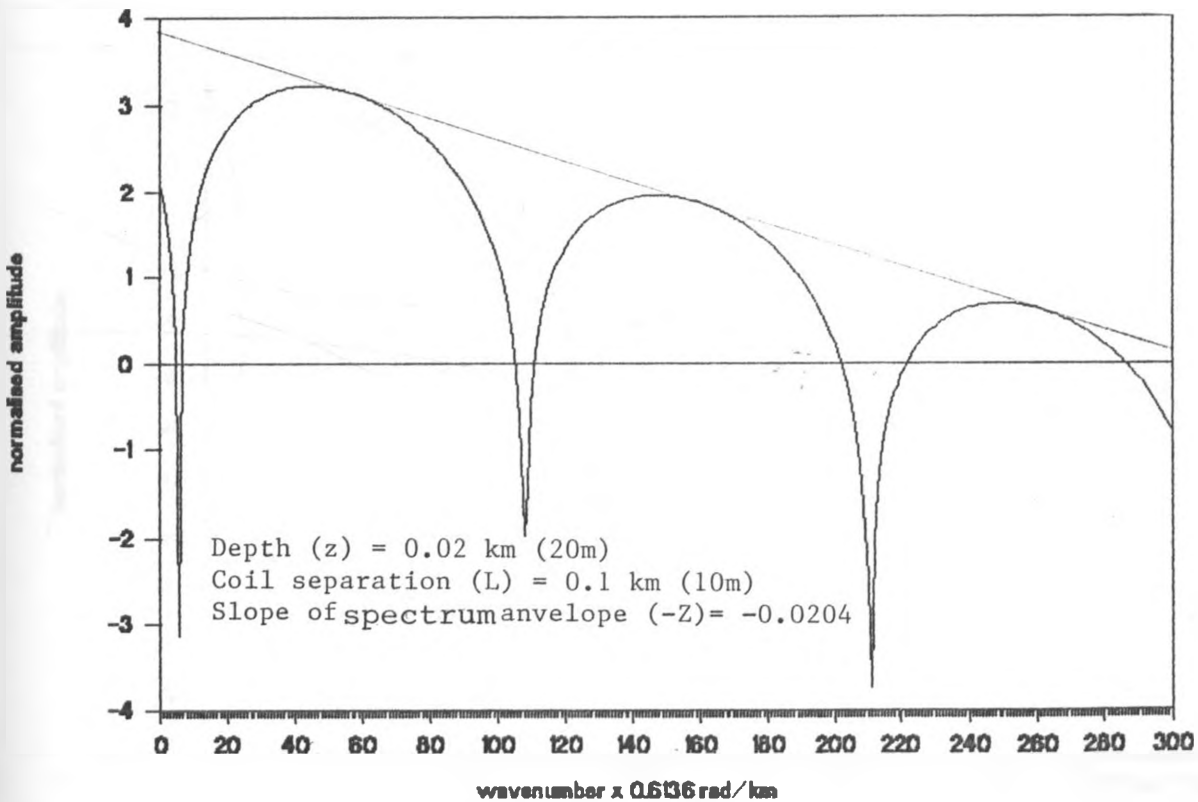


Fig. 3-6(b) Wavenumber-domain amplitude spectrum for the wire model

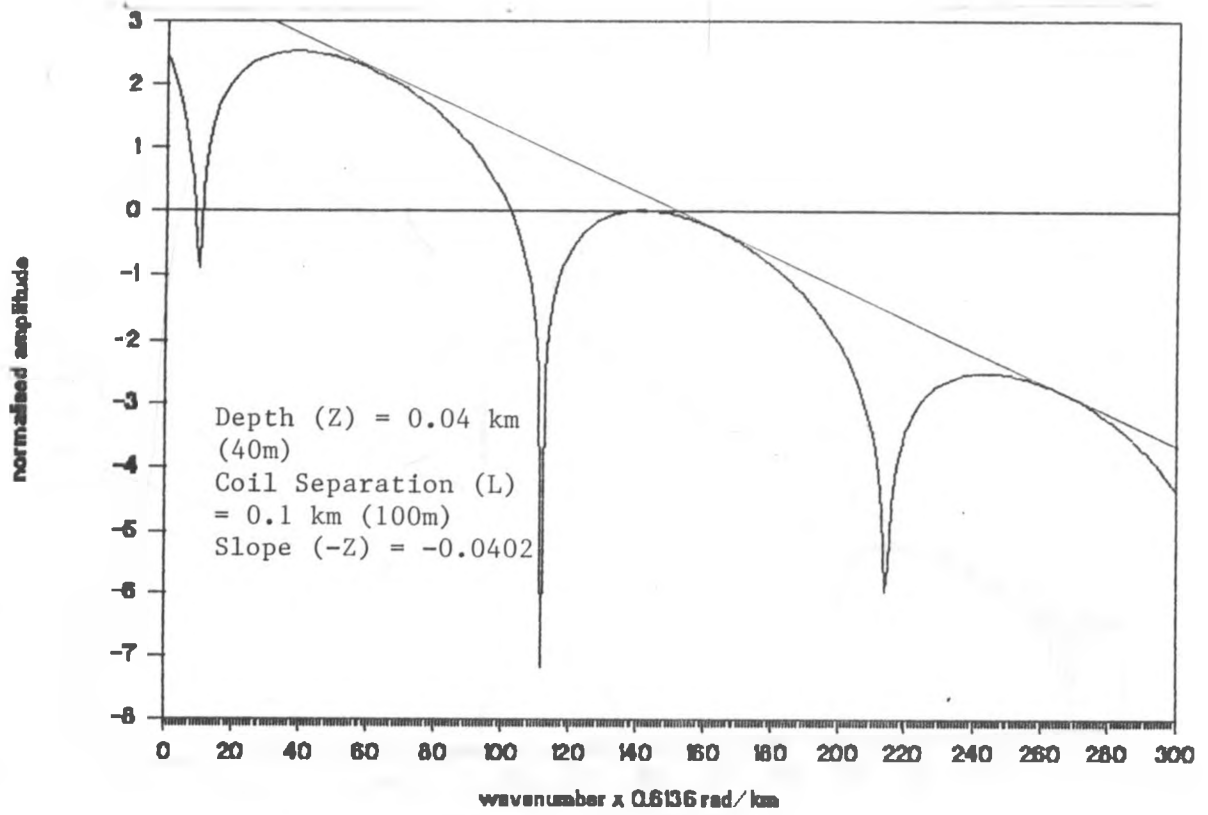


Fig. 3-6(c) Wavenumber-domain amplitude spectrum for the wire model

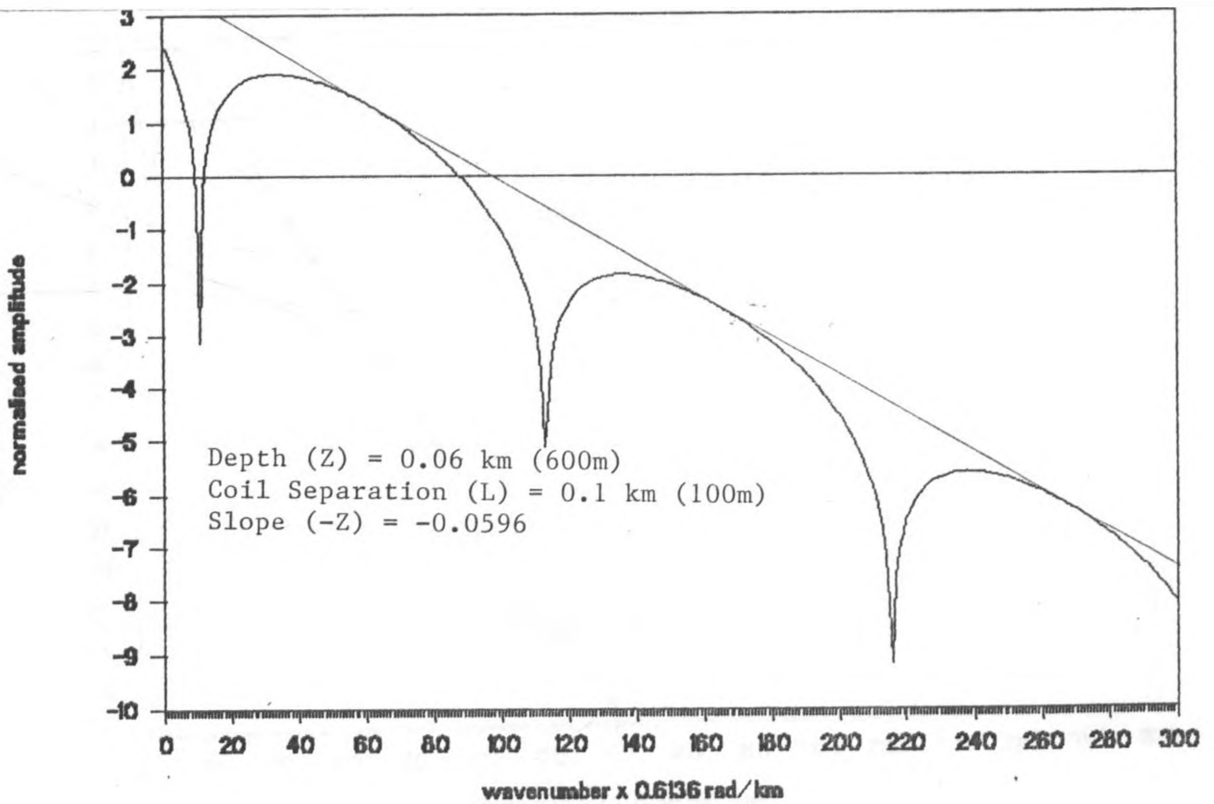


Fig. 3-6(d) Wavenumber-domain amplitude spectrum for the wire model

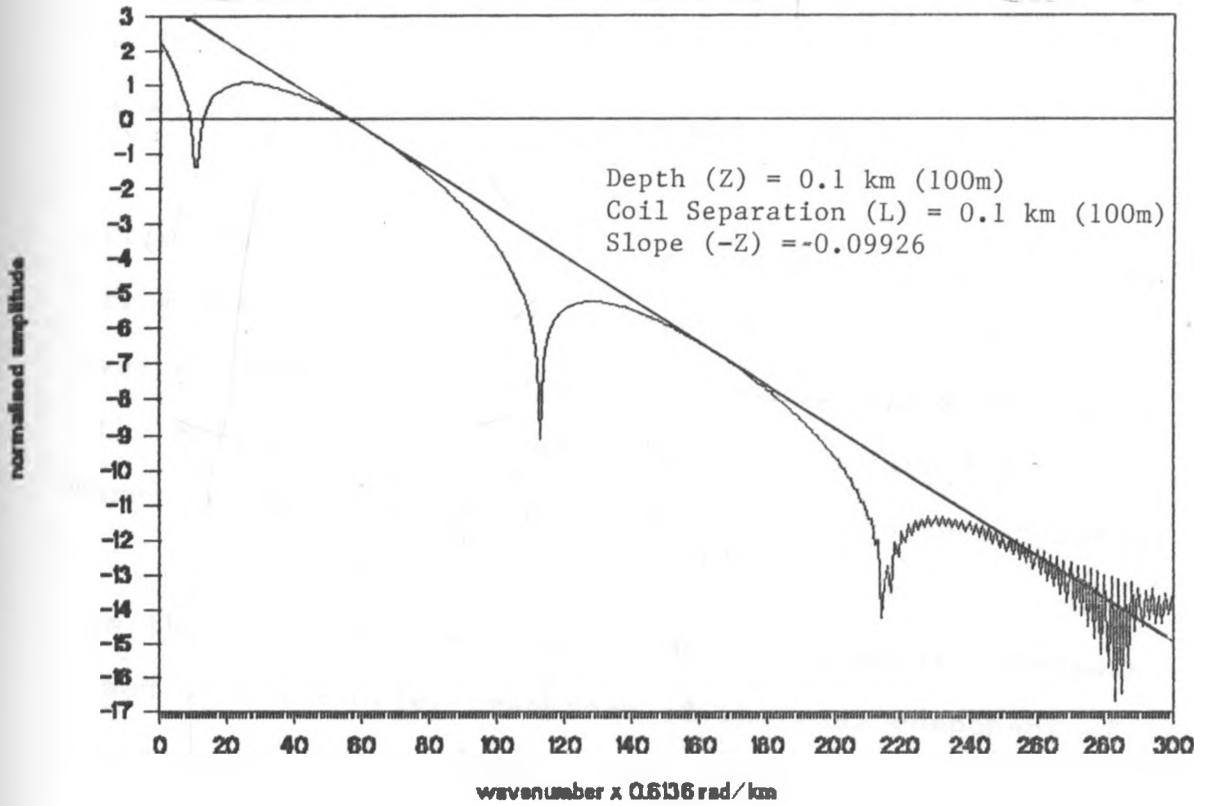


Fig. 3-6(e) Wavenumber-domain amplitude spectrum for the wire model

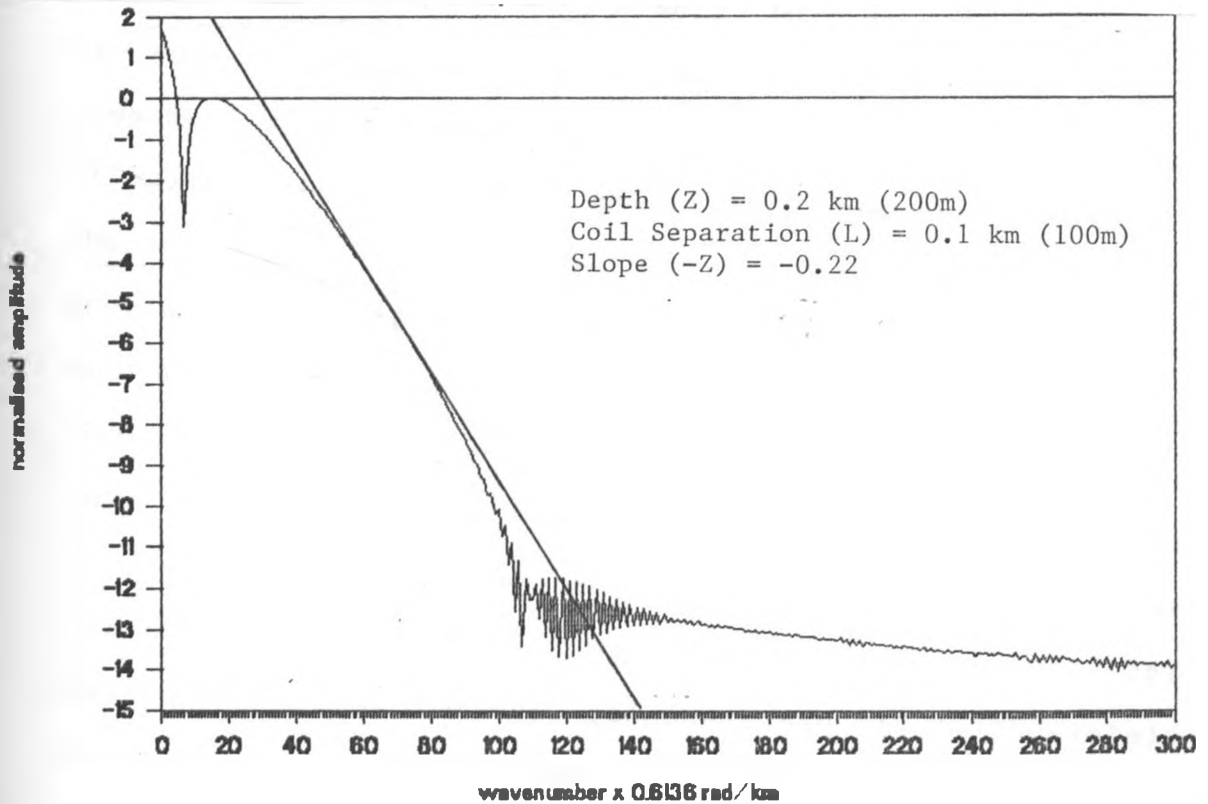


Fig. 3-6(f) Wavenumber-domain amplitude spectrum for the wire model

Table 3.1 summarises the results in which case the starting values of depth used to generate model curves are compared with the values determined from the slopes of the amplitude spectra derived from the same model curves.

From Table 3.1 it is very clear that the depths derived from the amplitude spectra agree very well with the true values. Note that a large depth beyond the resolution of the FFT (making it almost impossible to find the slope) was used to emphasise the applicability of the second method.

In the second method, the concept of harmonic analysis is used on the Fourier transform of the real component of the wire model response. As proved in chapter 4, the real component of the FT falls off to zero at the harmonics of the wavenumber (see equations 3.5 to 3.10). From this fact, depth can be estimated most simply. In order to determine the above condition, one needs to compute the real component of the Fourier transform using the DFT, then plot it against the wave number and finally find the values of the wavenumber at which the FT is zero. As was noted previously, the spectral information is available at zero harmonic thus making it necessary to consider only the first value of the wavenumber at which the FT falls off to zero. One obvious disadvantage of using the DFT is that it is uneconomical, in terms of both time and cost and is less accurate. In this work it was decided to use the FFT spectrum to derive the even component and fairly accurately determine the zero harmonic. Just to demonstrate the

Table 3.1. True and estimated values of depth determined from the slope of the amplitude spectrum of the wire model.

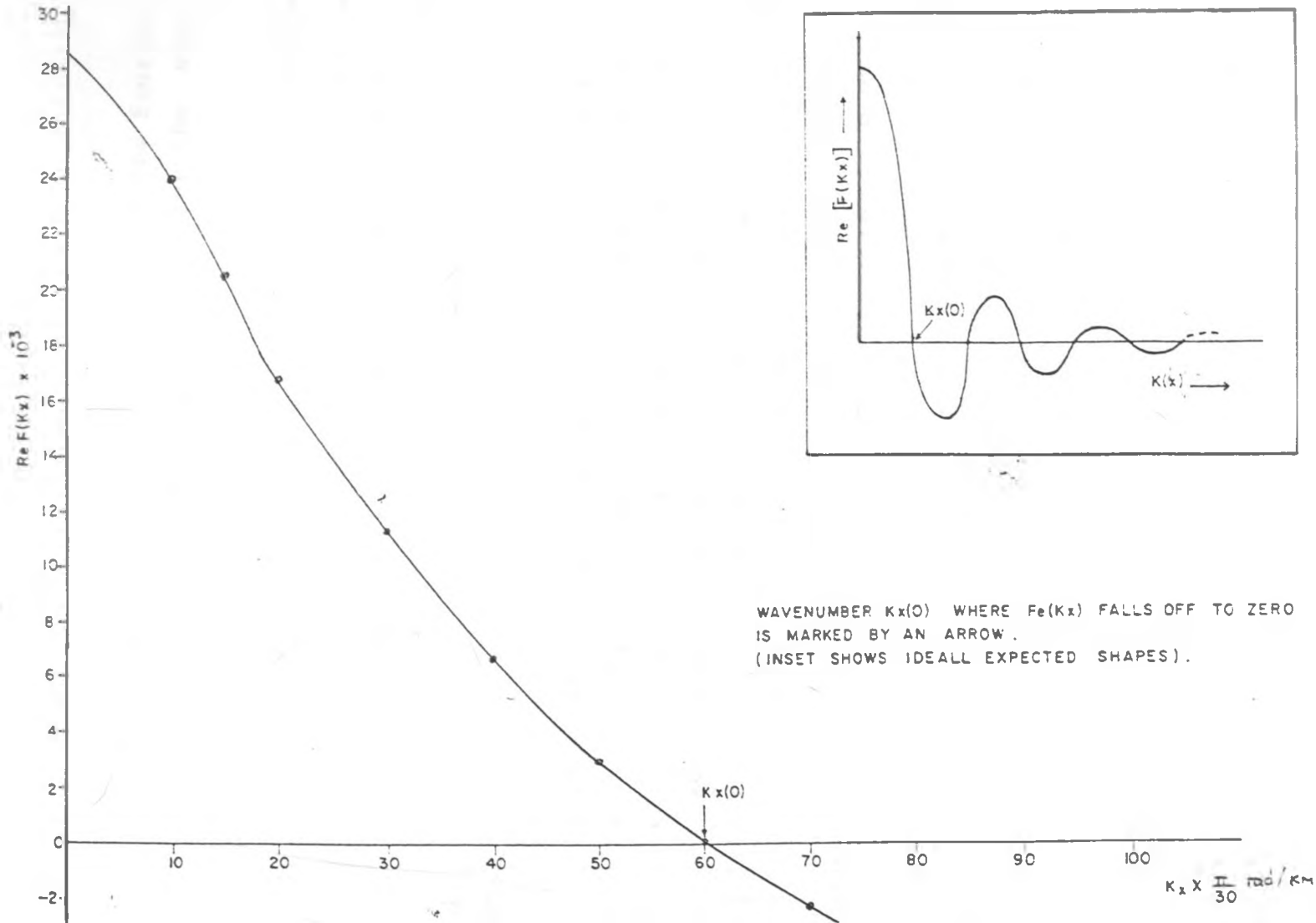
True Value (km)	Value estimated from slope (km)
0.01	0.0111
0.02	0.0204
0.04	0.0402
0.06	0.0596
0.10	0.0993
0.20 *	0.22 ± .005

(Estimates of depth are correct within + 0.05m or + 5×10^{-5} km., except the value with an asterik)

* This value is only a rough estimate since the resolution of the spectrum is poor and does not allow accurate determination of the slope

equivalence of the two Fourier transforms (ones calculated from the DFT and ones derived from the amplitude spectra), Figure 3-7 shows a plot of the Fourier transform against the wavenumber for a depth of 0.1km. Wavenumber $k_x(0)$ shows where the real component falls off to zero. If this plot is compared with the the Fourier transforms derived from the amplitude spectra, they are similar. This offers an economical method of using the amplitude spectrum for the two methods simultaneously. The justification of extracting the FT from the amplitude spectrum follows from the fact that, when the FT falls to zero, the amplitude of the spectrum becomes infinite. These are the points of discontinuity shown in Figure 3-2. For the zero harmonic we need to consider only the first point of discontinuity which is well defined in most cases even if the determination of the slope is difficult owing to poor spectral resolution at higher wavenumbers.

In extracting the real component, the values of the wavenumber and their corresponding amplitudes are read off in the neighbourhood of the first point of discontinuity (well to the left and right). The values of the logarithmic amplitude are then reconverted to FT values by taking an antilogarithm of each. The negative signs are easily fixed by inspection. Table 3.2 shows data extracted from the spectra in Figures 3-6(a) to 3-6(f) and the corresponding plots are shown in Figures 3-8(a) to 3-8(f). From the plots, it is very clear that the value of the wavenumber at which the real component of the Fourier transform falls to



WAVENUMBER $k_x(0)$ WHERE $F_e(k_x)$ FALLS OFF TO ZERO IS MARKED BY AN ARROW. (INSET SHOWS IDEALL EXPECTED SHAPES).

Fig. 3-7 Real component $[F_e(k_x)]$ of the Fourier transform of the wire model against wavenumber (k_x)

Table 3.2 Data used to plot the real component of the Fourier transform against wavenumber, $Kx(0)$ for the wire model.

Wavenumber (rad/km)	Depth (Km)					
	0.01	0.02	0.04	0.06	0.1	0.2
	Amplitude $\times .005$ (dimensionless)					
0.0000	4.43	8.16	11.67	11.77	9.51	5.47
0.6136	3.27	7.01	10.53	10.64	8.41	4.44
1.2272	1.74	5.50	9.06	9.21	7.06	3.25
1.8408	0.29	4.08	7.71	7.92	5.89	2.33
2.4544	-1.17	2.67	6.38	6.68	4.80	1.56
3.0680	-2.59	1.30	5.13	5.53	3.83	0.94
3.6816	-4.00	0.04	3.92	4.43	2.95	0.44
4.2951	-5.39	-1.35	2.76	3.42	2.16	0.05
4.9087	-6.76	-2.63	1.65	2.46	1.45	-0.27
5.5223		-3.86	0.60	1.57	0.82	-0.51
6.1359		-5.07	0.41	0.73	0.25	-0.69
6.7495		-6.24	-1.36	0.04	-0.25	-0.82
7.3631			-2.27	-0.77	-0.69	-0.91
7.9767			-3.13	-1.43	-1.08	-0.97
8.5903			-3.95	-2.05	-1.41	-1.00
9.2039				-2.62	-1.71	-1.01
9.8175				-3.14	-1.96	-1.00
10.4311				-3.62	-2.17	
11.0447					-2.35	
11.6583					-2.50	
12.2718					-2.62	
12.8854					-2.71	

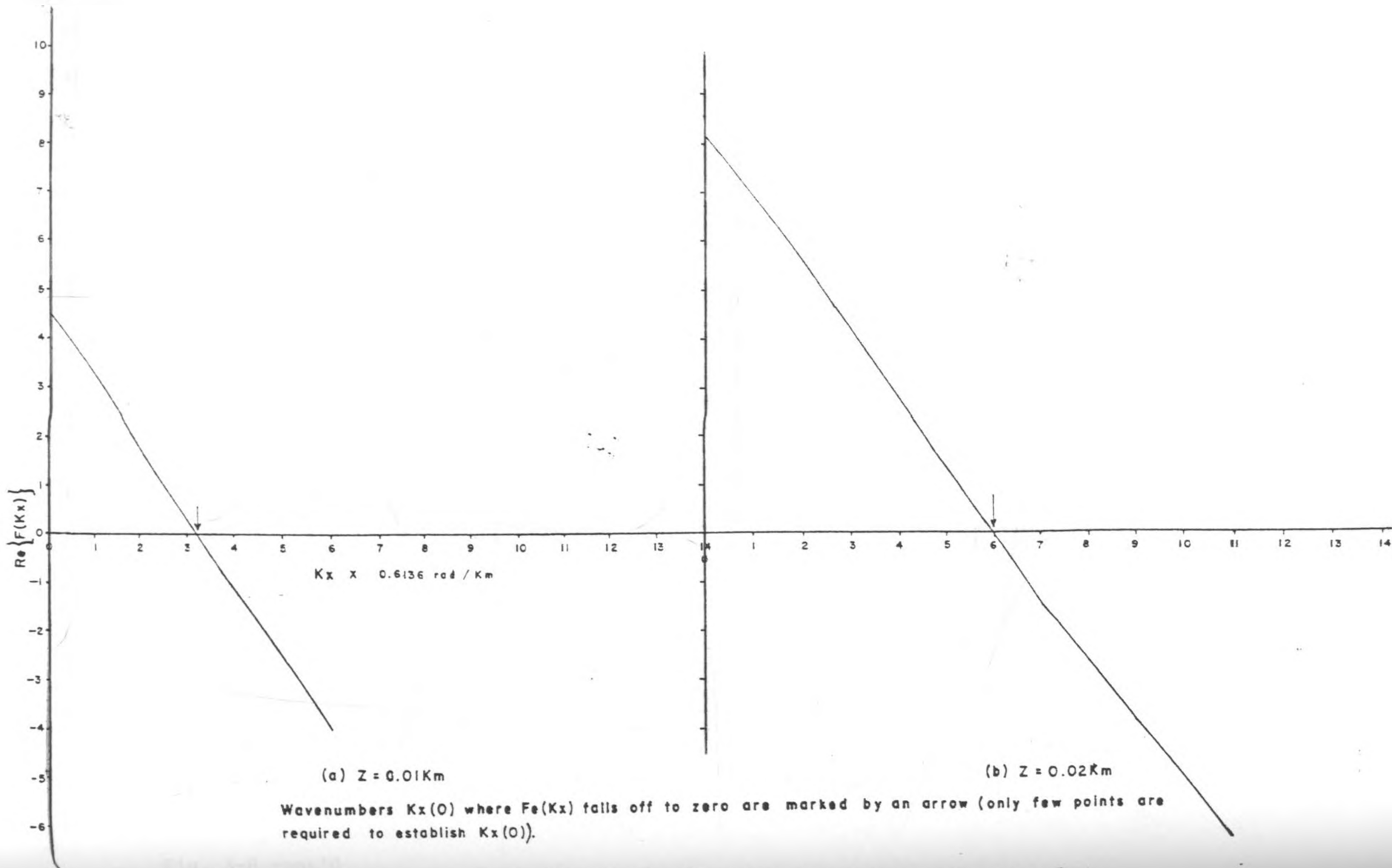


Fig. 3-8 Real component $[F_e(k_x)]$ of the Fourier transform of the wire model against wavenumber (k_x)

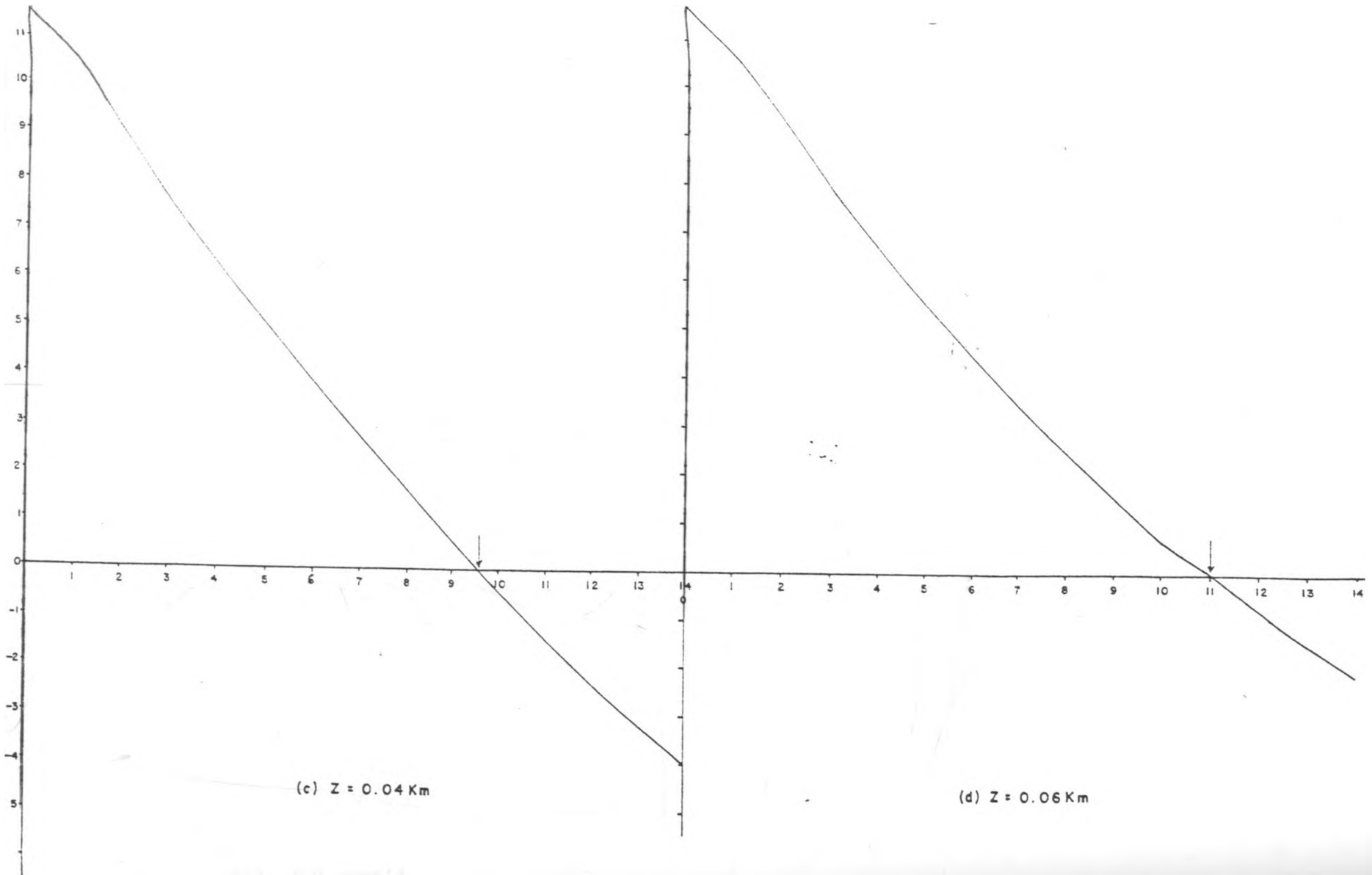


Fig. 3-8 cont'd

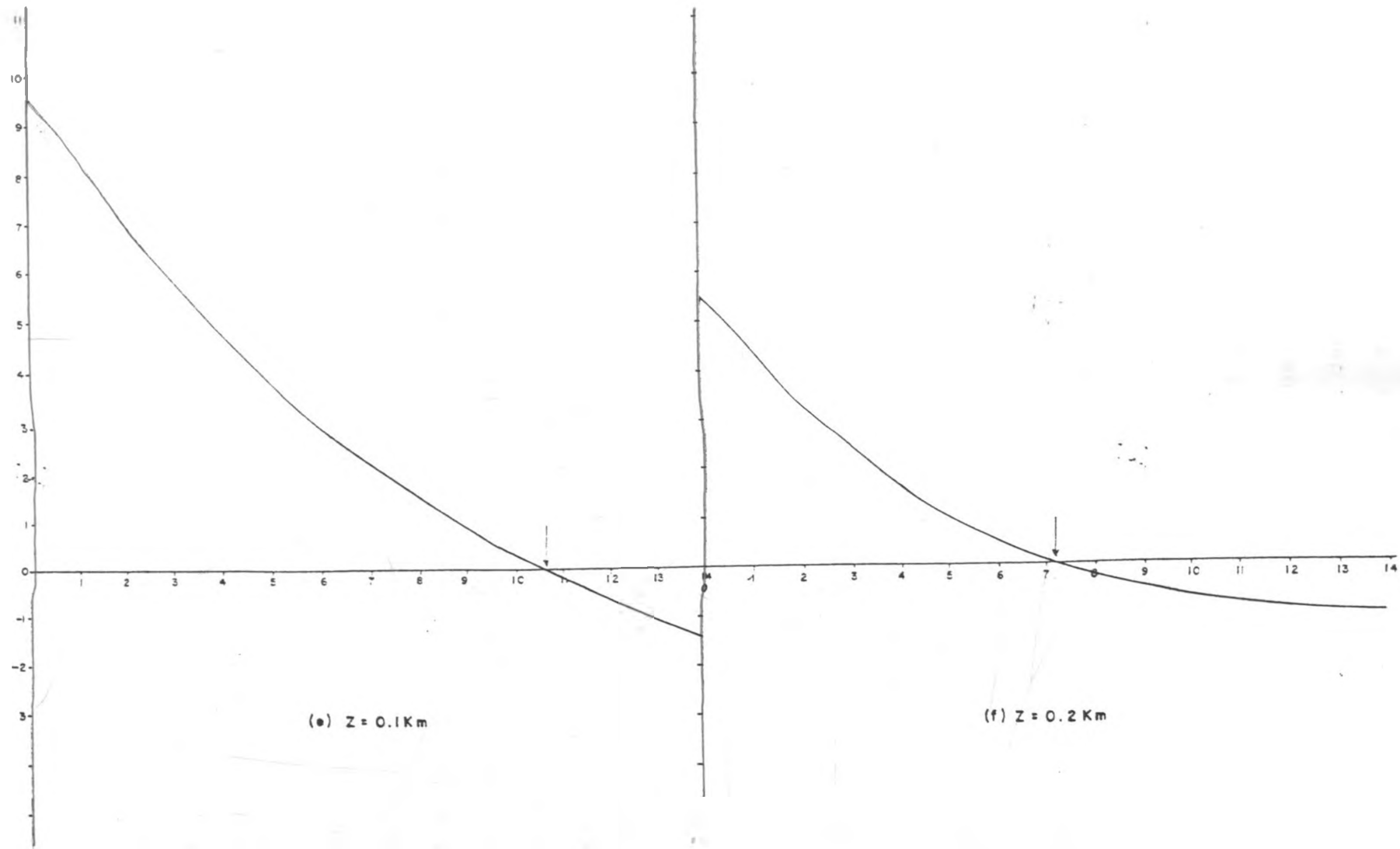


Fig. 3-8 cont'd

zero can be determined with better accuracy than using the discrete Fourier transform. The value of $k_x(0)$ from Figure 3-7 is approximately 6.28. Using Figure 3-5, the depth read off is 0.106 km (106m) which is less accurate. The real component derived from the amplitude spectrum gives the correct depth up to two decimal points.

This method suffers one major disadvantage in that it is ambiguous. For every value of harmonic determined, there are two depths that are estimated and choosing the correct one is difficult if this method is used alone. This fact follows from Figure 3-5. Mathematical justification of this also follows from equation (3.10) since upon solving for depth (z), the expression turns out to be quadratic and has two roots for depth (z).

The ambiguity above can be resolved by using the first method to estimate the depth, then the second method may be used to complete the determination more accurately. Note that the second method is applicable when the resolution of the amplitude spectra is not good enough to permit depth estimation from the slope. However, the rough estimate of depth should be used to check the ambiguity inherent in the first method.

To exemplify this, a depth of 0.2 km. is considered in which case the amplitude spectrum does not give adequate resolution to determine the depth from the slope (resolution is very poor beyond 70 rad/km). The rough

estimate of depth is 0.22 km. Of the two possible depths the value close to the rough estimate is considered when using the second method. It may be noticed that the wavenumber is expressed in radians for the plate model, and not radians per unit distance because the spatial units in the generation of the EM response of plate model are normalised with transmitter- receiver separation, (i.e. rad./km/km= radians).

The complete determinations of depth using the second method are summarised in Table 3.3. Again the estimated values agree very well with the true values.

3.2.2 The Plate Model Data

Anomaly profiles for the response of a thin plate model were generated using the program PLATE (Dyck et al., 1980) for various values of depth to the top of the plate. The full range profile length was 1.12 km (1120m) with an initial digitising interval of 10m. The profiles were digitised using the SPLINE algorithm (Crossley, 1982) thus reducing the digitising interval to 1.09482m and a total of 1024 reading stations. The interpolated anomaly profiles were then subjected to a 1024-point complex FFT to yield the amplitude spectrum which was then analysed for depth. This analysis is similar to that carried out for the wire model and involves calculation of the slope of the decay envelope of the spectrum described in the preceding section. An attempt is made to use harmonic analysis to recover depth.

Table 3.3. Results of using the second method (harmonic analysis) to estimate depth. The estimated values of depth are based on the zero harmonic.

true value of depth (km)	zero harmonic (rad/km)	Depth* estimate (km)
0.01	1.96	0.010
0.02	3.71	0.020
0.04	5.89	0.040
0.06	6.78	0.061
0.10	6.44	0.100
0.2	4.39	0.198

* estimated values are all accurate within + .0005 km or + 5cm

In testing the plate model, care is taken in order not to violate the condition specified in section 2.1.4 (Chapter 2) which is a rough guide to the minimum depth that is permissible in using the PLATE program. The values of depth used are: 0.02, 0.06 and 0.2 km from whose response the corresponding amplitude spectra are computed. A fairly high conductivity-thickness product of 50S and a frequency of 222Hz were used in order to obtain well defined space domain profiles.

Figures 3-9(a) to 3-9(c) show the wavenumber domain amplitude spectra for depths stated above. From the above plots, the wavenumber range in which the slope can be satisfactorily determined in order to estimate depth does not exceed 28 radians approximately, for a transmitter-receiver separation of 100m. Note that this range is dependent on the relative positions of the peaks of the amplitude spectra, which in turn depends on the depth used to calculate the profiles. In fact the width of the peak has the period of approximately $4\pi/l$ radians (see equation 3.4).

Table 3.4 summarises the results of using the profiles of

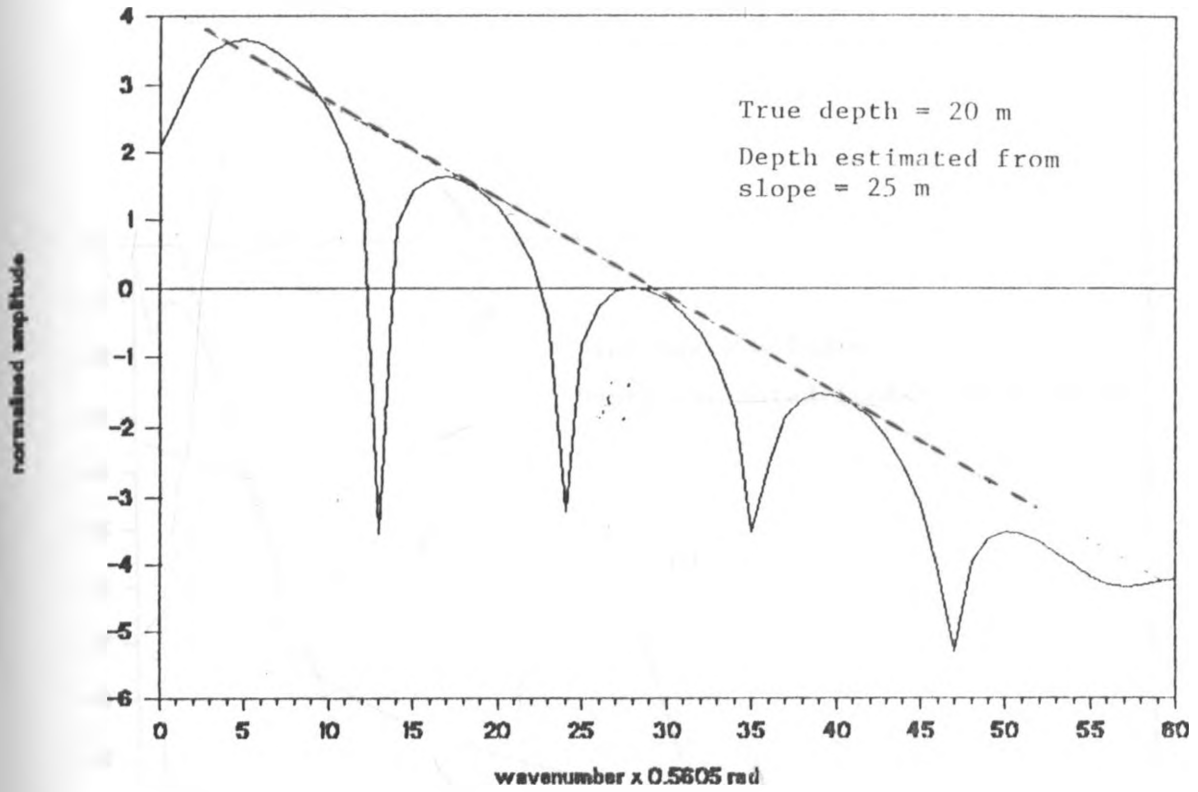


Fig. 3-9(a) Wavenumber-domain amplitude spectra for the plate model

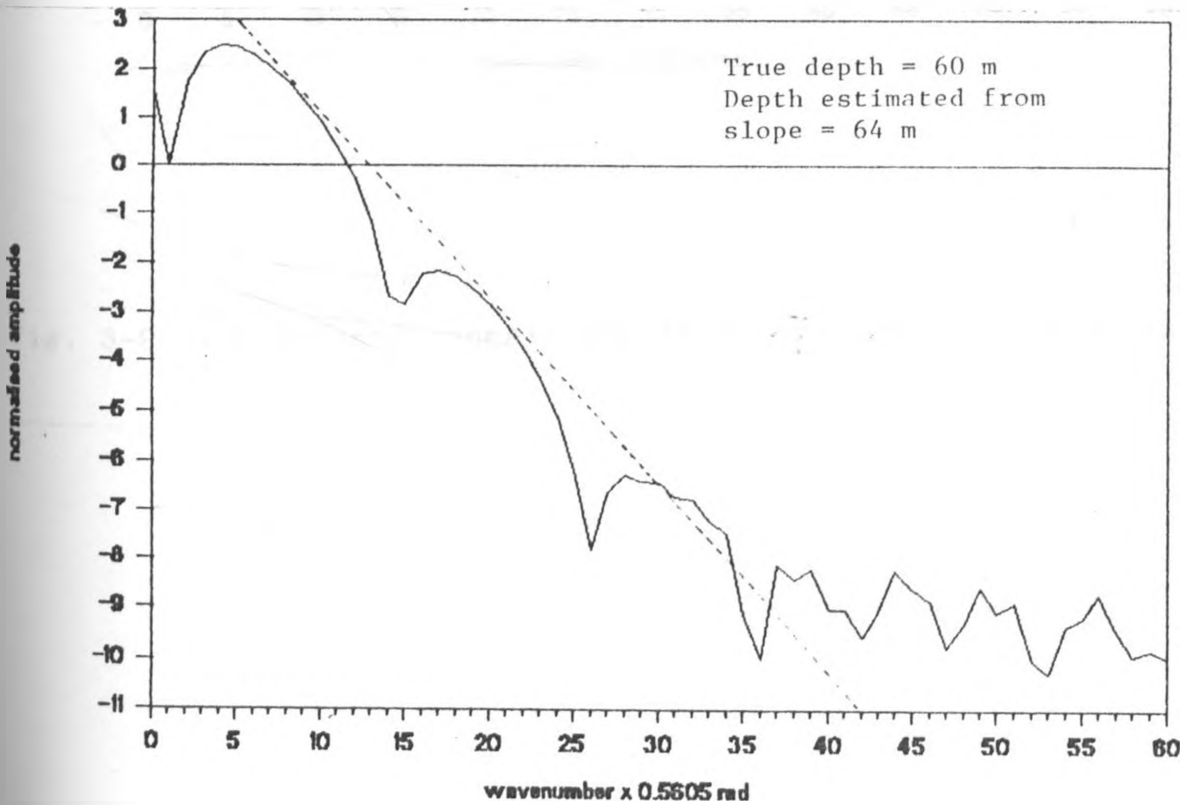


Fig. 3-9(b) Wavenumber-domain amplitude spectra for the plate model

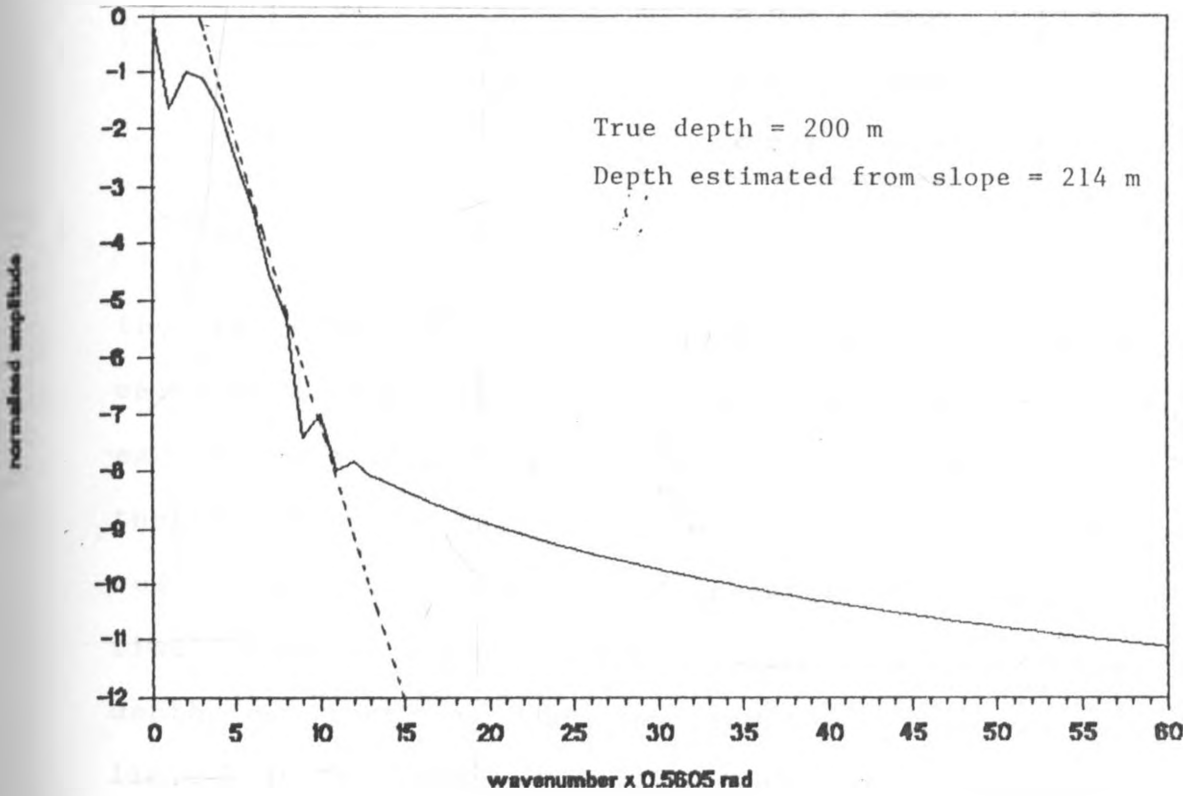


Fig. 3-9(c) Wavenumber-domain amplitude spectra for the plate model

Table 3.4 Depth estimates based on data generated using the plate model

True Dept (km)	estimated Depth (km)
.02	0.025 + .0005 -
.06	0.064 + .0005 -
.20	0.214 + .0005 -

the EM response for the depths specified above. The calculated slopes fairly well approximate the true depths except for a slight difference of about 3-5m in excess of the true depth. Other researchers (e.g. Bartel, 1990: pers. com.) have noticed the same difference while working on AEM time domain data generated using the PLATE program. For depths of over 200m, the amplitude spectrum is severely limited in the vertical range so that determination of the slope is unreliable (Figure 3-9(c)). The maximum depth of penetration is limited to about 150m with respect to the resolution of the amplitude spectrum.

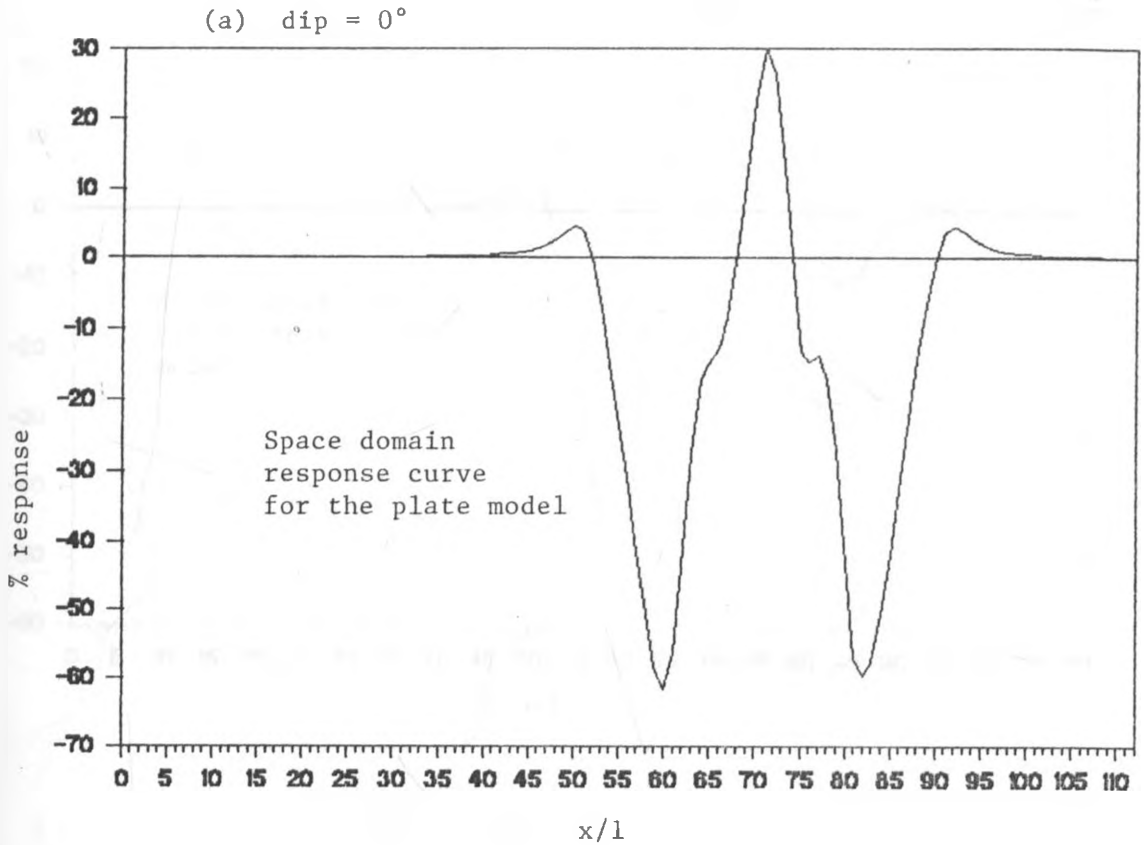
It was not possible to use the method of harmonic analysis to estimate depth in as much as the quality of the spectrum was not good enough to allow the determination of the zero harmonic and then use the graph in Figure 3-5. The complications arise from numerical inaccuracies associated with the PLATE program.

3.2.3 Effect of Dip on Amplitude Spectrum

The effect of depth on the amplitude spectrum has so far be noted to be an increase in slope with increasing depth in the wavenumber domain. In the space domain this has been manifested as broadening and dampening of the simulated anomaly profiles. The changes in slope in the amplitude spectrum in both the wire and the plate model have been demonstrated.

The effect of dip in HLEM anomalies on the other hand is interesting. Since the HLEM configuration is symmetrical, a range of dips within 0° - 90° were studied. Since so far the plate model amplitude spectra considered have been for vertical targets, the case for 90° dip is ignored. Figures 3-10(a)-(d) show a series of simulated field data profiles and their corresponding amplitude spectra. Both a very shallow dip of 5° and a horizontal target are considered.

Figures 3-10(a)-(d) shows the effect of increasing dip from 0° to 45° . It may be noticed that, spectral noise increases with decreasing dip. In fact, for horizontal targets the amplitude spectrum cannot reliably be used to estimate the depth by means of the slope. From Figure 3-10(a) , it is possible to make out an indistinctly decaying amplitude spectrum up to about 15 rad., which gives a depth estimate of about 34m. This is greater than the true depth by over 14m. While it is very difficult to use



Amplitude spectrum:

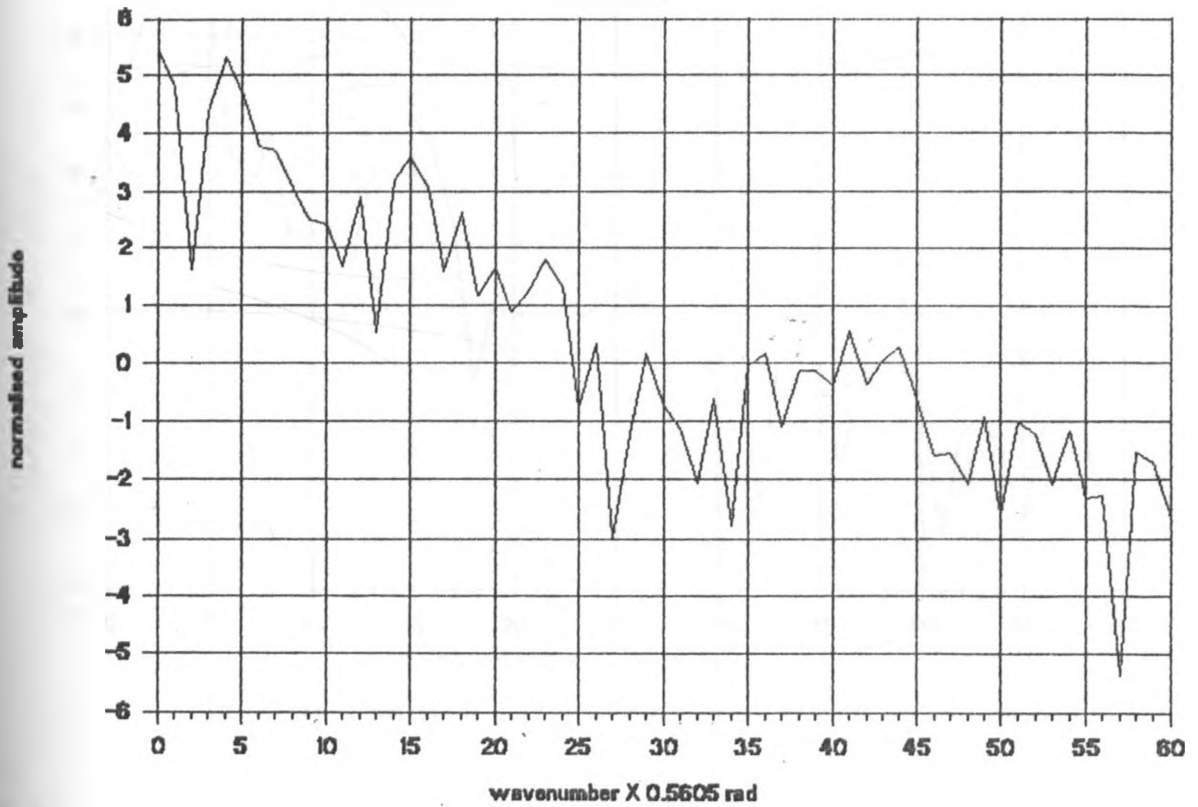


Fig. 3-10. Space domain profiles and their corresponding amplitude spectra for the plate model. Note anomaly response changes with

(b) dip = 5°

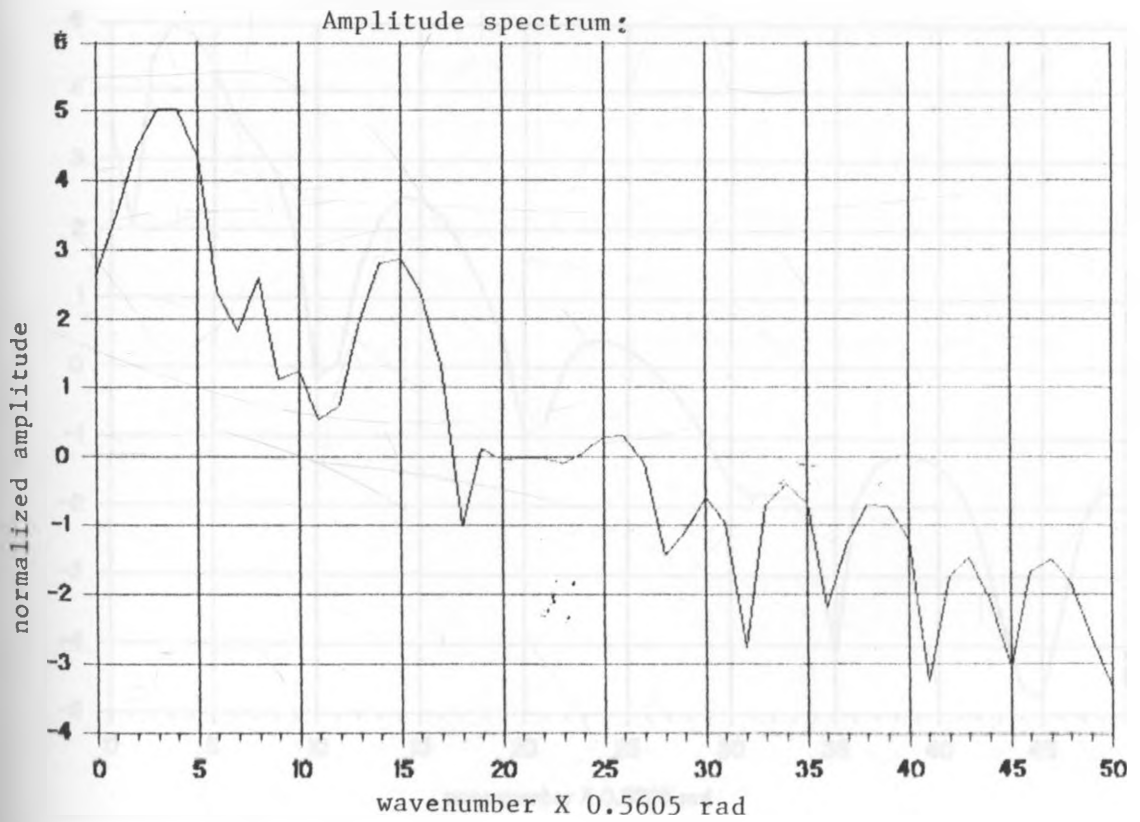
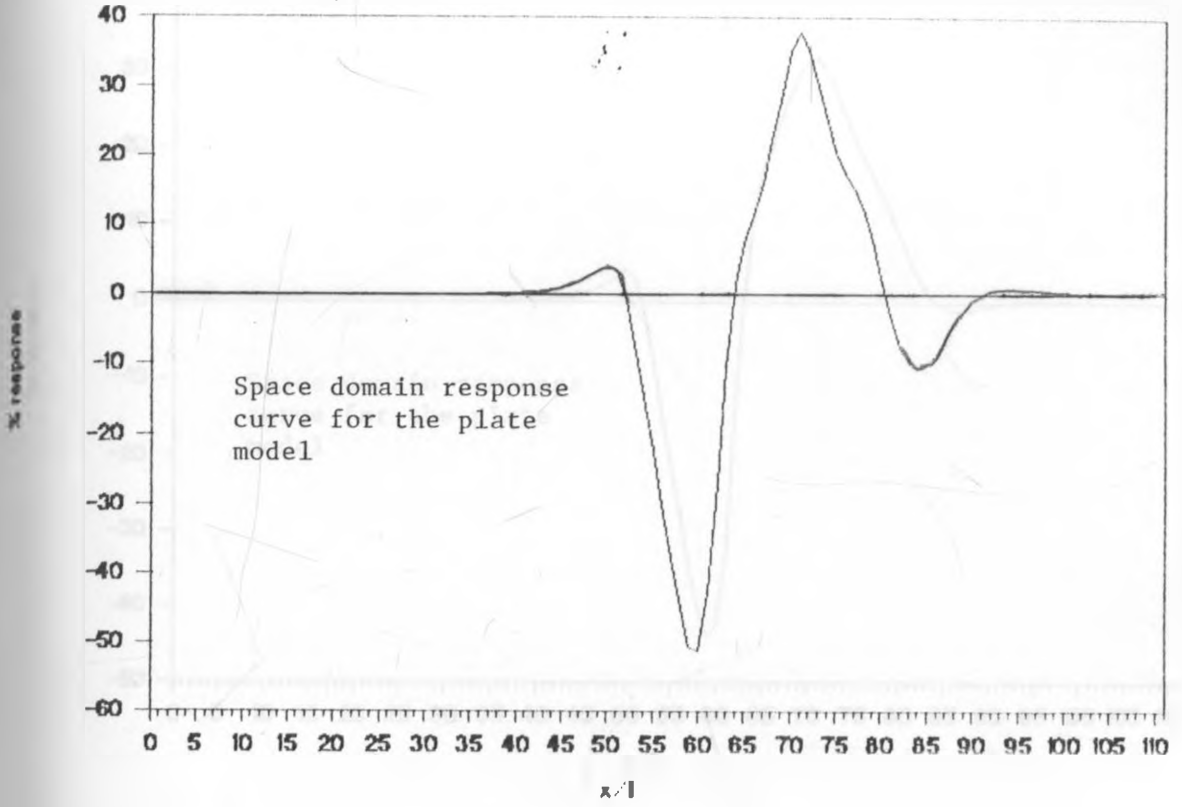
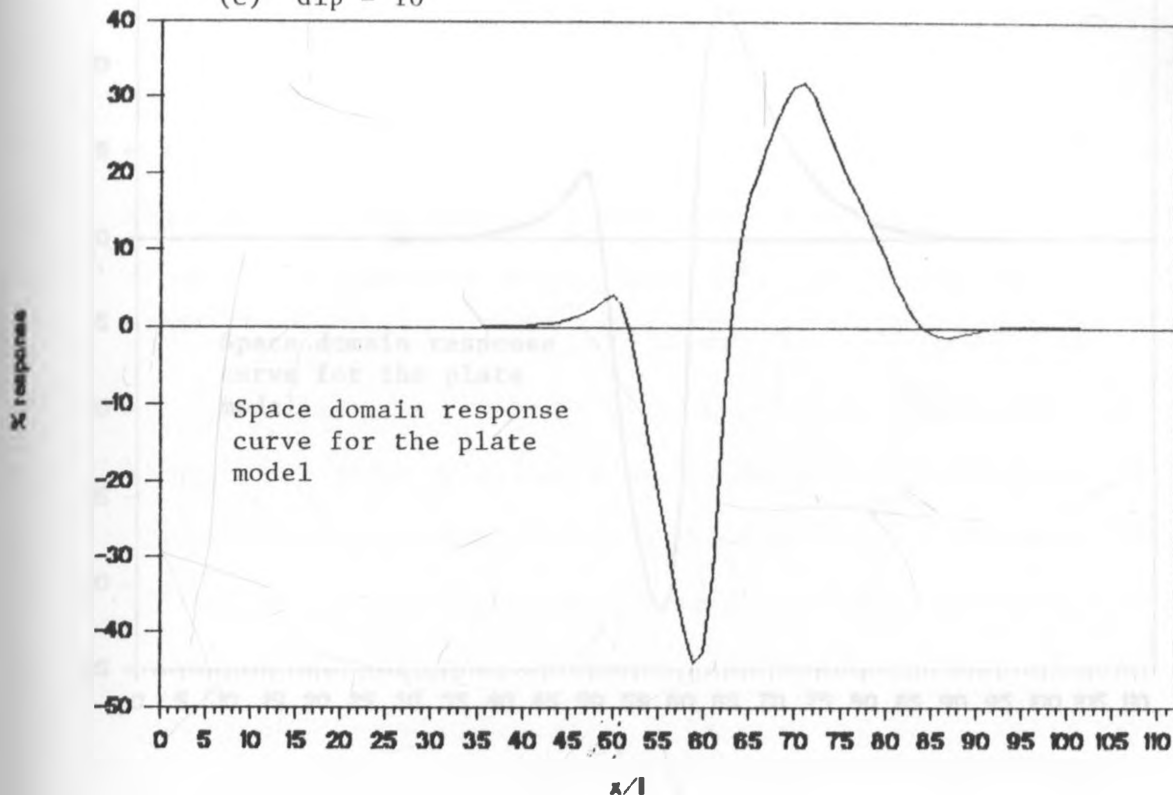


Fig. 3-10 contd.

(c) dip = 10°



Amplitude spectrum:

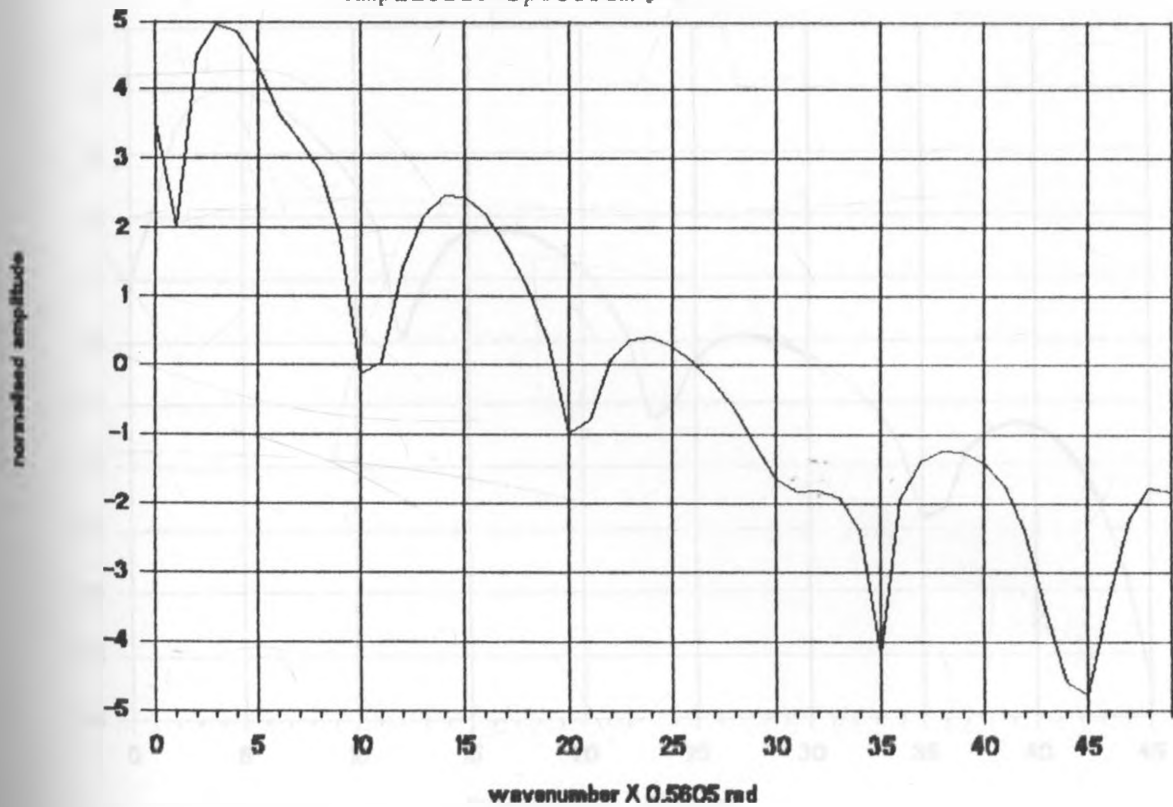
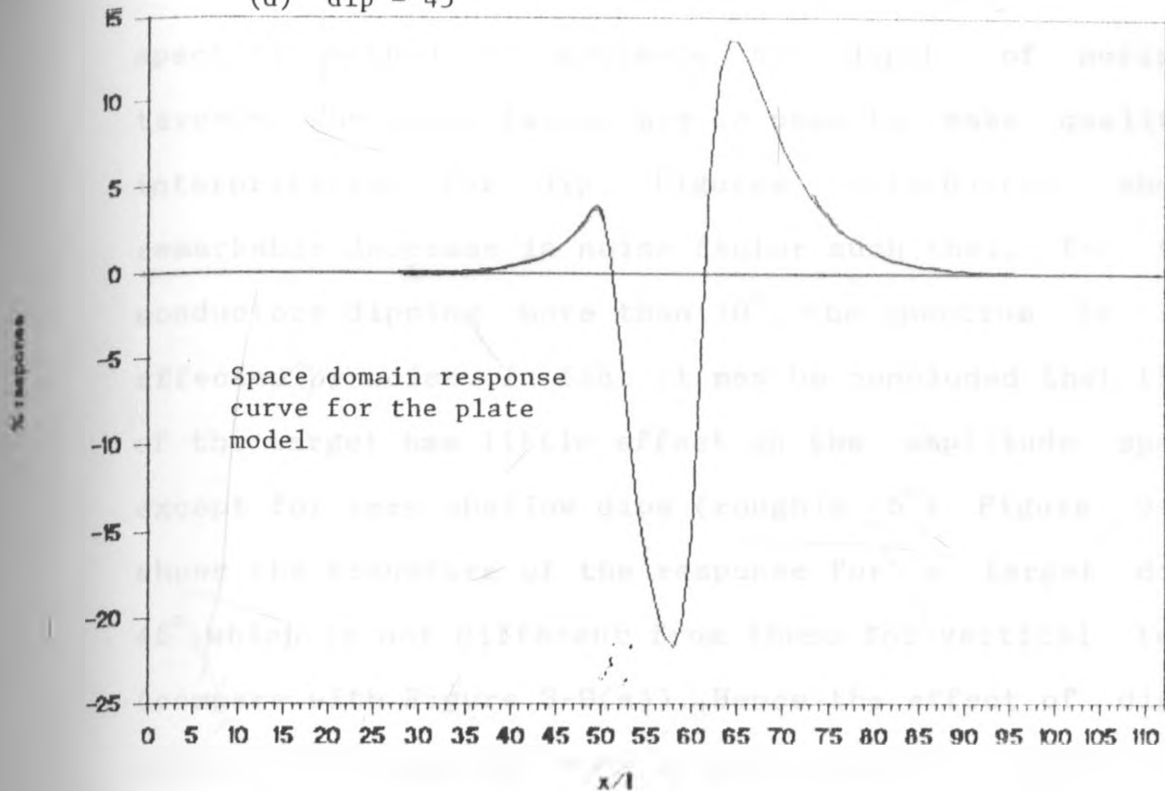


Fig. 3-10 contd.

(d) dip = 45°



Amplitude spectrum :

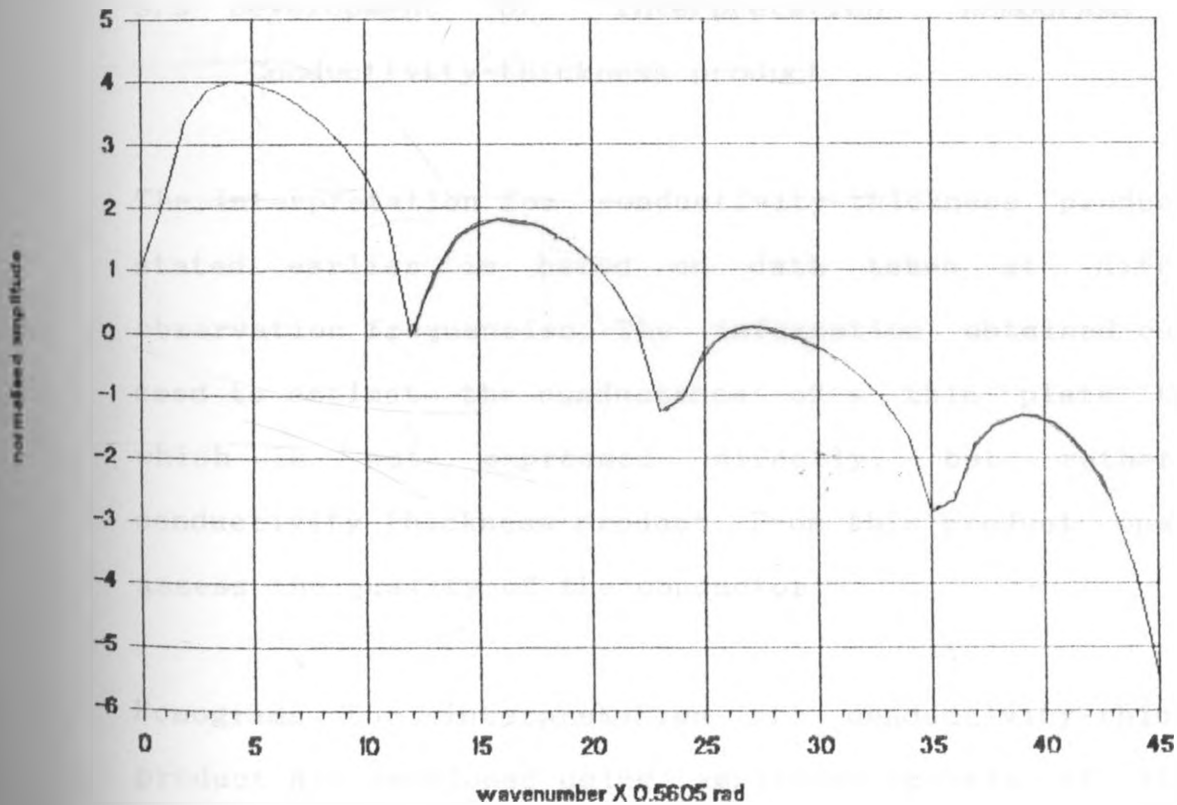


Fig. 3-10 concluded

spectral method to estimate the depth of horizontal targets, the noise factor may be used to make qualitative interpretation for dip. Figures 3-10(b)-(c) show a remarkable decrease in noise factor such that, for target conductors dipping more than 10° , the spectrum is little affected by noise. In fact it may be concluded that the dip of the target has little effect on the amplitude spectrum except for very shallow dips (roughly $<5^\circ$). Figure 3-10(d) shows the transform of the response for a target dip of 45° , which is not different from those for vertical targets (compare with Figure 3-9(a)). Hence the effect of dip can safely be disregarded when interpreting for depth in the wavenumber domain.

3.3 Development of Interpretation Nomograms for Conductivity-thickness product

The interpretation for conductivity-thickness product as stated earlier is based on data taken at different observation frequencies. The information obtained can be used to estimate the conductance of a thin plate target which is not expressed directly, but rather as conductivity-thickness product. From this product one can assess the quality of the conductor.

Nomograms for interpretation of conductivity-thickness product are developed using amplitude spectra of the EM responses for the plate model taken at the following frequencies: 222, 444, 888, 1777, and 3555 Hertz which are

the most commonly used operating frequencies in HLEM prospecting. Other sets of frequencies may be used to construct a similar interpretation nomogram. Different conductivity-thickness products are used for each set of five frequencies in an increasing order. In this work the conductances used range between 10 and 100 $S M^{-1}$.

In the transform domain the amplitude of the spectrum was determined at 16.81 radians for each frequency for every value of the conductivity-thickness product.

The amplitude scale was normalised with the amplitude of the highest frequency which is always equal to one. The same procedure can be used to construct nomograms if different values of frequencies or conductivities are desired.

The nomogram shown in Figure 3-11(a) was developed for the HLEM system using the specifications stated above. The vertical axis represents the normalised amplitude while the horizontal axis represents the conductivity-thickness product. The different curves represent the relative magnitude (to the highest frequency response) of the amplitude spectra using the five operating frequencies measured at 16.81 radians.

To use Figure 3-11(a), the interpreter should evaluate the amplitude spectra for the different frequencies at

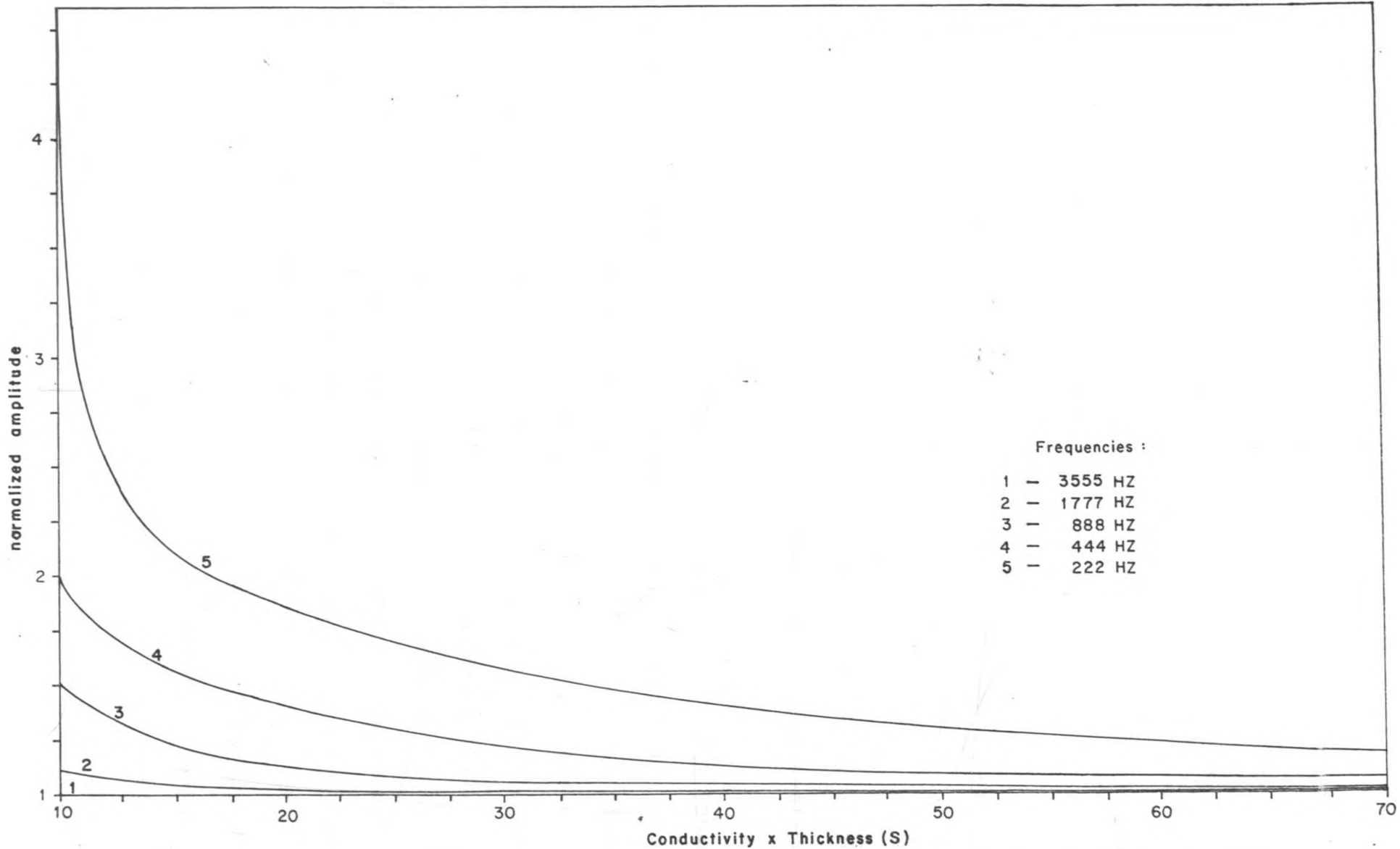


Fig. 3-11(a) A nomogram for determination of conductivity-thickness product for ground horizontal loop EM system. Vertical scale is normalised by the amplitude of the highest frequency and Spectra are measured at 22.42 rad.

approximately 16.81 radians and transfer them on a semilog-paper on the same scale as Figure 3-11(a). Normalisation by the highest frequency (3555Hz) value can be achieved by shifting vertically so that the highest frequency amplitude falls on the highest frequency curve in Figure 3-11(a). The relative spacing between the other frequency amplitudes can be matched by horizontal adjustment along the conductivity-thickness product axis. Once the amplitudes of the five frequencies are satisfactorily matched, the conductivity-thickness product can be read on the horizontal scale. The measured values are independent of dip or depth, and estimates of conductivity-thickness product from Figure 3-11(a) should be better than space domain determinations because the spectral analysis method relies on a broad base of data that has been transformed and it is unaffected by the migration of the peak anomaly in the space domain (Bartel and Becker, 1988).

It was noticed that at conductivity-thickness products higher than 100S the nomogram of Figure 3-11(a) cannot be accurately used to estimate the conductivity-thickness product since the amplitude curves crowd together and become almost 'parallel', making the match point ambiguous. Fortunately, the range used covers the conductivity-thickness product of most massive sulphide deposits. Reference to the nomogram in Figure 3-11(a) may be made in chapter 7 where field examples are tested.

Figure 3-11(b) shows a nomogram constructed from amplitude spectra read at 22.42 radians for a maximum value of the conductivity-thickness product of 50s. This nomogram can similarly be used the same way as the previous one. It emphasises the liberty of choosing any wavenumber (within a valid range) to construct the nomogram. An important problem that arises is the very rapid convergence of the curves with the wavenumber. However, using a larger scale this problem can be alleviated.

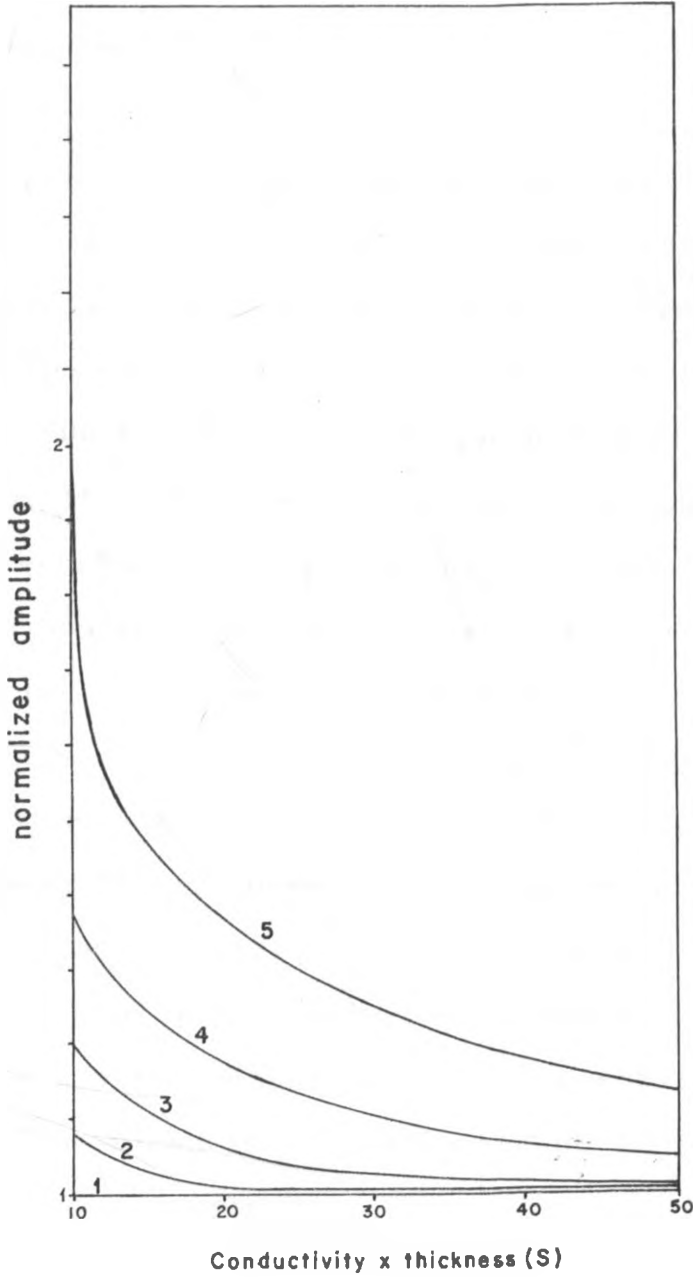


Fig. 3-11(b) A nomogram for determination of conductivity-thickness product for ground horizontal loop EM system. Spectra are measured at 22.42 rad.

CHAPTER FOUR

4.1 Field Studies in Western Kenya

4.1.1 Introduction

Field studies were carried out on data available from the Ministry of Environment and Natural resources. This data were taken from Western Kenya (Macharia and Barongo, 1982) which is largely a greenstone belt lying within the north-eastern flank of the Tanzanian Craton whose age ranges from 2800[±]120 to 2500[±]100 my (Dodson et al., 1975; Bell and Dodson, 1981). It is bounded to the east by the Mozabiquian mobile belt. This greenstone belt is similar to those found in Canada, Australia and Southern Africa (Sanders, 1964)-all of which have been subject to a lot of geophysical research for ore deposits.

The common mineralisation in the greenstone belt is gold in association with silver, both of which occur largely in small quartz veins or reefs, and metallic sulphides such as pyrite, chalcopyrite, pyrrhotite, galena and sphalerite. Several outcrops of pyrite deposits, commonly associated with thick graphite zones, can be seen in the area. Most mines in this area are no longer operational due to a decline of economic reserves.

4.1.2 Outline of Geology of The Area

Rocks in this area fall into four groups: The Nyanzian, the Kavirondian, the Basement and the Bukoban Groups. The four groups are in some areas overlain by Tertiary and

Quaternary lavas. Radiometric dating on rock samples has been carried out at various stages by Dodson et al. (1975), Saggerson (1978), Bell and Dodson (1981), Cahen et al. (1981) and Kagami et al., (1983). The Nyanzian Group (age 3100-2800 Ma) consists of acid, basic and intermediate volcanic rocks and their tuff equivalents. There are also gold bearing intrusive granites and interbedded sediments. The basic lavas consist of metabasalts and pillow lavas while rhyolites, andesites, dacites, welded tuffs and agglomerates make up the acid and the intermediate rocks. Present also are boulder conglomerates, quartzites and banded ironstones. The Kavirondian Group (age 2800-2500 Ma) occurs in association with the Nyanzian Group separated by an angular unconformity both with the same structural grain. The Kavirondian Group is a sedimentary derivative of the Nyanzian Group and consists of alternating sediments of mudstones, grits and conglomerates. Both groups are intruded by huge batholiths of granites and granodiorites. Other intrusives include post-Kavirondian ophitic quartz-diorite dykes. The highly metamorphosed Mozabiquian belt (age 750-500 Ma) to the east is younger than both the Nyanzian and Kavirondian Groups, while the Bukoban Group (age 1200-900 Ma) to the south represents both volcanic and sedimentation episodes at the margin of the Nyanzian Group.

4.1.3 Airborne Geophysical Survey

In late 1977, a combined airborne electromagnetic and magnetic survey was flown in the greenstone belt of Western

Kenya by Terra Survey Limited of Ottawa, Canada, on behalf of the Kenya Government. This airborne survey covered five discrete blocks of country and was aimed at selecting priority targets for ground follow up campaign in a quest for massive sulphide deposits. A towed-bird time domain MK 5 INPUT AEM system and a geometrics G-108 nuclear precession magnetometer were used. The survey was flown at a terrain clearance of 120 m and flight-line spacings of 200-500 m. AEM anomaly maps were constructed at scales of 1:25,000, 1:50,000 and 1:125,000. Less than 25% of all the AEM anomalies were considered to be due to probable bed-rock conductors, while a majority of the rest are due to the weathered layer.

4.1.4 Ground Geophysical Follow-up Survey

The data used to test the interpretive procedure developed in this work are taken from 'Area 1', which is part of the areas designated 'Areas 1-5' covering a total of 4,000 km². (Figure 4-1). The AEM anomaly maps show strong isolated cases associated with bedrock conductors and a majority of broad, relatively weak cases associated with surficial conductors. These were confirmed by drilling results (Macharia and Barongo, 1982) to be due to the effects of conductive overburden layer. This does not, however, rule out the possibility of massive sulphide deposits. The ground follow-up survey carried out soon after the completion of the AEM survey delineated interesting conductors some of which were proved to be disseminated sulphides through

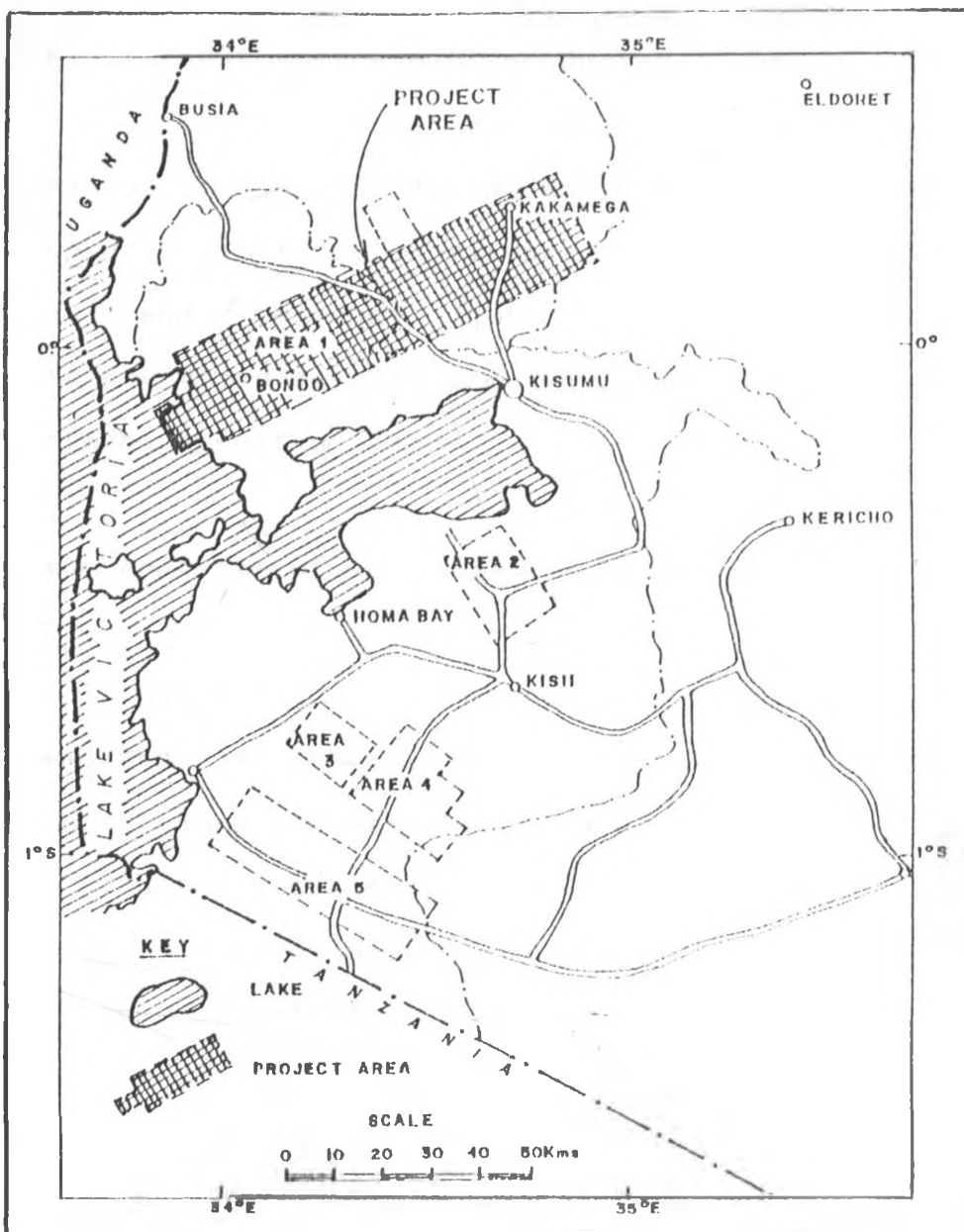


Fig 4-1. Map to show areas flown by combined INPUT AEM/AEROMAGNETIC survey in Western Kenya in 1977. Data used in this study is taken from the shaded area.

drilling (Macharia and Barongo, 1982; Barongo, 1983).

The ground follow-up initiated in January, 1978 concentrated in areas exhibiting promising anomalies ('Area 1'). The initial follow-up was based on vertical loop and VLF EM surveys. Later a HLEM ground survey using the Apex MaxMin II HLEM system was conducted which saw the acquisition of the data to be analysed in this work. The Field-work was done by the Mines and Geological Department of the Kenya; Ministry of Environment and Natural Resources (Macharia and Barongo, 1982). The data and their interpretation results are available from the ministry and department specified above.

4.2 Fourier Analysis of the Ground HLEM data

In chapter 3 synthetic data, which are noise free were transformed and as the results indicate the target parameters obtained through Fourier analysis are in good agreement with the starting model parameters. Here, the same procedure is used on the field data and hereinafter the parameters calculated using conventional techniques such as phasor diagrams and model curves will be compared with those obtained through Fourier analysis. This is due to unavailability of adequate drilling results.

Field data are prone to noise of various kinds, ranging from instrumental noise to that due to geological factors. Notably, field anomaly curves more often exhibit minor

anomalies superimposed on the major anomalies. By careful inspection, it is possible to smooth out these aberrations and consequently delineate the more prominent and desired anomaly for analysis. With noise levels of less than %1 relative to the peak anomaly in the profiles, one can always make some reasonable interpretation (Bartel and Becker, 1990)

For the purpose of interpreting for quality of the target conductor, profiles taken at the five operating frequencies, viz: 222, 444, 888, 1777, and 3555 Hz, should be used. Also, another important factor is the effect of conductive overburden layer. Anomaly profiles are selected where these effects are minimal. The overburden effects are manifest as shifting of the anomaly curves parallel to the vertical axis and less noticeably, a relative enhancement of the profiles. Methods for 'stripping' the overburden layer are available (Ferneyhough, 1985) but are not implemented in this work but are reserved for future work. However all the selected anomalies are treated in such a way as to minimise the effects of the overburden as will be described later. All in all, the fundamental objective is to make the anomaly profiles as ideal as possible without compromising the accuracy of the desired results.

There are two important effects of the overburden which are not taken care of in this work, namely :phase shifting and signal attenuation.

4.2.1 Procedure Adopted in Analysing the HLEM profiles

Profiles that are indicative of a vertically dipping plate are given preference. Those closely approximating the ideal (noise-free) profiles are selected. The following is a summary of the steps taken in analysing the profiles.

(a) Selection of anomaly profiles

The shapes of profiles closely approximating those generated either from the PLATE program (Dyck, et al., 1980) or the line current model (ideal cases) are selected for the five operating frequencies.

(b) Preparation of the anomaly profiles for interpretation

For purposes of calculating dip, a line parallel to the horizontal axis (traverse line) is drawn through the anomaly profile such that, the two trailing ends of the positive maxima are asymptotic to it, or approach this condition as much as possible. Missing trailing ends are extrapolated and any local anomalies are carefully smoothed out using the eyeball method.

(c) Fourier analysis

The selected profiles are suitably digitised and Fourier transformed using a 1024-point complex FFT. The amplitude spectrum is analysed in terms of the decay characteristics

and harmonic behaviour in order to determine depth. It is also used for estimating conductivity by means of the nomogram described in chapter 5 in which case the five operating frequencies become important.

(d) Estimation of dip

Dip is estimated by using a method described by (among others) Telford et al. (1990), and Grant and West, (1965). The ratio of the areas under the two shoulders of the anomaly curve become significant in this case. If the ratio is established then dip can be estimated with ease by using a graphical plot which represents the variation of the ratio with dip (David, 1966). Such a graph is shown in Figure 4-2.

4.2.2 Analysis of Field anomalies

Out of the many anomalies available from western Kenya only a few qualify to be subjected to the method of spectral analysis. The selected ones are mainly from Kaimosi, Ugenya and Yala areas. The noise factor which should be less than 1% of the largest negative peak anomaly (Bartel and Becker, 1990) is the major limiting factor. Though the anomalies were manually smoothed out to minimize geological noise, instrument noise, etc, the noise introduced by the overburden was hard if not impossible to manage. This can be appreciated in the useful range which can be attained in the wavenumber domain for determination of amplitude spectrum.

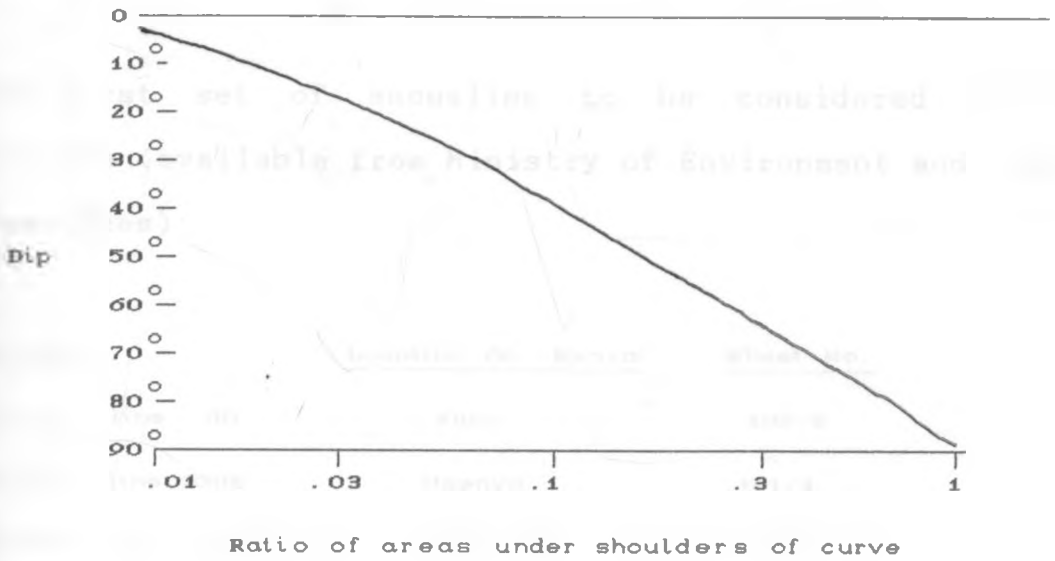
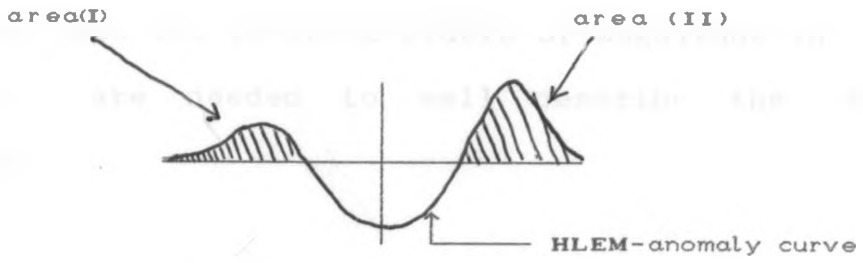


Fig. 4-2 Determination of dip of tabular conductor (After David, 1966)

One important fact to note is that high noise factor reduces the amount of useful range available for describing the spectrum by creating a noise 'floor'(Bartel and Becker, 1990). In fact two to three orders of magnitude in vertical resolution are needed to well describe the amplitude spectrum.

4.2.3 Results of Analysis

The first set of anomalies to be considered were as follows (available from Ministry of Environment and Natural Resources):

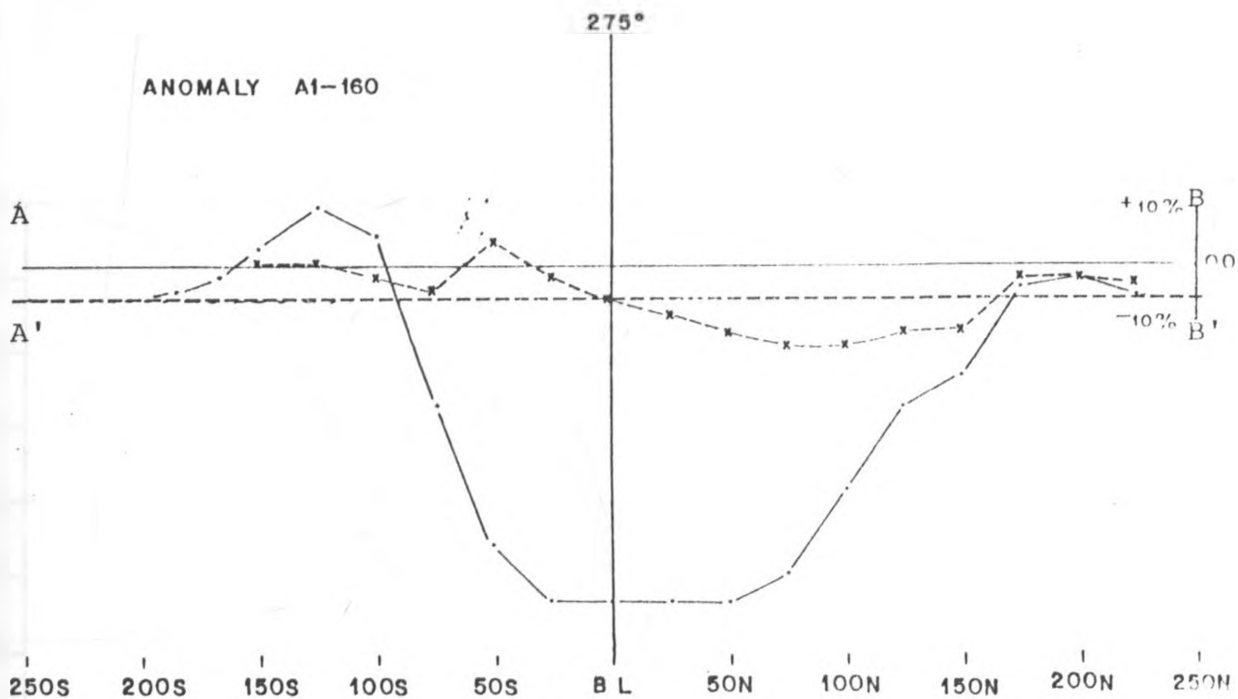
<u>Anomaly</u>	<u>Location (W. Kenya)</u>	<u>Sheet No.</u>
A1-160 line 00	Yala	102/3
A1-101 line 250E	Ugenya	101/4
A1-148 line 00	Yala	102/3
A1-221A line 250W	Kaimosi	102/4
A1-221A line 500W	Kaimosi	102/4

Anomaly profiles in this case were available only at two operating frequencies which makes them only analysable for depth using the spectral analysis method. The profiles for the first operating frequency (222 Hz) were considered owing to high noise factor at higher frequencies. The wavenumber range in which the spectrum was valid was up to 98.18 rad/km

(i) Anomaly A1-160 line 00

This is a fairly well defined anomaly. The maximum peak anomalies are -55 % and -9 % approximately for the real and the imaginary components, respectively. The imaginary part is very poorly defined and unreliable if phasor diagrams are used for interpretation of depth and conductivity-thickness product (Fig. 4-3(a)(i)). The real part is well defined except the trailing ends which are insufficiently determined. In order to make the anomaly approach the ideal shape, the traverse line is 'shifted' as described earlier in order to minimise the effect of conductive overburden. Shifting of the anomaly makes the imaginary part invalid. This makes the depth estimated using phasor diagrams unreliable since it can only be determined from unadjusted (unshifted) anomaly profile. This is an interesting case to do a comparison between results obtained using phasor diagrams and spectral analysis.

Figure 4-3(a)(ii) shows a plot of the computed amplitude spectrum of this anomaly. The spectrum is well defined and two slopes are determinable an average of which gives an error margin of + 6m. The estimated depth is about 74m. Interestingly, the depth estimated from phasor diagrams is extremely shallow (i.e less than 15 m.). This demonstrates how the conductive overburden severely affects the results. The spectral depth value, however, is not as much affected. (The conductive overburden effect tends to make the target



SCALE

0 50m

LEGEND

FREQUENCY (F) 222 Hz
COIL SEPERATION (L) 150 m

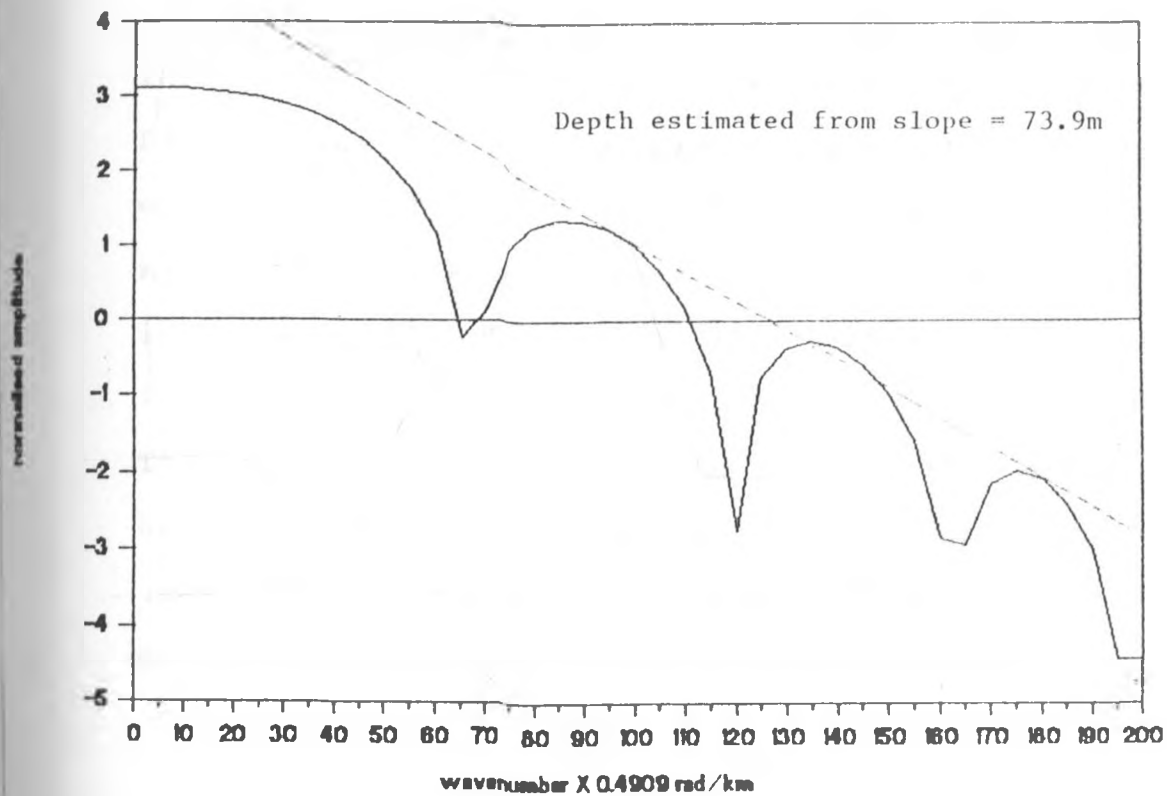
REFERENCE : IN-PHASE
QUADRATURE x---x---x



AB original traverse line

A'B' shifted traverse line to offset the effect of conductive overburden

Fig. 4-3(a).(i) Horizontal loop EM profile for the anomaly A1-160 at 222 Hz.



4-3(a)(ii) Amplitude spectrum for anomaly A1-160 line 00

look shallow. This effect is manifest in the conventional phasor diagram interpretation; apparently it is not evident in the spectral analysis case). The value of zero harmonic does not allow for determination of depth using the harmonic method(see Table 4.1 for results).

(ii) Anomaly A1-101 line 250 E

This is a well defined anomaly though the noise factor in the non-smoothed anomalies is over 1% of the peak anomaly. Both the real and the imaginary components are generally well defined. This is a case of low conductance since the magnitude of the real part is less than that of the imaginary part . The profile is 'shifted ' by redefining the traverse line as previously explained (Fig. 4-3(b)(i)). The peak negative values of the real and the imaginary parts are respectively -15% and -30% giving a depth estimate of less than 15m from phasor diagrams. This anomaly forms a good example for comparing the results obtained through the application of both the spectral analysis and phasor diagrams.

The computed amplitude spectrum for this anomaly is shown in Figure 4-3(b)(u) .The spectrum is well defined and allows fairly good determination of slope. Again a maximum and a minimum slope can be determined and the error margin is +9m. The estimated depth is 50m. This case is similar to the preceding one.

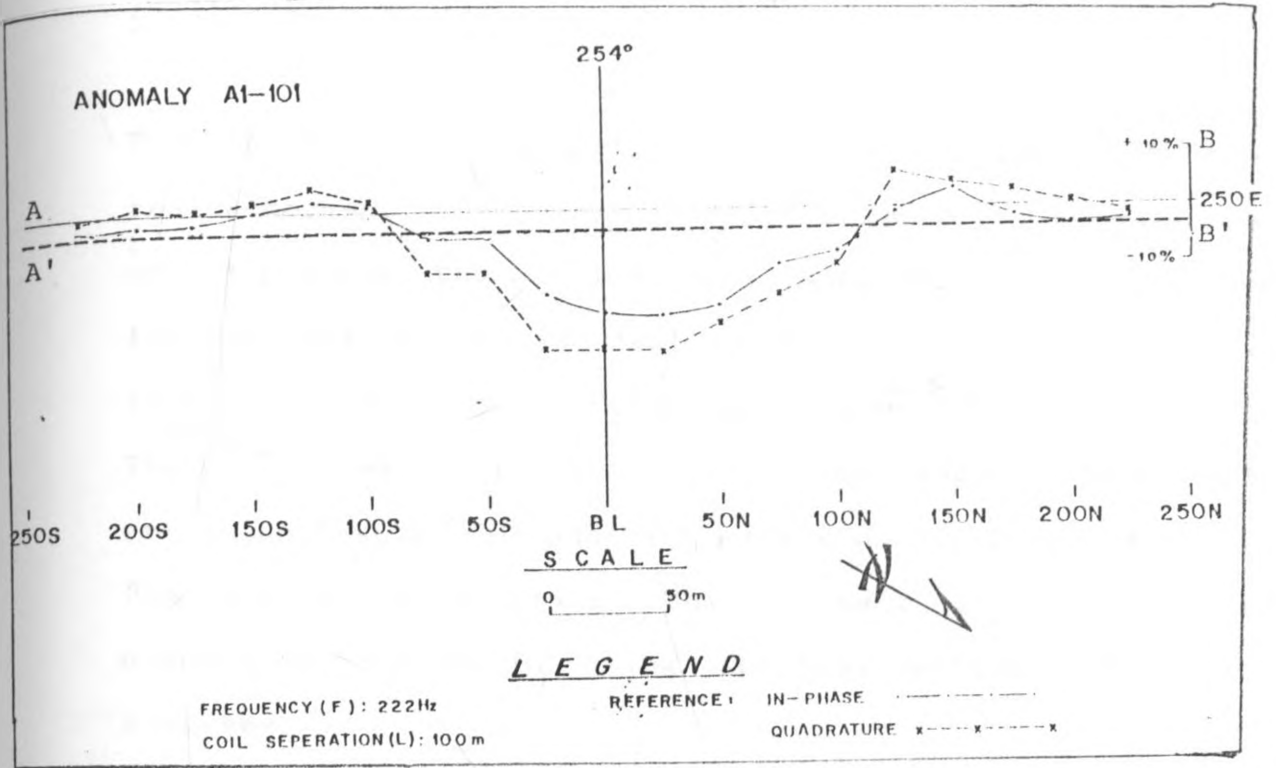


Fig. 4-3(b).(i) Horizontal loop EM profile for the anomaly A1-101 at 222 Hz.

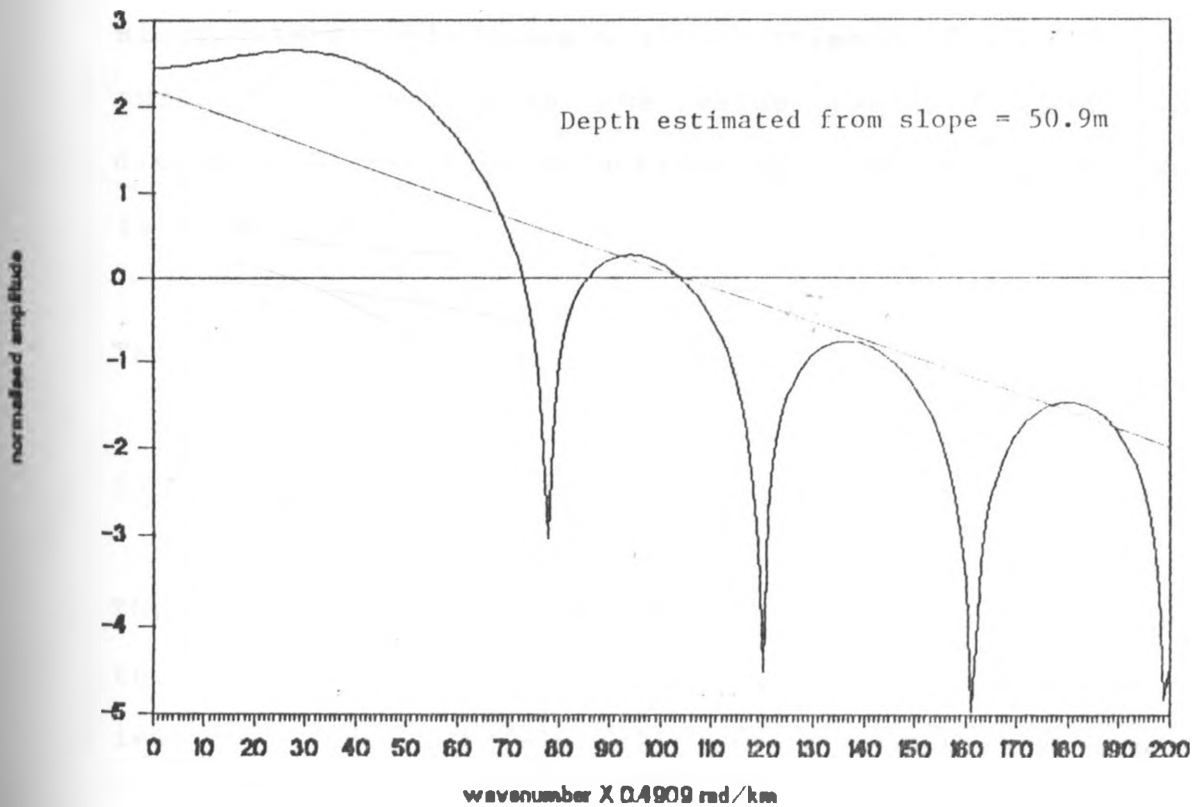


Fig. 4-3(b)(ii) Amplitude spectrum for anomaly A1-101 line 250E

The harmonic method is inapplicable in this case.

(iii) Anomaly A1-148 line 00.

This is also a fairly well defined anomaly especially the real component. The noise level for unsmoothed anomaly is over 1 percent. The pertinent peak anomalies do not lie on the same axis as should ideally be the case. The traverse line is redrawn for 'shifting' adjustment (Fig. 4-3(d)(i)). The peak anomalies for the real and the imaginary components are respectively -30% and -15% giving a depth estimate of 34m from phasor diagrams. This anomaly is suitable for comparison purposes in using spectral method and phasor diagrams.

The computed amplitude spectrum is shown in Figure 4-3(c)(ii). The spectrum is fairly well defined and the best slope determinable gives a depth estimate of 42m. This value agrees fairly well with the value reckoned using phasor diagrams. It may also be noticed here that the noise factor is fairly low.

The harmonic method cannot be applied in this case.

(iv) Anomaly 221A line 250W

This anomaly has the best defined real part as compared to the ones considered hitherto (see Fig. 4-3(d)(i)). The imaginary part is fairly well defined though much separated

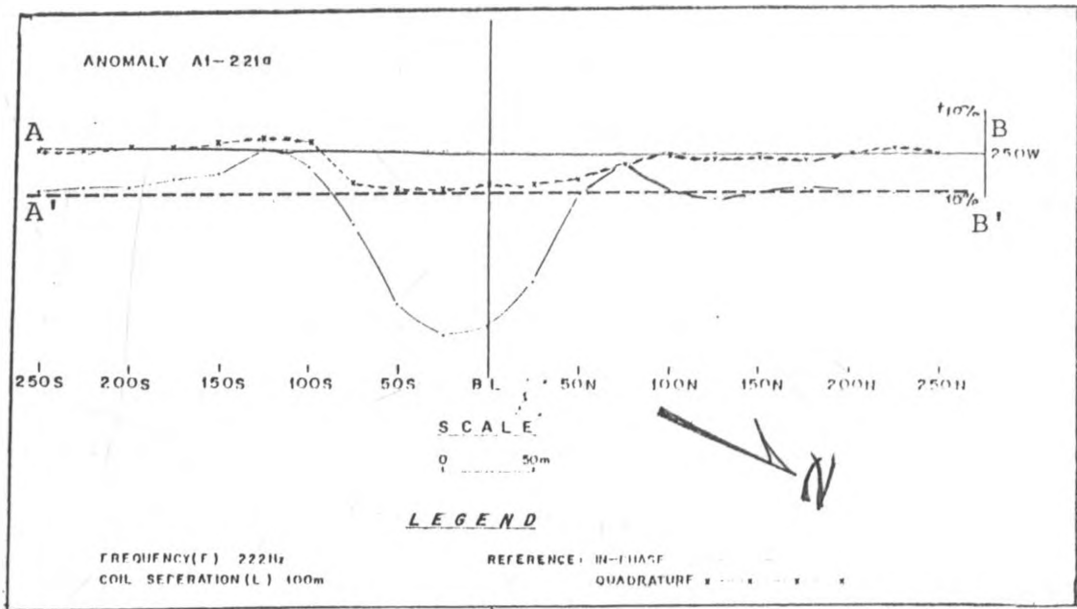


Fig. 4-3(d).(i) Horizontal loop EM profile for the anomaly A1-221A at 222 Hz

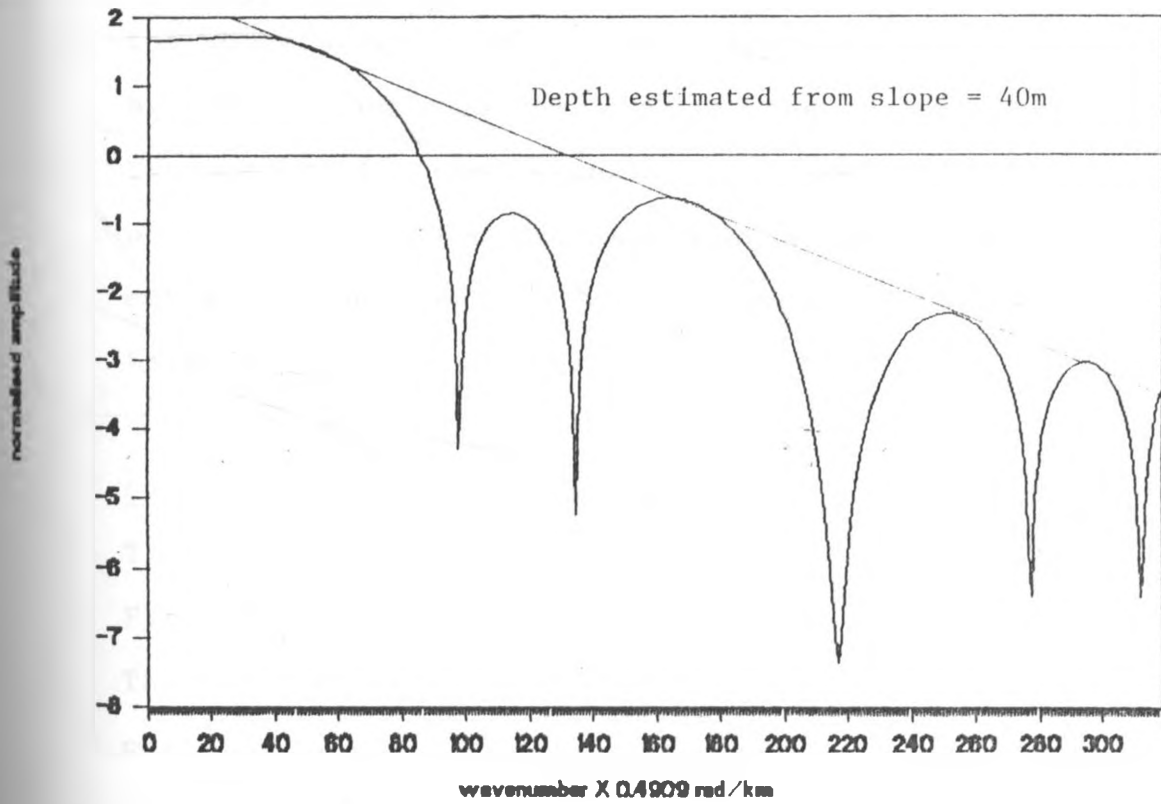


Fig. 4-3(d) (ii) Amplitude spectrum for anomaly A1-221A line 250W

and non-coincident with the real part. A 'shifting' adjustment of the traverse line makes the imaginary part invalid hence values of the peak anomaly for real and imaginary parts for use in phasor diagrams are read without any adjustment. Spectral analysis is performed on adjusted anomalies. The peak values for the real and the imaginary values are respectively -45% and -3% giving a depth estimate of 15m. From the increment of noise factor with frequency especially for the imaginary part and the separation of the two components, (real and imaginary) it is clear that this is a case in which the effect of conductive overburden is very severe, giving a very shallow depth interpretation by use of phasor diagrams.

Figure 4-3(d)(u) shows the computed amplitude spectrum for the above anomaly and it is fairly well defined. Except for a small incongruous second peak, the crests of the rest of the peaks lie in almost the same line. It was not possible to define a maximum or minimum slope in order to estimate error margin. The estimated depth is 40m. The harmonic method was again inapplicable.

(v) Anomaly A1-221A line 500W.

This anomaly is similar to (iv) above (compare with Fig.4-3(e)(i) below) and has the same limitations. The percentage values of the real and imaginary parts are respectively -45% and -2% with a 'shifting' adjustment giving a depth estimate of 15.4m using phasor diagrams. The unshifted case gives a

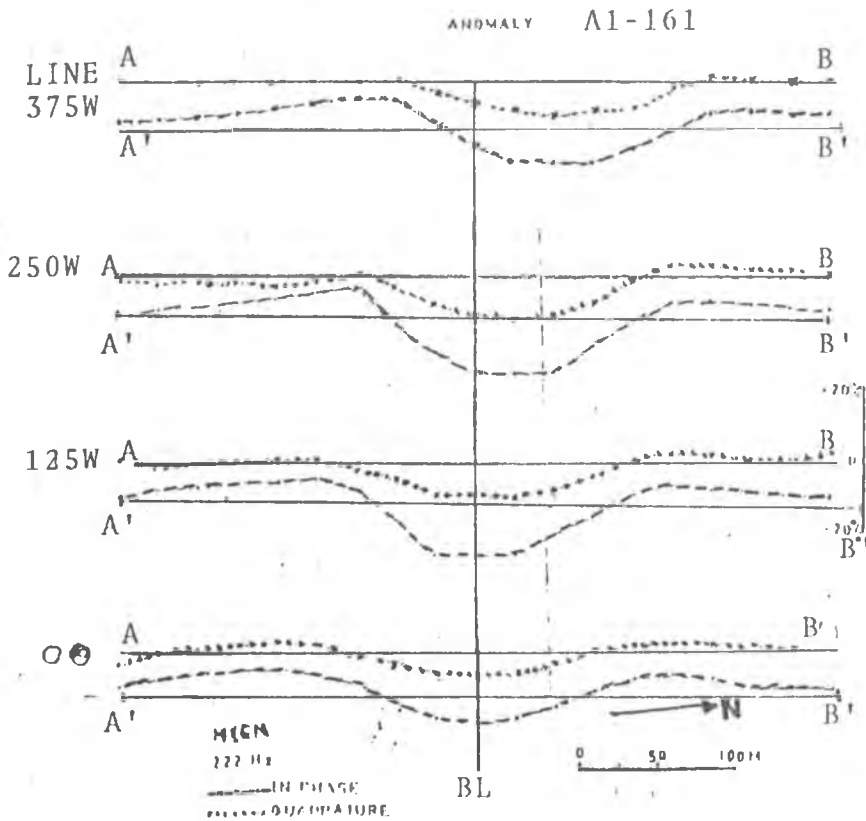
depth of less than 15m (see table 4.1).

Figure 4-3(e)(u) shows the computed amplitude spectrum. The maximum and minimum possible slopes that can be calculated give an estimated depth of about 42m with an error margin of $\pm 5m$. This case is similar to the preceding one.

The method of harmonic analysis was again inapplicable.

The second set of anomaly profiles to be considered were taken from anomaly A1-161 whose response profiles were taken along lines 375W, 250W, 125W and 00. The anomaly profile along line 375W was too noisy especially at the higher frequencies, and was consequently ignored. The anomalies were subjected to interpretation for depth at the first operating frequency. An attempt was made to interpret anomalies along lines 125W and 250W for conductivity-thickness product. Anomaly A1-161 was apparently suitable for conductance analysis because the anomaly profiles were available at the five operating frequencies. The anomalies are all well defined especially the real part. In general, these anomalies exhibit the same pattern with respect to shape at the corresponding frequencies. To avoid a duplication, a general description for all will suffice here as follows: The real part is well defined and has the expected shape for all the operating frequencies. For the first three frequencies viz 222, 444, 888 Hz the imaginary part is well defined besides having a noise factor relatively higher($>1\%$) than that in the real

(a) Frequency = 222Hz



Coil separation = 150m

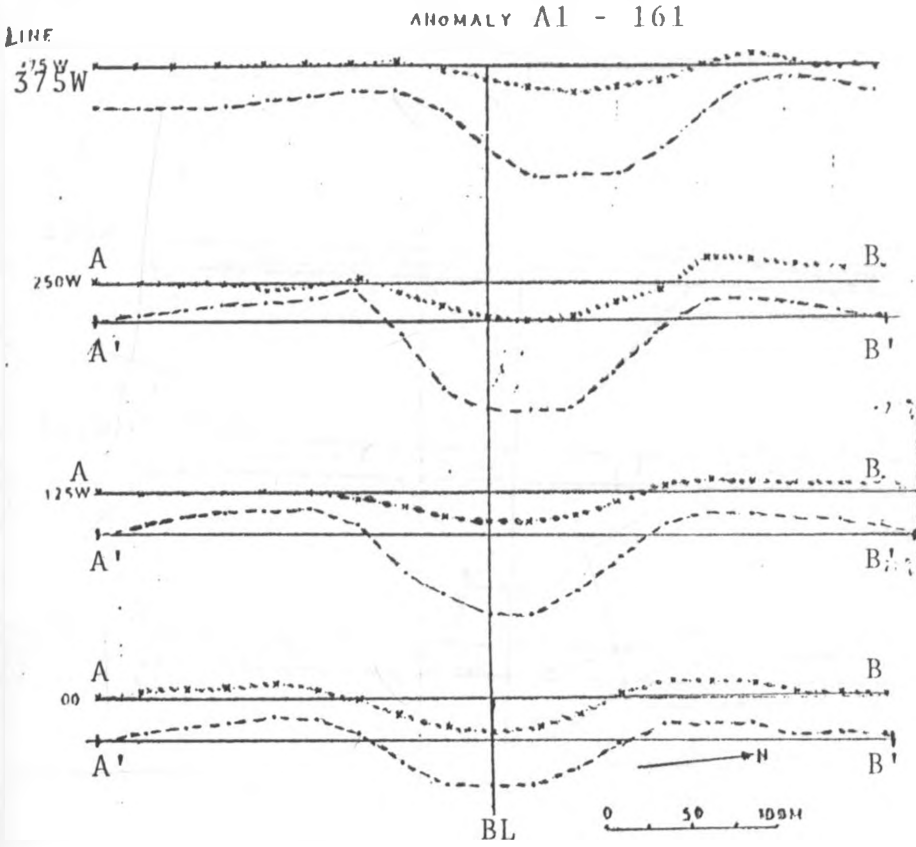
AB: original traverse line

A'B': shifted traverse line to offset the effect of conductive overburden

BL: baseline

Fig. 4-3(f).(i) Horizontal loop EM profiles for the five operating frequencies for anomaly A1-161

(b) Frequency = 444 Hz



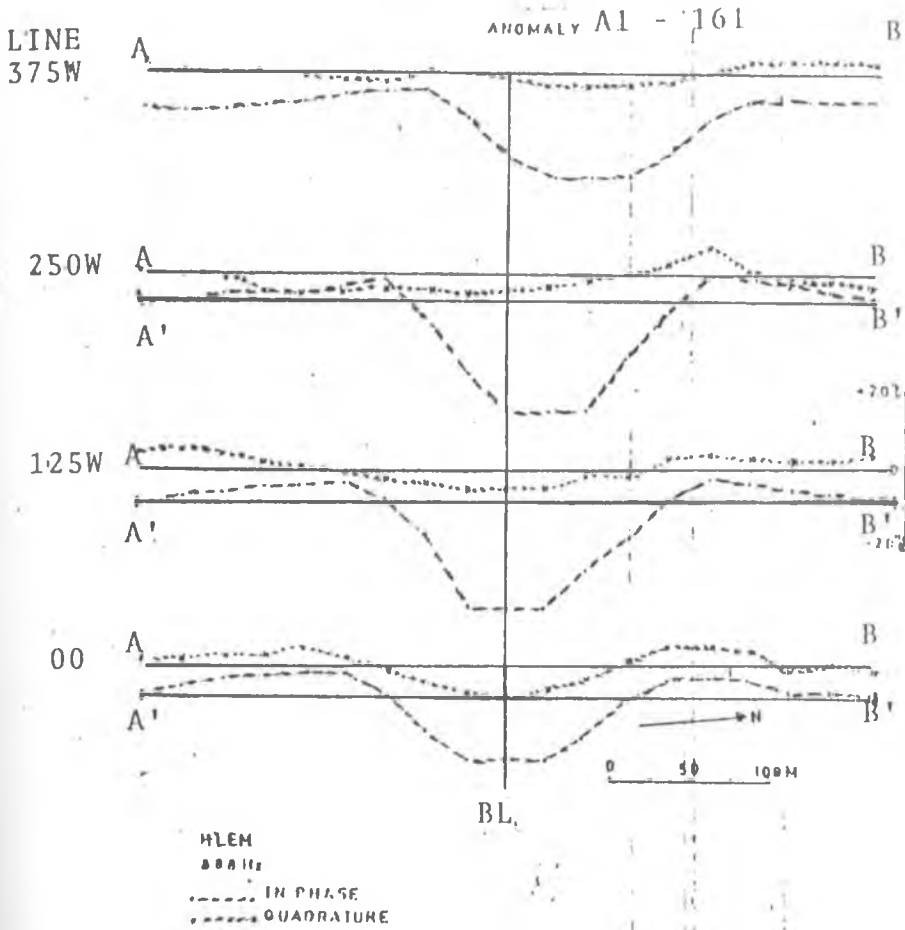
Coil separation = 150m

AB: original traverse line

A'B': shifted traverse line to offset the effect of conductive overburden

BL: baseline

(c) Frequency = 888Hz



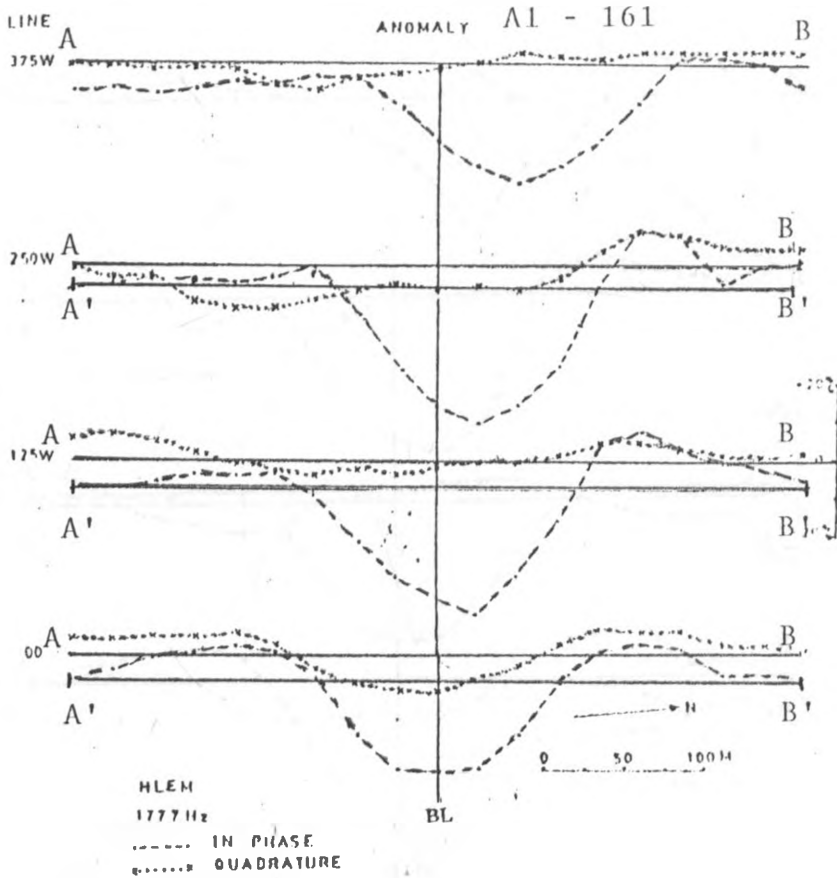
Coil separation = 150m

AB: original traverse line

A'B': shifted traverse line to offset the effect of conductive overburden

BL: baseline

(d) Frequency = 1777 Hz



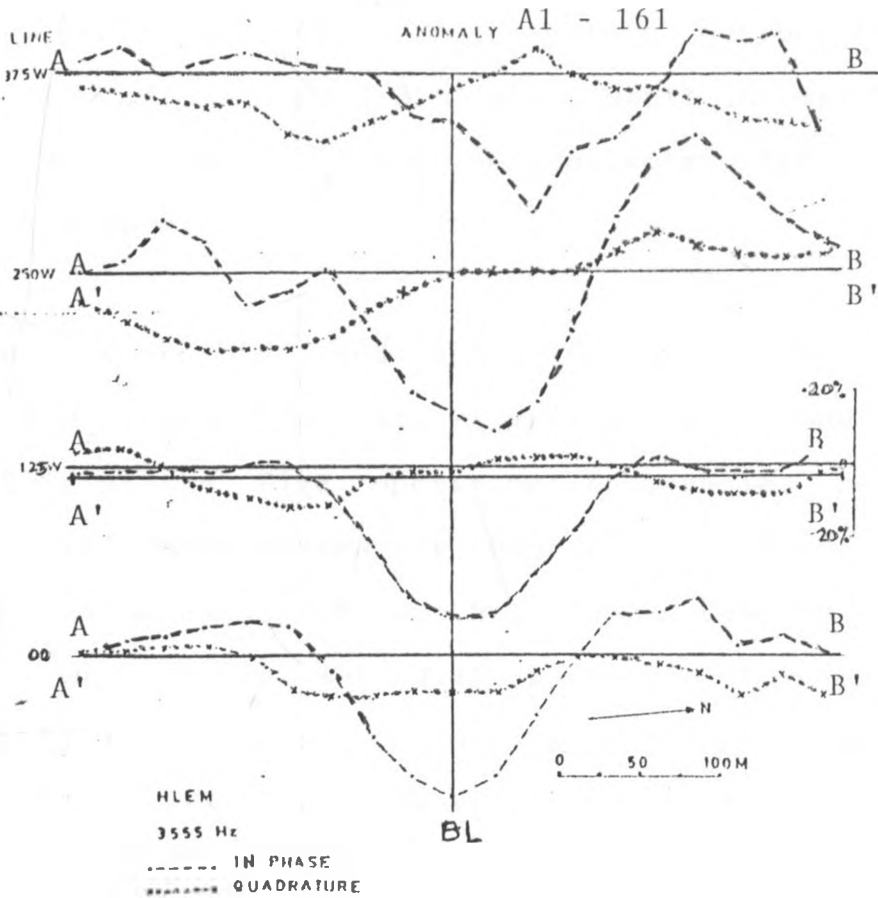
Coil separation = 150 m

AB: original traverse line

A'B': shifted traverse line to offset the effect of conductive overburden

BL: baseline

(e) Frequency = 3555 Hz



Coil separation = 150m

AB: original traverse line

A'B': shifted traverse line to offset the effect of conductive overburden

BL: baseline

NB: The amount of noise increases with the frequency of operation. This is mainly attributed to the effect of conductive overburden

part. At the remaining two frequencies, 1777 and 3555, Hz the imaginary part becomes considerably noisy (>5%). Another notable factor is that in all the anomalies the imaginary part is shifted vertically by about 5-10%, an aberration attributed to the effect of conductive overburden. Figures 4-3(f)(u) ,4-3(g) and 4-3(h) shows depth interpretation for lines 00, 125W and 250W respectively. The spectra are reliably good.

Figures 4-4(a)-(e) and 4-5(a)-(e) give the respective amplitude spectra for the anomaly A1-161 along lines 125 and 250W at the five operating frequencies respectively. Within the valid wavenumber range given earlier, depth could be estimated easily from the slope. However, the noise factor was too high making it impossible to determine the conductivity-thickness product. Any attempt to determine the latter parameter always gave totally unreliable results.

One interesting case lies in the amplitude spectra for lines 125W and 250W at 444Hz. These are exemplary of the expected amplitude spectra suitable for determining the conductivity-thickness product.

The only case that lent itself to harmonic analysis procedure to recover depth was anomaly A1-161 line 00. The useful wavenumber range was very limited (<62 rad/km). The available range gave an unreliable depth estimate from the slope of about 116m (see Fig. 4-3 (u)). The value of zero harmonic for which the real part falls to zero was reckoned

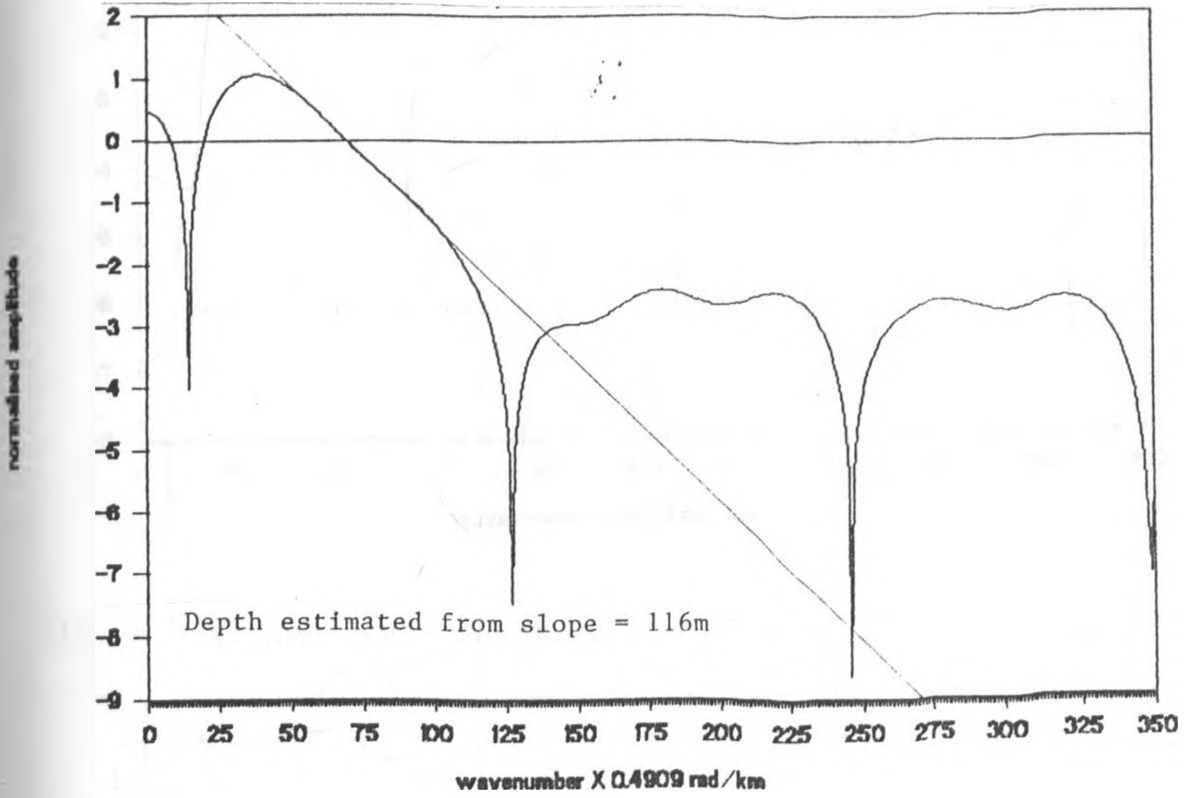


Fig. 4-3(f)(ii) Amplitude spectrum for anomaly A1-161 line 00 at 222Hz.

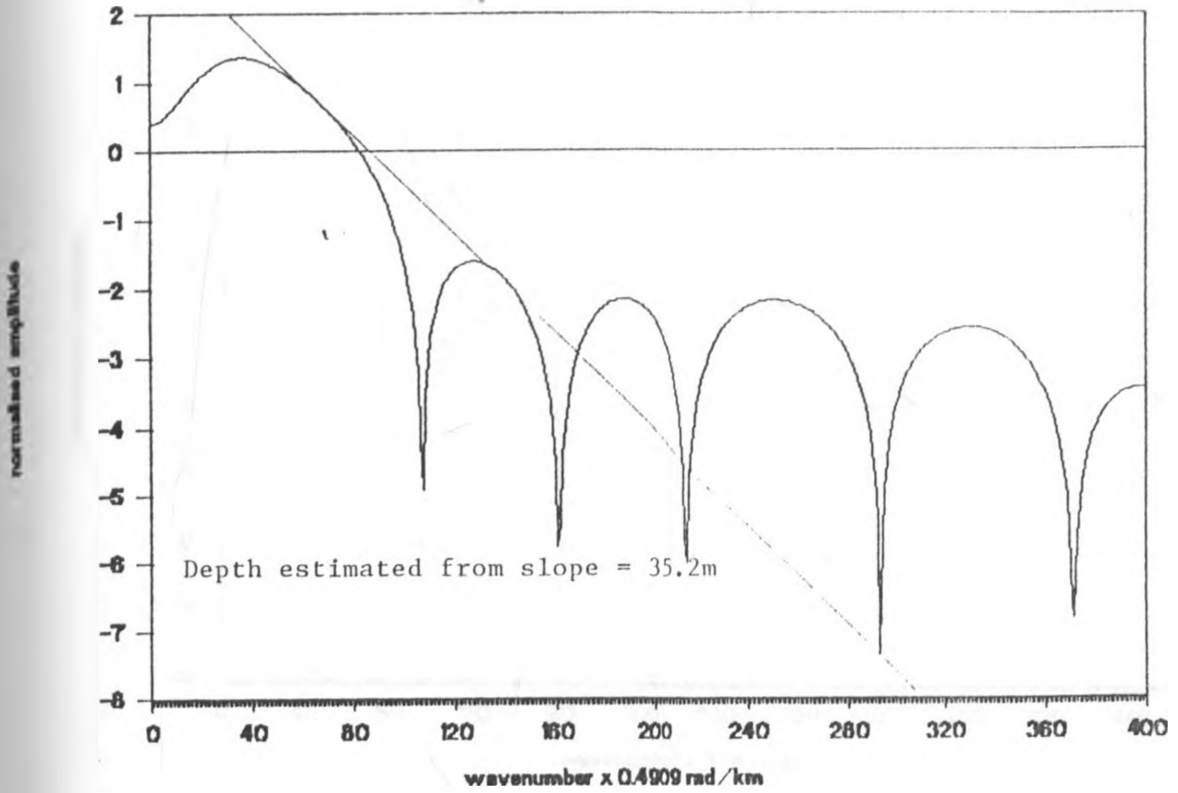


Fig. 4-3(g) Amplitude spectrum for anomaly A1-161 line 125W

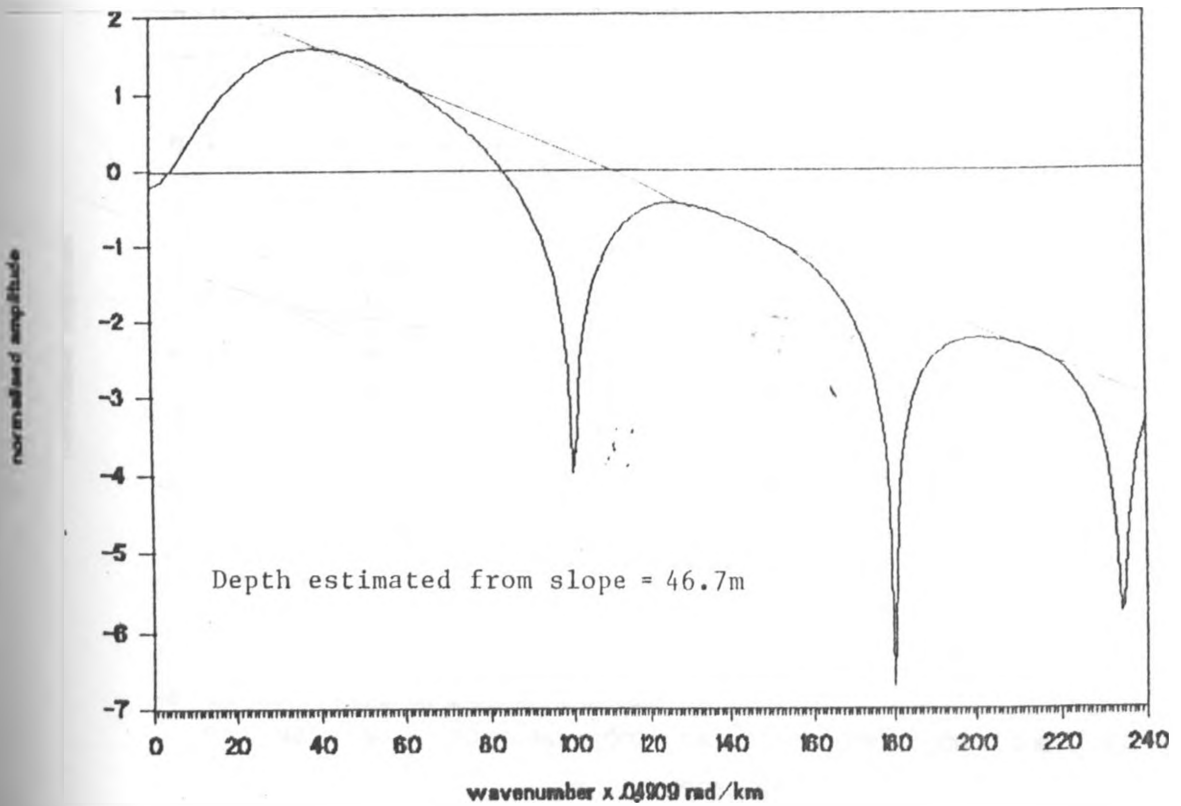


Fig. 4-3(h) Amplitude spectrum for anomaly A1-161 line 250W

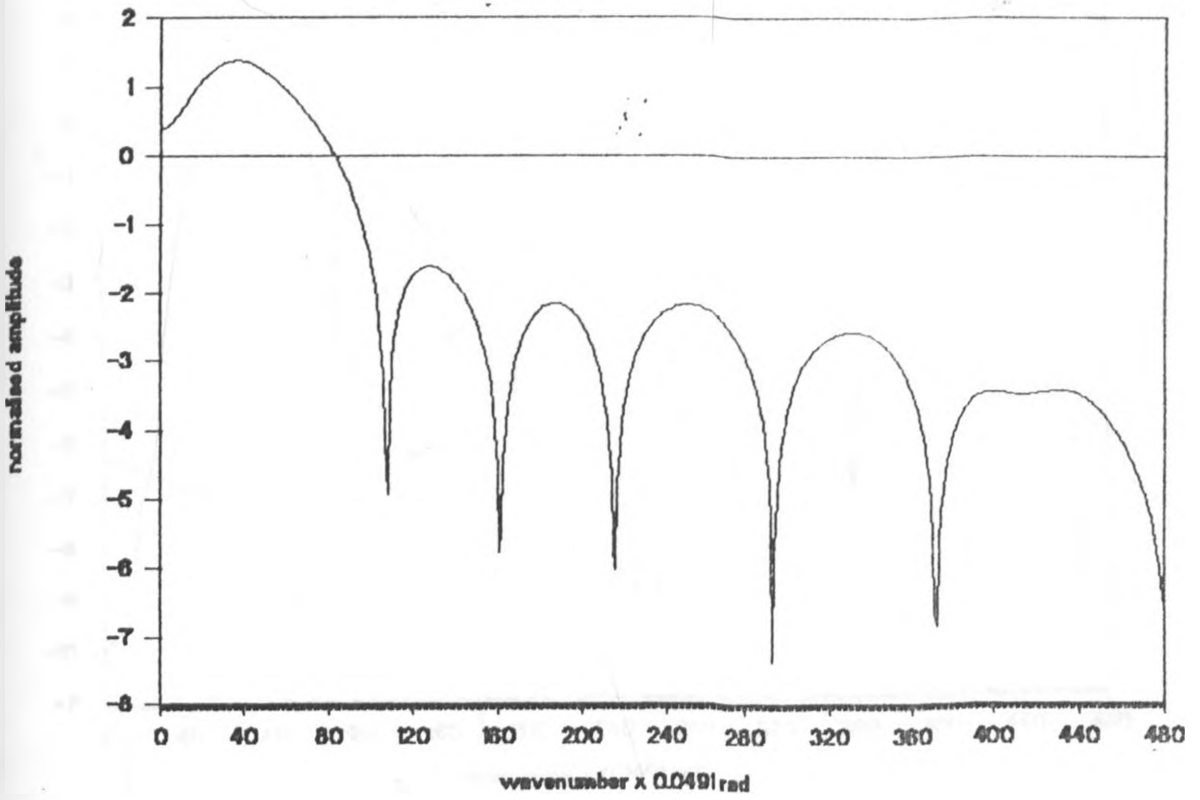


Fig. 4-4(a) Amplitude spectrum for anomaly A1-161 line 125W at 222 Hz.

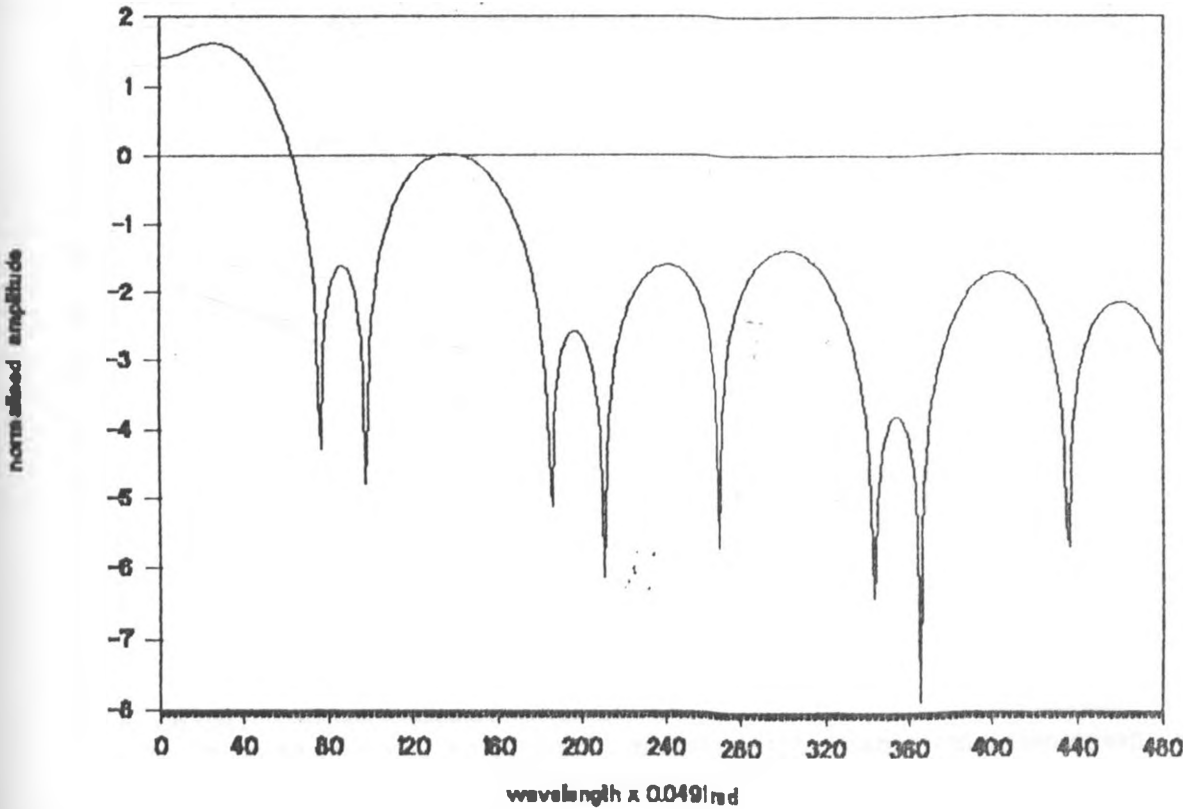


Fig. 4-4(b) Amplitude spectrum for anomaly A1-161 line 125W at 444 Hz.

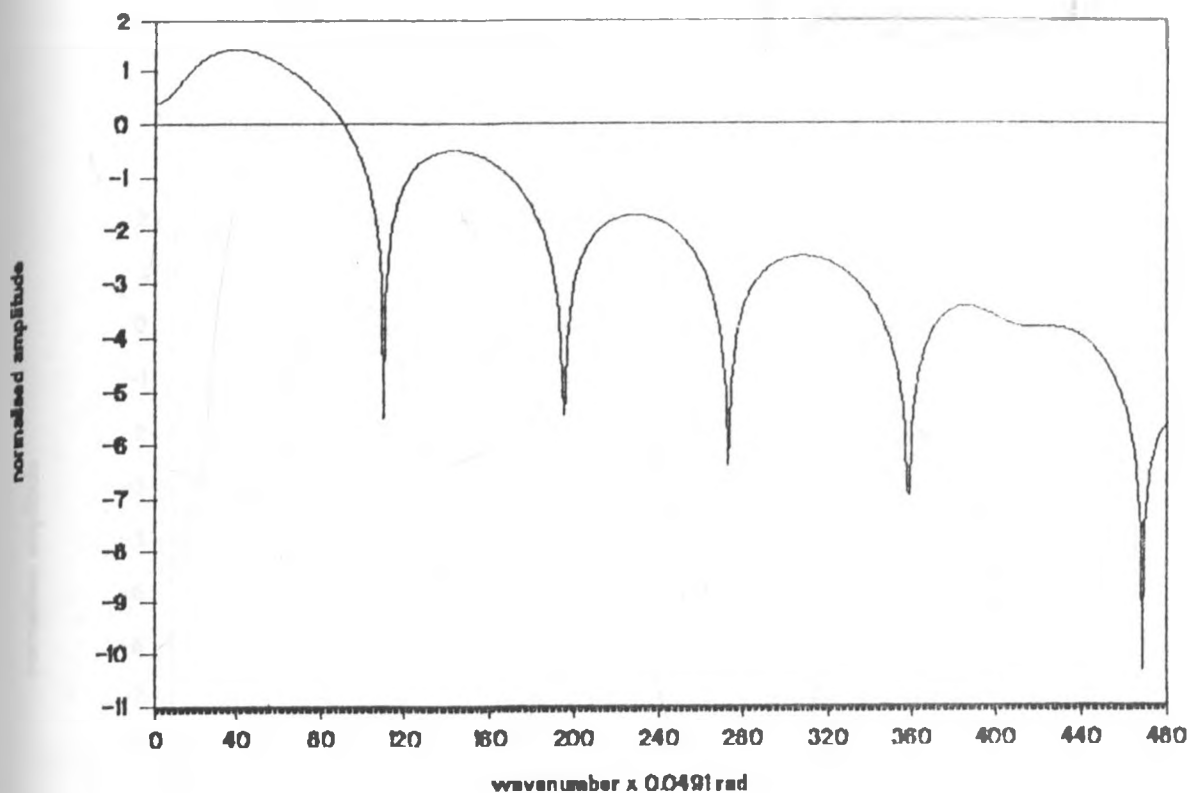


Fig. 4-4(c) Amplitude spectrum for anomaly A1-161 line 125W at 888 Hz.

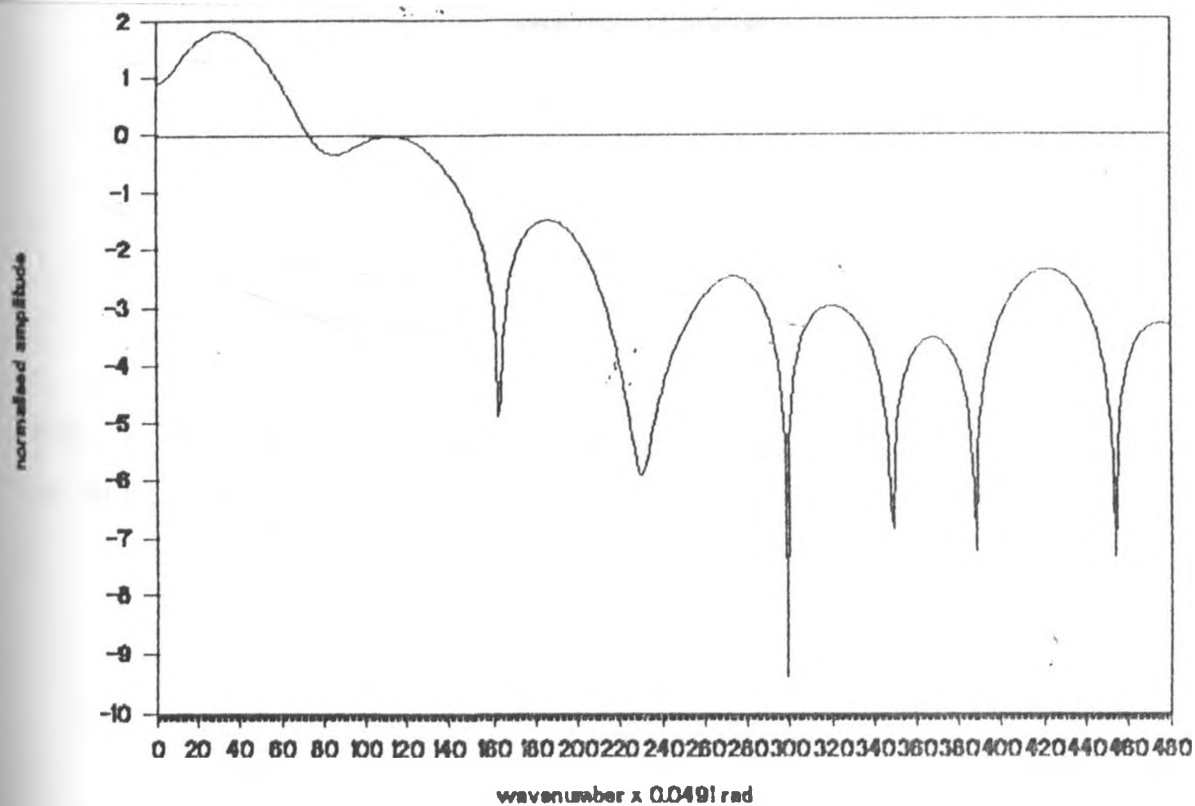


Fig. 4-4(d) Amplitude spectrum for anomaly A1-161 line 125W at 1777 Hz.

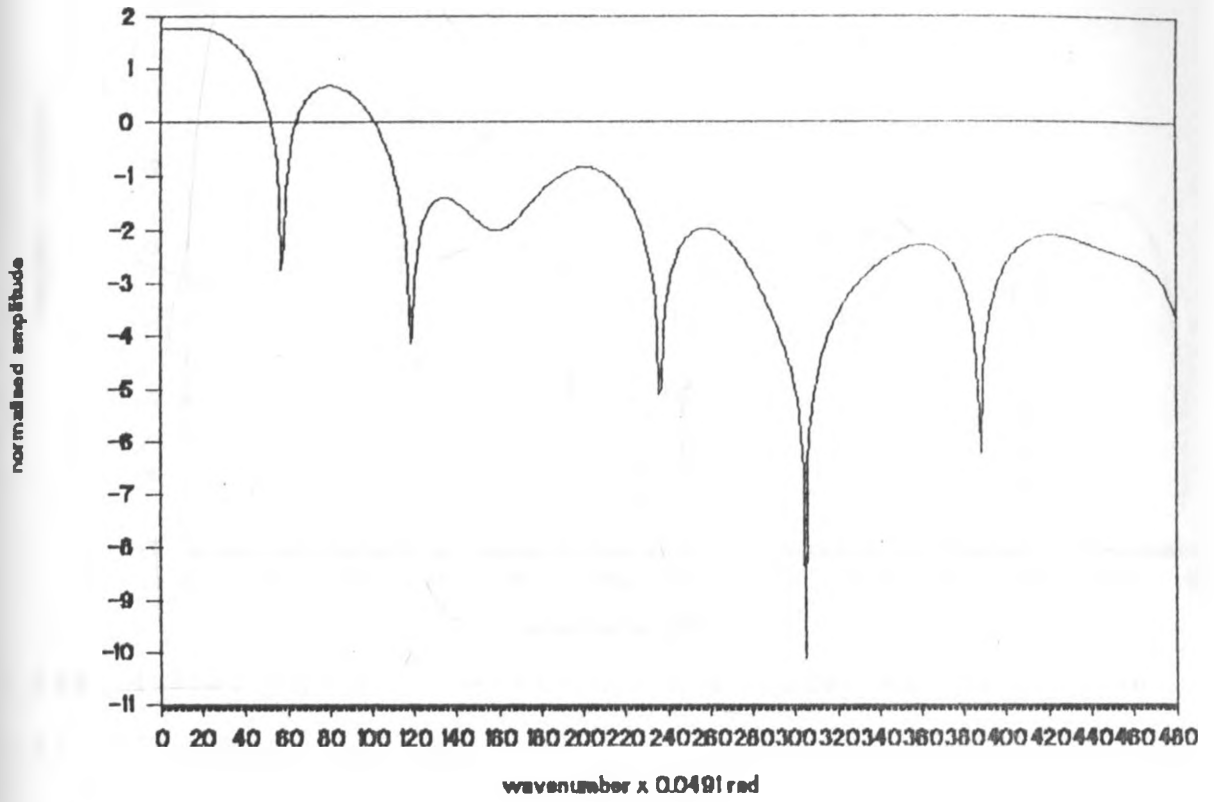


Fig. 4-4(e) Amplitude spectrum for anomaly A1-161 line 125W
at 3555 Hz.

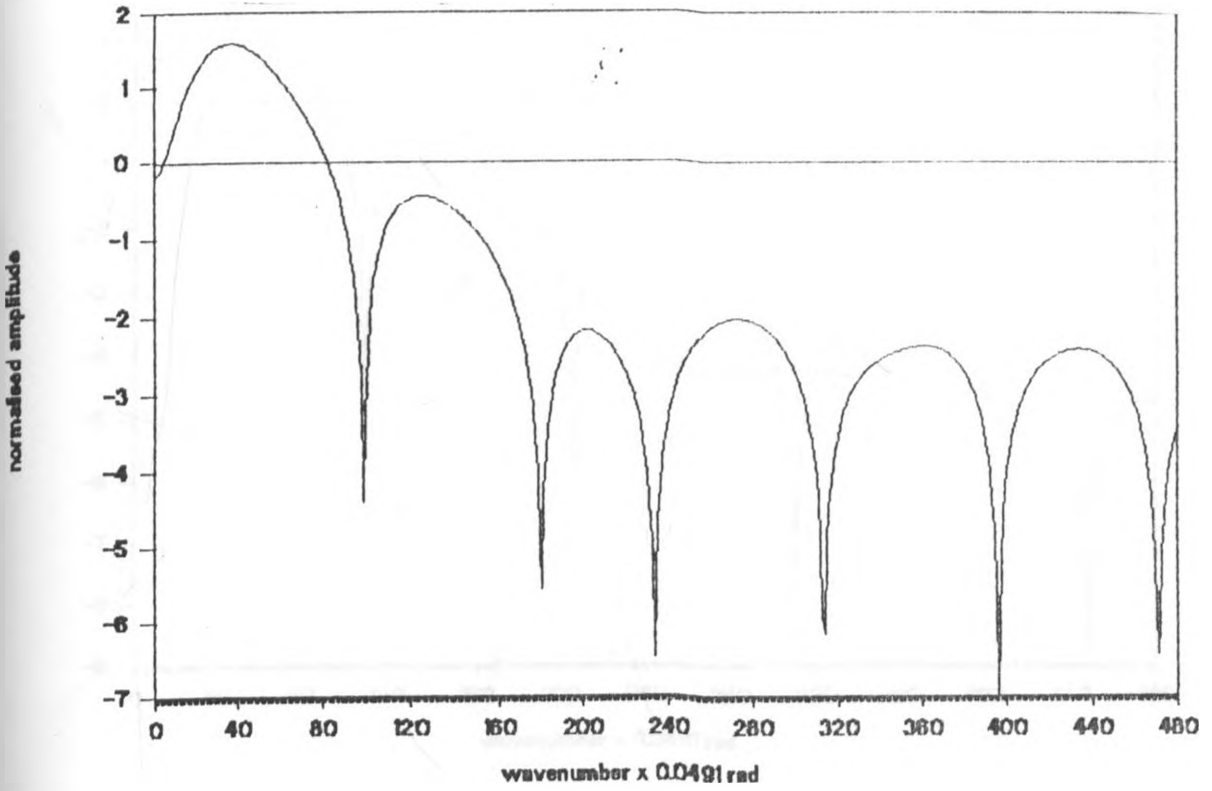


Fig. 4-5(a) Amplitude spectrum for anomaly A1-161 line 250W at 222 Hz.

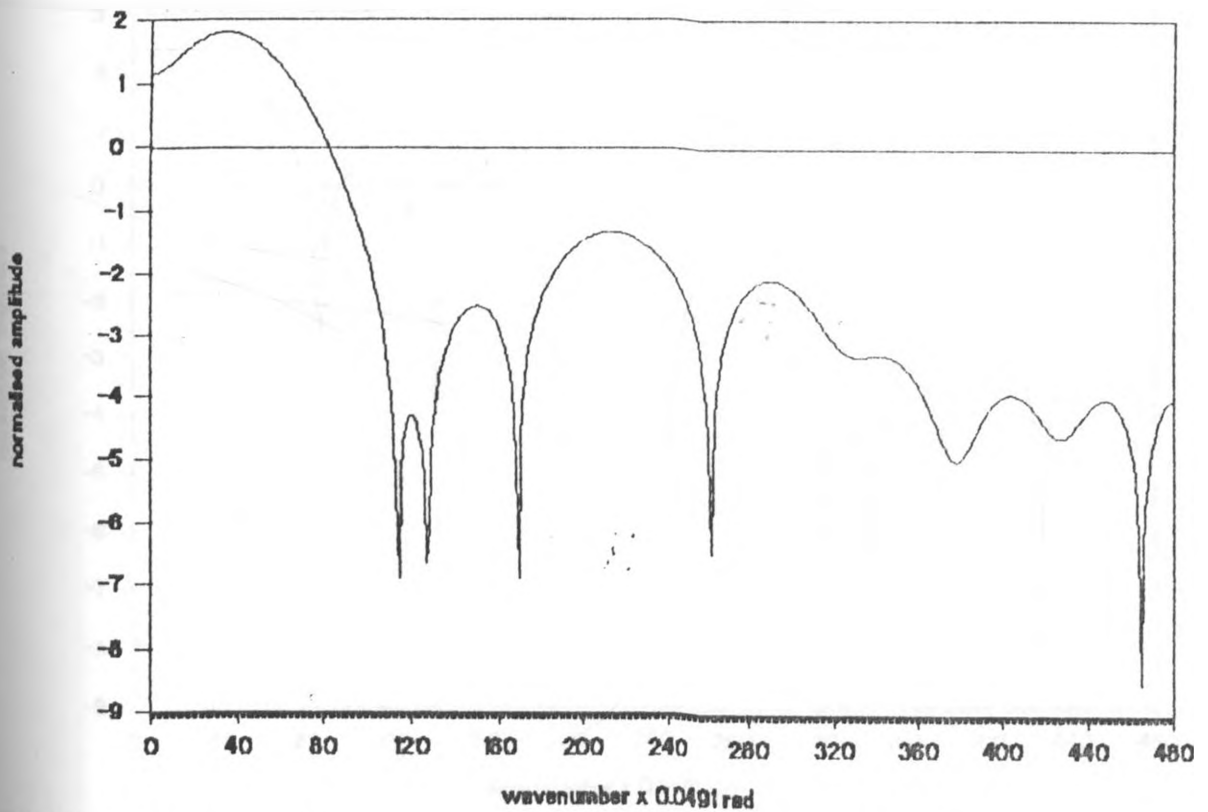


Fig. 4-5(b) Amplitude spectrum for anomaly A1-161 line 250W at 444 Hz.

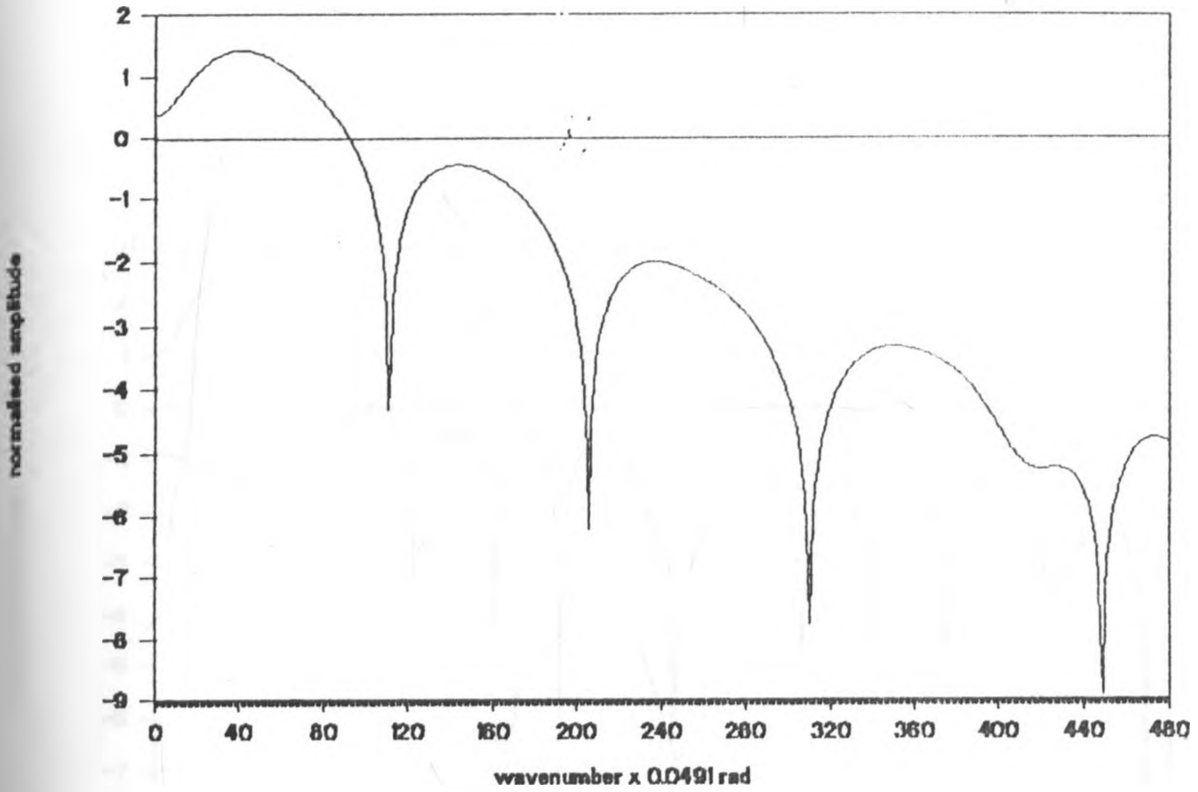


Fig. 4-5(c) Amplitude spectrum for anomaly A1-161 line 250W at 888 Hz.

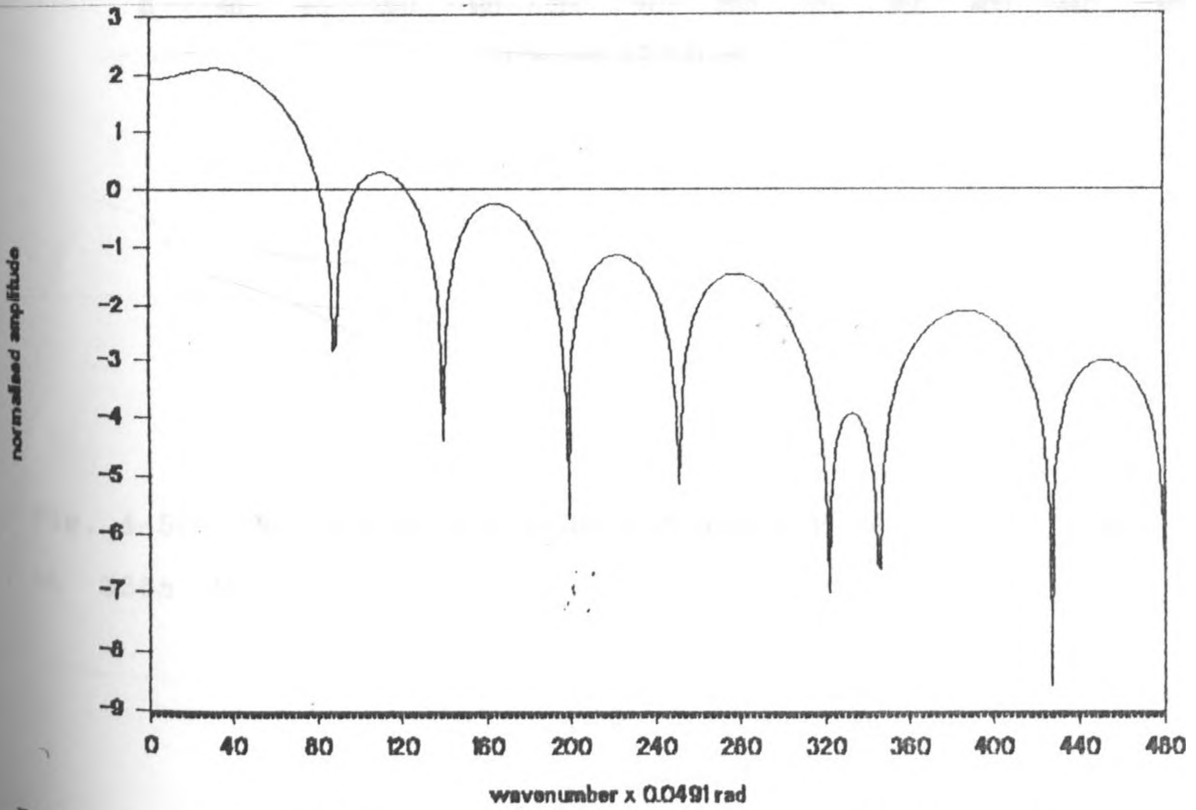


Fig. 4-5(d) Amplitude spectrum for anomaly A1-161 line 250W at 1777 Hz.

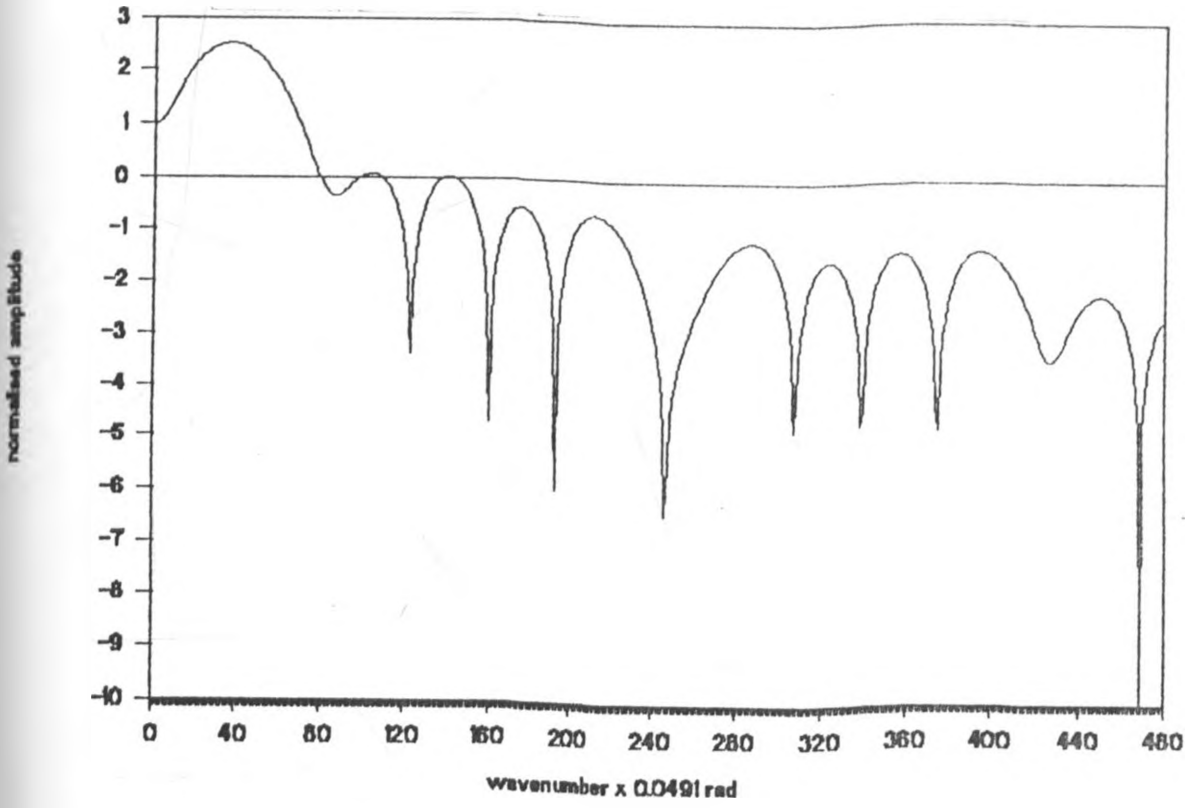


Fig. 4-5(e) Amplitude spectrum for anomaly A1-161 line 250W at 3555 Hz.

as 6.38 radians which using figure 3-6 gave a depth of about 100m.

Table 4.1. Tabulated results of depth analysis for field anomalies.

(a) Table of results of depth analysis obtained using phasor diagrams for all anomalies taken at 222 Hz.

Anomaly/line	$d(= D/l)$	$l(m)$	Depth (m)
A1-161 line 250 W.	0.238	150	34.5
A1-161 line 125 W.	0.250	150	37.5
A1-148 line 00	0.170	200	34.0
A1-221A line 250W	0.150	100	15.0
A1-221A line 500W	(a). 0.154 [*]	100	15.4
	(b). <0.100	100	<10.0
A1-101 line 250E	<0.100	150	<15.0
A1-160 line 00	<0.100	150	<15.0

* The anomaly has been adjusted by shifting the traverse line accordingly to reduce noise. # (b) represents the peak amplitudes read for unadjusted anomaly.

(b) Tabulated results of depth analysis estimated by means of spectral analysis.

Anomaly/line	max. slope	min. slope	mean slope	depth (m)
A1-161 line 125 W	-0.0352	-0.0352	-0.0352	35 +1
A1-161 line 250 W	-0.0467	-0.0467	-0.0467	47 +1
A1-148 line 00	-0.0415	-0.0415	-0.0415	42 + ?
A1-221A line 250W	-0.0399	-0.0399	-0.0399	40 +?
A1-221A line 500W	-0.0473	-0.0368	-0.0420	42 +5
A1-101 line 250E	-0.0599	-0.0428	-0.0509	51 +8
A1-160 line 00	-0.0815	-0.0662	-0.0739	74 +8

(c) Tabulated results of depth estimates based on the spectral method and phasor diagrams.

Anomaly/line	depth estimate (m)	
	spectral est.	Phasor diag. est.
A1-161 line 125 W	35 +1	34.5
A1-161 line 250 W	47 +1	37.5
A1-148 line 00	42 +?	34.0
A1-221A line 250W	40 +?	15.0
A1-221A line 500W	42 +5	15.4
A1-101 line 250E	51 +8	<10.0
A1-160 line 00	74 +8	<15.0

CHAPTER FIVE

5.1 Discussion of Results

Synthetic data from the current filament model when analysed in the wavenumber domain yield estimates of depth that agree very well with the starting values used to generate space domain anomaly curves. Both the slope and harmonic analysis have been proven to work in this case. The plate model data generated using the program PLATE however in the transform domain shows some slight difference between the value of depth estimated from the slope and the true value. This difference may be explained in part to be due to numerical inaccuracies associated with the plate program. Moreover the induced current pattern whose sum total effect is a current concentrated on the edges of the plate does not absolutely confine itself to the edges but there is a degree of "spreading" or "smearing" of the current on an area near the edges of the plate. The current filament hence takes the average position of this current region which will always give an excess depth estimate.

Edge effects of the net current flow could also be another source of error. We note that the current flow approaches that of a current filament at/near the centre of the plate and away on either side there is a fanning out effect such that the flow is no longer linear but confined to a broadening region towards the vertical edges. The

response anomaly calculated will hence be derived from this current distribution which would obviously give a larger estimate of depth.

Bartel (pers. comm.) noticed that all depths calculated were in excess by about 3-5m regardless of high frequencies/early times or large conductances while working on time domain synthetic data. In his case, he attributes the error to a migration of the equivalent current filament towards the centre with time (Dyck, 1981; Barnett, 1984; Bartel and Becker, 1990) and in part due to numerical inaccuracies associated with the PLATE program. Better accuracy can be achieved by using the solution for the EM response of a dipping half-plane recently published by Weidelt (1983). The response generated using the PLATE program should approach this model as much as possible, however, the slight differences arise which adversely affect the results of using the harmonic analysis concept as briefly discussed below.

The harmonic analysis method works excellently for the wire model, however, for the plate model data, it is inapplicable. The value at which the real component of the Fourier transform falls to zero is too big to allow the use of Figure 3-5 (Chapter 3). It is deduced that, for the same reasons, that the estimated depths using the plate model are in excess of the true depths, by a few metres, the harmonic analysis method fails. It is apparent that the

slightest departure of the model from the wire model produces considerable harmonic distortion, thus fatally affecting the harmonic analysis method. One important source of difficulty is also noise introduced by digitisation of the profiles whose effect is to adversely affect the resolution of the FFT and consequently the spectral information available at the harmonics.

In the several field examples analysed in Chapter 4, the results of analysis cannot be fully validated owing to inavailability of drilling or excavation data. A deductive approach is used to add credence to the validity of the results obtained from field data analysis. While the theoretical background elucidates the validity of using the wire as a rudimentary model, it is not always the case in nature. Departures from this model are inevitable in nature so that results are not absolutely reliable. It must be borne in mind that many factors contribute towards the many sources of difficulty as will be discussed shortly.

From the tabulated results of analysis and examination of the anomaly profiles analysed, various deductions can be made regarding the reliability and credibility of the results. Data that were analysed were available in anomaly profile graphs, which necessitated the extraction of the values of response along the profile for Fourier transformation. This was accomplished by reading off the values from the profiles. The objective of this research was to develop a spectral analysis procedure for interpreting

the depth and quality of a thin plate-like subsurficial target conductor. In most cases dip and conductance are very easy to evaluate directly from the observed field data. While attempts were made to evaluate both depth and conductance, the former parameter became the main product of the work. The various parameters whose interpretation was carried out are discussed below plus the possible sources of error.

(i) Depth :

The depths estimated using phasor diagrams are smaller than those obtained by means of spectral analysis. The difference is in the range 1-8m for the anomalies that are not seriously affected by noise. This agreement is clearly seen in the estimates of depth for anomalies A1-161 for lines 125W and 250W , and A1-148 line 00. An important aspect of the spectral method is that it gives fairly consistent depth estimates lying between 35m and 50m. This excludes anomaly A1-160 line 00 which gives a relatively higher value. It is to be borne in mind that these anomalies are taken from more or less the same geological environment and in that respect the depth of occurrence should be fairly consistent. Interpretation for depth carried out by Barongo (1987) for anomaly A1-161 using Nair's free air phasor diagrams gives depths of 45m and 40m for lines 125W and 250W respectively. These results also do not depart much from spectral values.

There are several important factors to consider which may be the source of error. The most significant in this case is the effect of conductive overburden. The nomograms used for interpretation of the target parameters are based on conductors embedded in free space. In this case the host medium in the field situation is assumed to be an insulator when carrying out interpretation. Conductive overburden introduces the most serious aberrations or noise in the response profiles and two cases can be considered regarding the relationship between it and the target. As is well understood, tropical terrains possess a thick (20m-60m) mantle of overburden which is a product of weathering and has appreciable conductivity. The effect of the overburden is to enhance the anomaly profiles especially if it is in contact with the target. This effect makes interpretation difficult at higher frequencies which explains why only anomaly profiles at the lowest frequency were considered. Interpreted anomalies also show that the target conductors appear shallow and less conductive at higher frequencies (Barongo, 1987). It is apparent that the spectral method is less sensitive to this effect, since examining anomalies, A1-221a line 250W and 500W, A1-101 line 250W and A1-160 line 00, we see that they have been severely affected by the overburden giving unrealistic shallow depths especially the last two. It may be deduced that the masking effect of the overburden is so severe that the anomaly source is basically the overburden which in this case represents horizontal infinite sheet conductor.

Results obtained with spectral analysis however are indicative of deep seated conductor (see Table 4.1) which is more credible.

Another notable source of error is the fact that the host medium is not a perfect insulator. This further complicates the target EM response, more so if the target conductivity is poor or comparable to that of the host medium. The situation is further aggravated by the embedding of the target conductor into the overburden. The EM response of such situation is very difficult if not impossible to formulate. Delineation of bedrock conductors using EM methods in the greenstone belt of Western Kenya has worked well and has indicated that the hosting rocks are highly resistive in most cases hence the conductive overburden becomes more significant.

Field data used here contained significant noise which was mainly due to geological factors. Other sources could be due to instruments used, manmade EM sources, incidental changes in transmitter-receiver separation, etc. Geological noise is mainly due to minor variations in geology, and consequently variations in porosity, permeability, pore-fluid composition, main alteration minerals and structural controls of the mineralisation and host rock are inevitable. These will cause undesirable effects such as lateral variations in conductance whose EM response will be superimposed on the major anomaly. Depending upon the position of these aberrations on the major anomalies,

careful smoothing may fairly eliminate them. For instance, if the maximum peak anomaly of the noise coincides with the peak of the major anomaly and are in the same direction, smoothing will definitely lead to an enhanced peak anomaly leading to erroneous interpretation. This emphasizes that manual smoothing does not always guarantee total elimination of background effect. Bartel (1988) has shown that noise should be less than one percent of the peak anomaly response to allow a reasonable range in the wavenumber domain to measure the amplitude spectrum decay. This can be observed in the amplitude spectrum plots where the modulation pattern becomes almost horizontal beyond 100 rad/km.

Interpretation for depth using harmonic analysis was attempted on field data with very little success. Only anomaly A1-161, line 00 was interpretable in this respect. The zero harmonic was reckoned to be 6.387 rad/km from the amplitude spectrum, which gave a depth of about 100m through the use of Figure 3-6. The slope of the spectrum which was poorly defined gave a depth of 116m. This values are not very different though the depth is too much exaggerated. Phasor diagrams give a depth of 60m. These results are not very reliable but at least demonstrate that the harmonic method is workable. The inefficacy of this procedure can be explained in part to be due to harmonic distortion introduced by noise factors discussed above. The theory behind the harmonic method is based on an infinitely conductive wire model *sensu stricto*. The wire is assumed to

be infinitely thin and infinitely conductive. Departures from these constraints in practical cases may render the method ineffective. This is so because in field examples we deal with conductors of finite conductance and width. The main drawback here is mainly the deviation of field cases from the wire model. It must be emphasised that slight deviations will be manifest as large harmonic distortions in the wavenumber domain. This effect may be recognised by the non-periodicity of the modulation pattern in the amplitude spectra for field cases.

(ii) Conductivity-thickness product.

The above parameter is of utmost importance in evaluating the quality of massive sulphide deposits. Though methods of evaluating it rapidly and directly from field data are available, futile attempts were made to recover it from the field data using the spectrum plots. Anomaly A1-161 was the most suitable on lines 125W and 250W. The spectra were relatively good, however it was hard to read the respective amplitudes at a selected wavenumber and then use the nomogram in Figure 3-11 for the interpretation of conductivity-thickness product. This was on the one hand due to the modulated nature of the amplitude spectrum and noise in the field data on the other. Also the peaks of the amplitude spectrum do not have a constant width. An attempt to digitise the data aggravated the noise factor making it even harder to make interpretation. This effect may be attributed to spectral leakage and picket fence

effect discussed under fast Fourier transform in Chapter 2. Amplitude spectrum as exemplified in Figures 4-4(b) and 4-5(b) are the anticipated ones for field cases where noise effects are minimal. These can easily be used to estimate conductivity-thickness product. In general conductivity-thickness product is relatively difficult to estimate in this case.

5.2 Conclusions and Recommendations

The main product of spectral analysis method of EM data interpretation is a simple estimate of the depth to the equivalent current axis in the target. This is based on the decay of the amplitude spectrum in the wavenumber domain which is primarily dependent on the depth from the receiver to the current axis in the target.

A study of this sort will perhaps raise more questions than it can possibly answer. Nevertheless, it opens more avenues of investigation which can be pursued in order to come out with a more consummate and a universally applicable method. The first problem that merits thorough investigation is the undesirable effect of conductive overburden. Ferneyhough (1985) discusses a development for mitigating the overburden effect by treating it as a low pass filter. His procedure would require modifications in order to apply it on ground HLEM situation, which is an interesting avenue of research. Another important investigation would be the applicability of the spectral analysis method on target bodies of different geometries, for instance a sphere,

prism, and pipe. These should be pursued in the light of current patterns induced by the transmitter in the targets.

The harmonic analysis method which elegantly works for the wire model should be pursued further to establish why it fails for the plate model. Noise in the field profiles seems to be the major limitation in using this method.

Another problem that requires attention is the modulating factor in the amplitude spectrum which impresses a series of peaks on the spectrum. If this factor (of the form $\sin K_x^{1/2}$) can be eliminated, the spectrum would be easy to use in estimating the conductance of the target conductor. This factor has one undesirable effect in that it can make the components of the FT zero and consequently the amplitude spectrum infinite (i.e. the logarithm is not defined), which may cause the FFT to fail. However this happens on very rare occasions.

It was noted in the analysed field profiles that, data was taken with the main interest being the peak anomalies. The spectral analysis method requires data for the whole anomaly profile which should be taken carefully and at a smaller interval. It is then clear that data taken at points removed from the axis of the conductor along the anomaly profile may not be reliable because the researcher is concerned with the peak anomalies. This was noticed as an increment in noise factor when digitisation was

tried. In fact, undigitised profiles gave better amplitude spectra.

This study has also led to the adaptation of the PLATE program to a microcomputer which was originally designed to run on a Main Frame computer. Modelling can now be done on a microcomputer although the PLATE program requires considerable amount time to run (approx. 45 min to calculate the EM response of one profile only).

REFERENCES

- Annan, A.P., 1974, The equivalent source method for electromagnetic scattering theory and its geophysical applications: Ph.D Thesis, Memorial Univ. of Newfoundland.
- Avarantchev, L., and Lebel-Drolet, S., 1980, Catalogue des gites minéraux du Québec: Ministère de L'Énergie et des Ressources, DPV-744.
- Barnet, G.T., 1984, Simple inversion of time-domain electromagnetic data: Geophys., v.49, p.925-993.
- Barongo, J.O., 1977, magnetic model theory in the analysis of vertical gradient anomaly: M.Sc. Thesis, Queen's University, Canada.
- _____ 1983, Geophysical investigations for kimberlite pipes in greenstone belt of Western Kenya: Journal of African Earth Sciences, v. 1, p. 235-253.
- _____ 1985. Spectral analysis of the vertical gradient of the total magnetic field anomalies due to two dimensional dipping dikes: Kenya Journal of Science and Technology Series A6(1): p. 49-58.
- _____ 1987, Geophysical detection of mineral conductors in tropical terrains with target conductors partly embedded in the conductive overburden: Geophys.

Prosp., 35, p. 368-589.

Bartel, D.C., 1988, Spectral analysis in airborne electromagnetics: Ph.D Thesis, Univ. of California, Berkeley.

Bartel, D.C., and Becker, A., 1988, Application of spectral analysis in AEM data interpretation: geophysical Abstracts: Univ. of Toronto.

1990, Spectral analysis in airborne electromagnetics: v. 55, no. 10, p. 1338-1346.

Bell, K., and Dodson, M.H., 1981, The Geochronology of the Tanzanian Shield: Journal of Geol., v.84, p.109-128.

Bendat, J.S. and Piersol A.G., 1971, Random Data Analysis and Measurement Procedures: John Wiley Inc.

Bhimasankaran, V.L.S., Nagandra, R., and Seshagiri Rao, S.V., 1977, Interpretation of gravity anomalies due to finite inclined dikes using Fourier transformation: Geophys., v. 42, p. 51-59.

Brigham, E.O., 1974, The Fast Fourier Transform: Prentice-Hall Inc., Englewood Cliffs, New Jersey.

Cahen, I., Snelling, N.J., Delhal, J., Vail, J.R., Bonhomme, M., and Ledent, D., 1981, The Geochronology and Evolution of Africa: Clarendon Press.

- Corbet, J.D., 1961, An empirical demonstration of geophysical methods across the caribou deposit, Bathurst N.B.: Transactions CIMM, v. 64.
- David, W.S., 1966, Electromagnetic parameters of some sulphide orebodies: Society of Exploration Geophysicists, Mining Geophysics: v.1, p. 227-241.
- Dodson, M.H., Gledhill, A.R., and Shackleton, R.M., 1975, Age differences between archean cratons of eastern and southern Africa: Nature 254, p. 315-318.
- Dolan, W.M., 1960, A versatile approach to EM scale modelling: Paper presented at SEG meeting, Galvestone, Texas, no. 10.
- Dyck, A.V., Bloor, M., and Vallee, M.A., 1980, User manual for Programs PLATE and SPHERE: Research in Appl. Geophy., Univ. of Toronto, Canada.
- Ferneyhough, A.B., 1985, The quantitative interpretation of airborne electromagnetic data: Ph.D Thesis, Univ. of Toronto, Canada.
- Fleming, H.W., and Brooks, R.B., 1960, Geophysical case history of clear water deposit, North Uمبرland Co., New Branswick, Canada: Transactions CIMM, v. 64
- Geldart, L.P., and Sharma, B., 1968, Analysis of gravity anomalies of two dimensional faults using Fourier transforms: Geophys. Prosp., v. 16, p. 76-93.

Gilbert, J.E., 1960, Distribution and general characteristics of the massive sulphide deposits of the Province of Quebec: CIMM Bulletin, v. 53, no. 575, p. 128.

Grant, F.S. and West, G.G., 1965, Interpretation Theory in Applied Geophysics: McGraw Hill Book Co. Inc., 583 pp.

Hedstrom, H., and Parasnis, D.S., 1958, Some model experiments related to EM prospecting with special reference to airborne work: PH.D Thesis, McGill Univ., Montreal, Canada.

Kagami, H, Maruyama, T. and Adachi, 1983, Geochronological study of the Maragoli granite in the Tanganyika Craton in Suswa: K., Ed., Eighth preliminary Report of African Studies: Nagoya Univ. (Earth Sciences 5).

Keating, B.J., 1960, Massive sulphide deposits in Nova Scotia: CIMM Bulletin, v. 53, no. 574, p.81.

Keating, P.B., 1987, The inversion of time domain airborne electromagnetic data using the plate-model: Ph.D Thesis, McGill Univ., Montreal, Canada.

Keller, G.V. and Frischknecht, F.C., 1966, Electrical Methods in Geophysical Prospecting: Pergamon Press Inc.

- Lamontagne, Y., and West, G., 1971, Electromagnetic response of a rectangular thin plate: Geophys., v. 36, p. 1204-1222.
- Lindgren, W. , 1933, Mineral Deposits, 4th Ed., New York: McGraw-Hill, 930 pp.
- Macharia, H.T., and Barongo, J.O., 1982, Report on geophysical follow-up of INPUT AEM anomalies in western Kenya(areas 1 to 5): Investigation note 1982/83.
- McKay, D.G., and Paterson, N.R., 1960, Geophysical discoveries in the Mattagami district, Que: CIMM Trans., v. 53.
- Murthy, K.S., and Mishra, D., 1980, Fourier transform of the general expression for the magnetic anomaly due to a long horizontal cylinder: Geophys., v. 45, p. 1091-1097.
- Odegard, M.E., and Berg, J.W., 1965, Gravity interpretation using the Fourier integral: Geophys., 30 p. 424-438.
- Palacky, G.J., 1975, Interpretation of INPUT airborne electromagnetic measurements in areas of conductive overburden: Geophys., v. 40, p. 490-502.
- Parasnis, D.S., and Hedstrom, H., 1958, Some model experiments related to EM prospecting with special reference to airborne work: Geophys. Prosp., v. 6, no.4.
- Rao, K.G.C., and Avasthi, D.N., 1973 Analysis of Fourier spectrum of the gravity effect due to two dimensional triangular prism: Geophys. Prosp., V. 21, p. 526-542.

- Rattew, A.R., 1962, Helicopter-Borne EM and radiometric survey, Coronation Mine, Sask: CIMM trans., v. 35.
- Riley, C., 1959, Saturation prospecting-a new concept(?): CIMM Bulletin, v. 52, p. 44-46.
- Saggerson, P.T., 1978, Metamorphic map of Africa: Commission for the Geological Map of the World, UNESCO.
- Sanders, L.D., 1964, Copper in Kenya, Memoir No. 4, Ministry of Natural Resources, Geol. Surv. of Kenya.
- Sharma, B., and Geldart, L.P., 1968, Analyses of gravity anomalies of two dimensional faults using Fourier transforms: Prosp. V. 16. p. 76-93.
- Slitcher, L.B., and Knopoff, L., 1959, Field of an alternating magnetic dipole in the surface of a layered earth: Geophys., v.24.
- Stanton, R.L., 1960, General features of the conformable 'pyritic' ore bodies, pt. 1 - Field Association: CIMM Bulletin, March, p. 90 - 94.
- Taylor, F., 1976, Digital Processing in FORTRAN: Lexington Books, Toronto, London.
- Telford, W.M., Geldart, L.P., Sherrif, R.E., and Keys, D.A., 1990, Applied Geophysics; Cambridge Univ. Press, London.

Wait, J.P., 1951, Oscillating magnetic dipole over a horizontally stratified earth: Canada Journ. of Phys., v. 29.

Wait, J.P., 1954, 1955, 1956, Mutual coupling of loops over a homogeneous ground: Geophys., v. 19, p. 290-296; v. 20, p. 630-637; v., 21 p. 479-484.

1959, On the electromagnetic response of an imperfectly conducting thin dyke: Geophys., v. 24, p. 167-171.

Ward, S.H., 1958, The role of geophysics in exploration in New Brunswick: CIMM Bulletin March, p. 90 - 94.

Weidelt, P., 1983, The harmonic and transient electromagnetic response of a dipping dyke: Geophys., v. 48, p. 934-952.

Wesley, J.P., 1958a, Response of a dyke to an oscillating dipole: Geophys., v. 23, no. 1 p. 128-133.

1958b, Response of a thin dyke to an oscillating dipole: Geophys., v. 23, p. 134-143.

West, G.E., 1960, Quantitative interpretation of electromagnetic prospecting measurements: Ph.D Thesis, Univ. of Toronto.

William, M., 1984, Geophysical Data Analysis: Discrete Inverse Theory: Academic, Press Inc.

APPENDIX 1

THE PROGRAM PLATE

Program Structure

The program is structured to make optimal use of reusable calculations when the response of more than one model is desired. This is reflected in the flow chart.

Main program

The program MAIN (PLATEO in this work) controls the main operation of the program. Access is controlled such that two main streams can exclusively come into operation, that is, the case for fixed transmitter and for moving transmitter. In this work, only the moving transmitter option is described.

Moving Source Option

The first step is to decide the structure of the output file. Here the profile mode is chosen so that output is presented as the response at given normalised positions in space, i.e., profile output.

The next stage involves the generation or retrieval of eigenpotentials and eigenfunctions. The only required parameter is the aspect ratio of the plate.

Alternatively, Previously generated eigenpotentials may be retrieved from the library. If they are not available, a new set must be generated. Note that the program stores the functions along with aspect ratio of plate and a number of integration parameters.

If the eigenvalues and functions are available, the other step is to input the parameters of the plate geometry (see the flow-chart). For dipole-dipole system, the reference point of the plate is always the origin of the general co-ordinate system.

The next stage is to input the dipole-dipole system geometry including positions along the profile at which the response is to be calculated. Distance along the profile is measured in units of the dipole separation. After all geometrical parameters have been input, calculations commence forthwith. The profile loop is executed once for each position in space at which the response is desired in either spectral or profile mode. The first profile loop contains the following functions:

- (1) All geometric parameters are transformed into the plate co-ordinate system via subroutines ROT1, ROT2, ROT3.
- (2) Primary field excitation coefficients are calculated using subroutine PETE5. These are the coupling coefficients between the transmitting dipole and the eigencurrents in the plate.

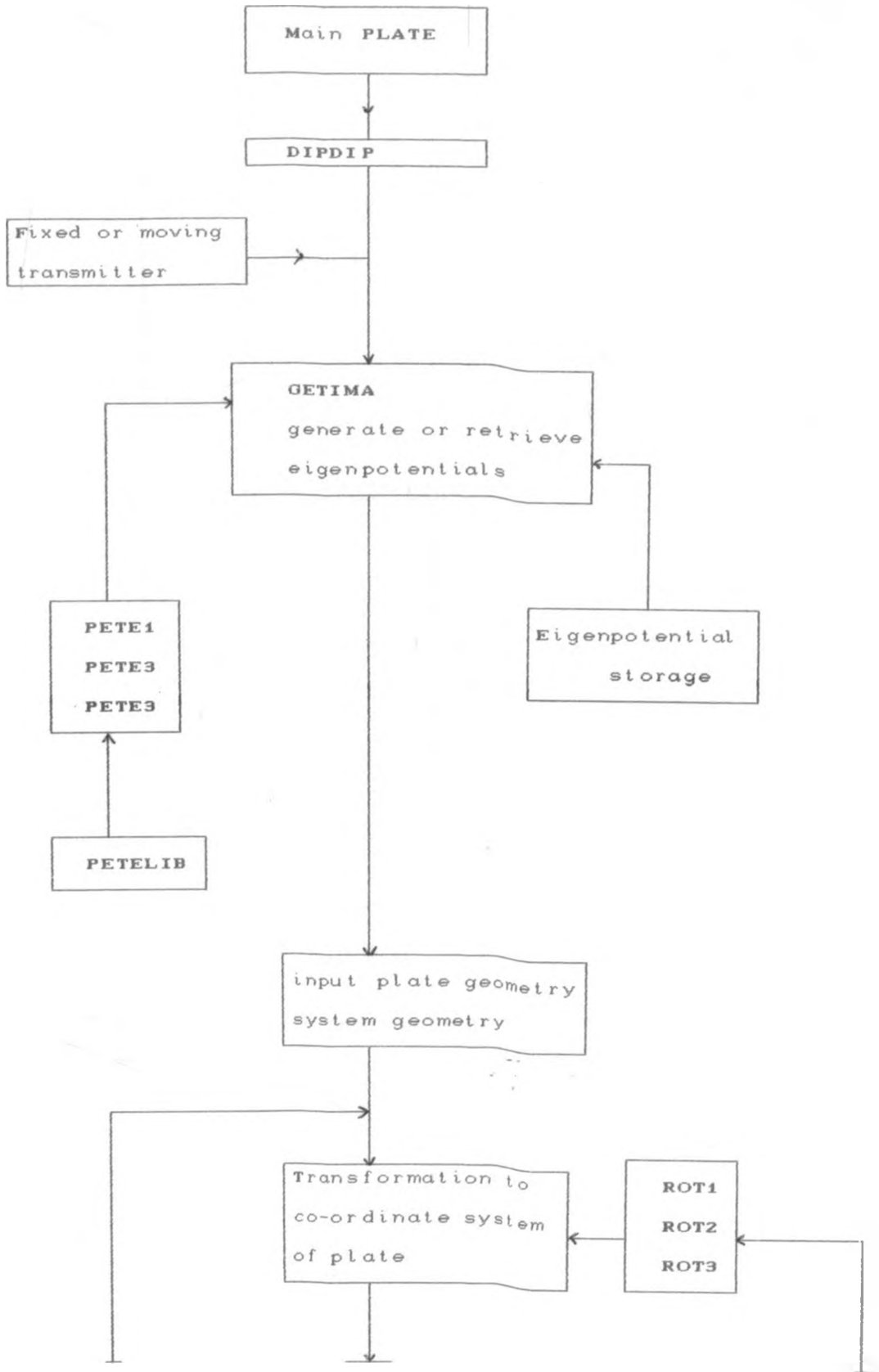
(3) Secondary field coefficients are calculated using subroutine PETE7. These are the coupling coefficients between the receiver dipole and the eigencurrents in the plate. (4) The final stage is the transformation of the magnetic field components back into the co-ordinate frame of the field system. The second profile loop contains the following functions:

(1) Subroutine GETIMC performs the time or frequency response part of the synthesis and the convolution of the system waveform with the electromagnetic response. The first time through this loop subroutine GETIMB is accessed, which allows the input waveform parameters as well as input of the spectral parameters (frequency in this work). On subsequent passes through the loop, control to the subroutine is passed via a call to GETIMC at a suitable entry point. The actual convolution is performed via subroutine SPONS.

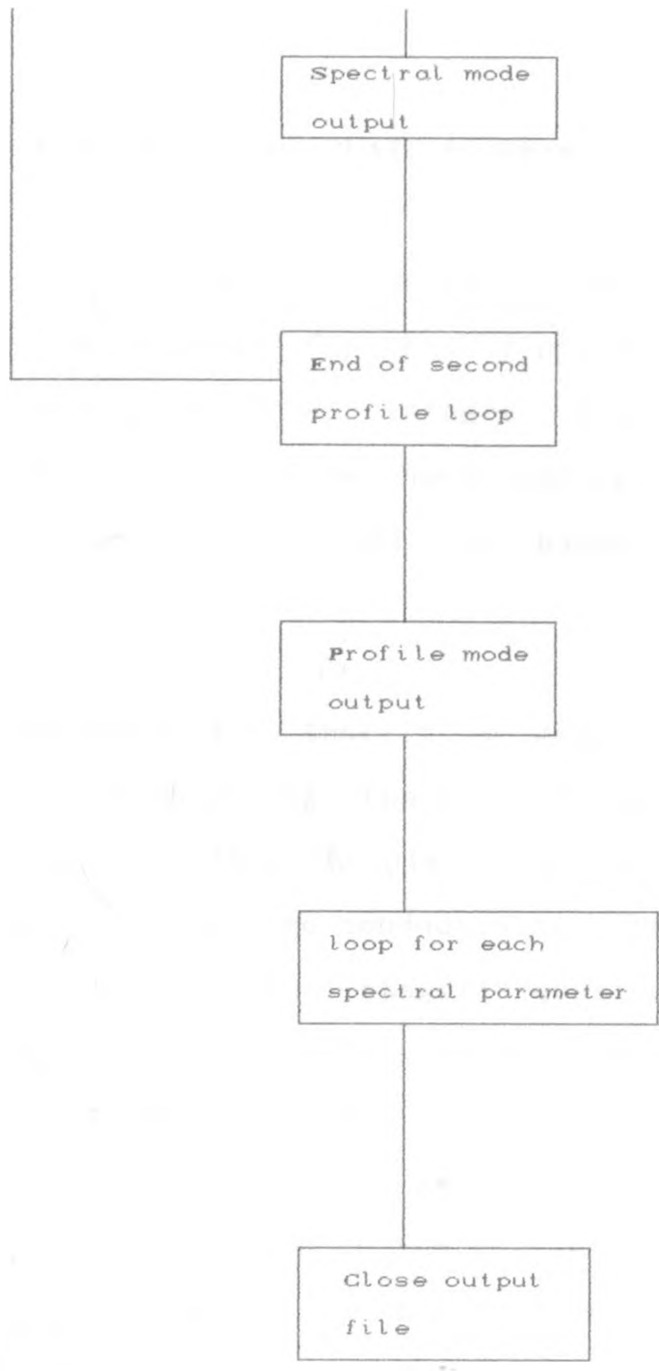
(2) The electromagnetic calculations are prepared for output. Normalisation of the primary field at the receiver location is carried out at this point.

In the present research, profile mode has been selected so that in the output, the next loop will be executed once each spectral parameter has been input. The output is written to a file. Inphase and quadrature values are output when working in the frequency domain. The program structure is summarised in the flow chart shown

below:



Flowchart for the PLATE program (after Dyck et al., 1980)



Flowchart concluded.

APPENDIX 2

THEORETICAL BACKGROUND OF THE PLATE PROGRAM

Annan (1974) developed a numerical procedure for determining the EM response of a thin dipping rectangular plate in free space based on integral equation for a conductive plate in a uniform host medium. The PLATE program by Dyck et al., (1980) is based on his development.

The plate is constrained so that it is geometrically and inductively thin, in which case the skin depth effect δ , $\left[(\sigma \mu \omega / 2)^{-1/2} \right]$ is greater than the plate thickness. The host medium is assumed to have zero conductivity. This reduces the problem to that of surface integral equation in terms of the unknown solenoidal surface currents and the known incident electric field. The total electric field, E , in an anomalous zone of conductivity σ_l embedded in a medium of conductivity σ_n may be written as the sum of an incident and a scattered field, $E_i(r)$ and $E_s(r)$ respectively;

$$E(r) = E_i(r) + E_s(r) \quad 2:1$$

The scattered field, $E_s(r)$, is caused by scatter currents J_s , due to the presence of anomalous conductor. The scatter currents may be expressed as;

$$J_r(r) = (\sigma_l - \sigma_n) E(r) \quad 2:2$$

The scatter field E , may be expressed in terms of a Green's tensor, $\bar{G}_{e_j}(r|r')$, which represents the electric field at r due to a unit current dipole at r' ;

$$E_s(r) = \int_v J_s(r') \bar{G}_{e_j}(r|r') d^3r' \quad 2:3$$

Equation 2:1 may be rewritten as ;

$$\frac{J_s(r)}{\sigma_t - \sigma_n} = \int_v J_s(r') \bar{G}_{e_j}(r|r') d^3r' = E_s(r) \quad 2:4$$

which is the integral equation for the scattering current at any point in the anomalous region. Since the plate is inductively thin, equation 2:4 reduces to:

$$\frac{K_s(r)}{\sigma_t s} - i\omega \mu_0 \int_v K_0(r') g(r|r') d^2r' = E_s(r) \quad 2:5$$

The conditions $K_s =$ and $K_s \cdot e_3 = 0$. ensure that K_s is solenoidal and confined to the plane of the plate. This means that K_s may be expressed in terms of a scalar current potential U as;

$$K_s = \nabla \times U e_3 = -e_3 \times \nabla U \quad 2:6$$

The scalar current stream potential, U , can be expanded as a linear combination of Chebychev polynomials, Φ_i , and

unknown coefficients, which is an expression of the induced current ;

$$U = \sum_{i=1}^N \Phi_i C_i \quad 2:7$$

Applying the Galerkin method results into a set of linear equations which can be expressed in matrix form:

$$\left[\frac{1}{\sigma_1 s} [F] + i\omega\mu_0 [L] \right] [C] = i\omega\mu_0 [H] \quad 2:8$$

The above matrix equation may be solved routinely. Alternatively, it may also be solved in terms of a weighted eigenvalue problem (Annan, 1974). Annan defines [F], the integral resistance matrix and [L], the general inductance matrix, both of which combine to form the general impedance matrix, [Z]. Thus, equation 2:8 can be expressed as:

$$[Z] [C] = -i\omega\mu_0 [H] , \quad 2:9$$

Where ,
$$[Z] = \frac{[F]}{\sigma_1 s} + i\omega\mu_0 [L]$$

and, [C] = eigencurrent coefficients.

The weighted eigenvector method is very useful since the eigenvectors and eigenvalues are only a function of the plate dimensions. A solution for the eigencurrent coefficients, [C], is totally decoupled in terms of electrical and geometrical plate properties. Finally the secondary magnetic field, H, due to the source currents k_s , is calculated by means of Biot-Savart law:

$$H^s(r) = \sum_{n,m}^N H_{nm}(r) C_{nm}, \quad 2:10$$

where:

$$H_{nm}(r) = \nabla \int_S g(r|r') \nabla' \times \phi_{nm}(r') d^2r'.$$